JOURNAL OF GEOPHYSICAL RESEARCH, VOL. 103, NO. C7, PAGES 14,395–14,450, JUNE 29, 1998

Coupled Ocean-Atmosphere Response Experiment (COARE): An interim report

J. S. Godfrey,[1] R. A. Houze Jr.,[2] R. H. Johnson,[3] R. Lukas,[4]
J.-L. Redelsperger,[5] A. Sumi,[6] and R. Weller[7]

Abstract. This paper is an interim report on results of the Coupled Ocean-Atmosphere Response Experiment (COARE), conducted from November, 1992, through February, 1993, in the equatorial western Pacific. Early work has emphasized data from single platforms or sensors; more profound, cross-cutting research, using multiple data sets to address ocean-atmosphere interaction, is only now yielding results. Three episodes of the intraseasonal oscillation (ISO) occurred during COARE. Atmospheric effects extended well outside the tropics. Each ISO episode was accompanied by numerous deep convective events, loosely organized on lengthscales from 10 - 10,000 km and timescales from hours to weeks. Similar lengthscales and timescales were evident in all atmospheric variables and in sea surface temperature (SST). We report detailed observations of precipitation and winds from shipborne and airborne radars; atmospheric heat and moisture budgets from sounding arrays; boundary layer properties and fluxes from ships, buoys, and aircraft; ocean heat and freshwater budgets; and numerous ancillary observations. Emphasis has been on achieving accurate heat, momentum, and freshwater fluxes, on documenting the diurnal cycle, on understanding the role of freshwater fluxes in controlling SST, and on obtaining the morphology of typical convective events. Large-scale context is provided by satellite observations and numerical weather prediction (nwp) output. However, comparison of in-situ data with nwp products shows systematic discrepancies with winds, scales of convective events, and surface fluxes. Some new parameterizations and early modeling results are reported. Further improvements in modeling the coupled ocean-atmosphere system are anticipated, based on COARE results.

1. Introduction

As discussed elsewhere in this volume, the initial concept for the Tropical Ocean-Global Atmosphere (TOGA) program had two main initiatives. Large-scale, low-intensity monitoring of the upper tropical oceans was to be maintained for a period of 10 years to provide an observational background for testing models of interannual climate variability. Simultaneously, a heirarchy of models of the coupled ocean-atmosphere system were to be developed, which would use the increased supply of data first to test the predictive skill of these models and then (if they were skillful) to start experimental predictions of climate variability.

However, near the start of the TOGA decade (1985-1994) it was recognized that the initial strategy might contain a significant gap, relating to deep convection in the western tropical Pacific. The highest sea surface temperatures (SSTs) in the world occur in this region; mean wind speeds are extraordinarily light, which is certainly an important cause for the existence of the global SST maximum there. These calm conditions are sporadically disturbed by westerly wind bursts (WWBs) along the equator, which play a major role in El Nino-Southern Oscillation (ENSO) events. ENSO warm event years can be distinguished from other years largely by the greater frequency and strength of WWBs and the related eastward migration of the warm pool [*Gill and Rasmusson*, 1983; *Picaut and Delcroix*, 1995]. While WWBs are closely linked with ENSO, they also have very vigorous dynamics of their own, on timescales of 30-60 days [*Madden and Julian*, 1971]. This phenomenon is now known as the intraseasonal oscillation (ISO). As an example of this strength, twin tropical cyclones frequently form near the terminus of a WWB, rotating oppositely on either side of the equator [*Keen*, 1982]. The intense convective activity is always confined within the "warm

[1]Commonwealth Scientific and Industrial Research Organization, Hobart, Tasmania, Australia.
[2]Department of Atmospheric Sciences, University of Washington, Seattle.
[3]Department of Atmospheric Science, Colorado State University, Fort Collins.
[4]Department of Oceanography, University of Hawaii at Manoa, Joint Institute for Marine and Atmospheric Research, Honolulu.
[5]Meteo-France Centre National Recherche Meteorologique, Tolouse.
[6]Centre for Climate System Research, University of Tokyo, Tokyo.
[7]Woods Hole Oceanographic Institute, Woods Hole, Massachusetts.

Paper number 97JC03120.
0148-0227/98/97JC-03120$09.00

pool" of the western Pacific and eastern Indian Oceans, defined by SST > 28°C. However, eastward propagating equatorial Kelvin waves emanating from these events are clearly apparent both in the atmosphere [*Madden and Julian*, 1971, 1994; *Knutson and Weickmann* 1987; *Milliff and Madden*, 1996] and in the Pacific Ocean [e.g., *McPhaden et al.*, 1988; *Kessler et al.*, 1995]. WWBs induce dramatic effects in the ocean, with SST drops of 1°C and 1 m s^{-1} changes in zonal current in a week [*McPhaden et al.*, 1988, 1992; *McPhaden and Hayes*, 1991].

Early coupled climate models were able to simulate many aspects of ENSO quite successfully by treating the atmospheric circulation as a passive, equilibrium response to the ocean's SST field [e.g., *Cane and Zebiak*, 1985]. The episodic nature of ISO events is in effect smoothed over in such models, both within the atmosphere and the ocean. However, despite the success of such models, it was felt that averaging over events as obviously energetic and nonlinear in nature as ISOs might cause significant loss in potential predictive skill, so that in order to achieve the overall aims of TOGA the dynamics of ISOs needed to be understood in their own right. The TOGA monitoring program [*McPhaden et al.*, this issue] was not designed to address the sorts of questions relevant to understanding the WWBs. Therefore a special process study was devised as part of TOGA, the Coupled Ocean-Atmosphere Response Experiment (COARE). A detailed account of the rationale for COARE (its aims and its design) was given by *Webster and Lukas* [1992], so the description given here is quite brief.

1.1. Design Considerations for COARE

The warm pool is the center of the heaviest rainfall and strongest latent heat release on the planet, as the Walker Circulation and the west Pacific trades all converge on this region [e.g., *Webster*, 1983]. Changes in convection here can affect atmospheric circulation over much of the globe. Early motivation for COARE came from experiments with atmospheric general circulation models (AGCMs), which revealed that, at least in the AGCMs available at the time, the atmosphere was extraordinarily sensitive to small (0.5°C) perturbations in SST in the western equatorial Pacific [e.g., *Palmer and Mansfield*, 1984]. A possible explanation for this sensitivity is that because of the global SST maximum in this region the atmospheric boundary layer moisture content (which depends nonlinearly on temperature) is exceptionally high and vigorous convection extending to the tropopause is commonplace. In any case, such model sensitivity to small SST changes highlighted the need for more information regarding two questions.

1. Observationally, are convective events over the warm pool related to SST changes there? *Gadgil et al.* [1984] and *Graham and Barnett* [1987] found that while SSTs in excess of 27.5°C were a necessary condition for large-scale deep convection to occur, (monthly mean) SSTs above 27.5°C were largely uncorrelated with indices of convection such as outgoing longwave radiation (OLR) or near-surface wind convergence. However, monthly means are too coarse to resolve relationships on the 30-60 day timescale. *Krishnamurti Krishnamurti et al.* [1988] showed, using 10-day average SSTs for 1 year, that a very striking peak in SST variability occurs in the western equatorial Pacific on the 30-60-day timescale and to a lesser extent in the Bay of Bengal. These peaks are presumably related to the ISOs, but whether the SST variations somehow cause the ISO convection, or the ISO winds and clouds cause the SST changes, or both, was not known.

2. What causes SSTs to change within the warm pool region? In the eastern equatorial Pacific (i.e., outside the warm pool) the huge interannual SST changes are primarily controlled by horizontal advection and/or changes in temperature of the upwelled water. However, the much smaller, but climatically very significant, SST changes in the western equatorial Pacific seemed to be controlled by air-sea heat exchanges [*Meyers et al.*, 1986]. Specifically, Meyers et al. found that changes in the sum of shortwave input and evaporative heat loss correlated rather closely with the SST changes in this region that led ENSO events.

The *Meyers et al.* [1986] result showed that if one is to understand SST changes in the warm pool, first emphasis must be placed on obtaining accurate surface heat fluxes. Unfortunately, predicting SST changes of 0.5°C over 3 months (typical warm pool changes near the start of an ENSO event) requires heat fluxes to be accurate to 10 W m^{-2}; annual mean climatologies published in the 1980s showed discrepancies of over 50 W m^{-2} in this region [e.g., *Godfrey and Lindstrom*, 1989]. A large part of the uncertainty was found to be due to problems with commonly used flux algorithms [*Bradley et al.* 1991; *Godfrey et al.*, 1991]. Models of both the atmosphere [*Miller et al.* 1992] and the ocean SST [*Gent*, 1991] suggested that rainfall patterns and SST were remarkably sensitive to small changes in the parameterization of latent heat flux at low wind speeds. The design of COARE therefore emphasized careful measurement of all fluxes into the region, of rainfall as well as of heat fluxes, because rainfall is a quantitative measure of latent heat release to the atmosphere. Furthermore, rainfall can affect SST changes through the stabilizing influence of freshwater input into the upper ocean [*Lukas and Lindstrom*, 1991].

A further consideration in designing COARE was that phenomena needed to be studied on a variety of space scales and time scales. The convective clouds and precipitation, which are the key linkage between the surface fluxes and the large-scale atmospheric circulation, are highly intermittent in time and space and exhibit a wide spectrum of scales [*Mapes and Houze*, 1993; *Chen et al.*, 1996]. In undisturbed conditions, convective clouds may be at most a few kilometers in depth. Under increasingly disturbed conditions, buoyant elements begin to reach tropopause heights. In very disturbed situations the clouds reaching high levels become areally extensive, in the extreme being referred to as "superconvective systems" and "superclusters" [*Nakazawa*, 1988; *Mapes and Houze*, 1993; *Chen et al.*, 1996]. When these large deep convective systems are present, they are accompanied by the whole spectrum of smaller convection. Changes in the strength or frequency of the convective population over the warm pool cause changes in wind patterns over regions far distant from the convective events at their center [*Mapes and Houze*, 1995; *Mapes*, 1996]. The changes in winds and radiation lead to changes in ocean circulation and SST over broad regions, and the SST changes (and associated changes in air temperature and humidity) feed back on the rainfall patterns.

These feedback processes are known to be important for the ENSO mechanism. It is not yet known whether they are important also on the ISO timescale, though *Lau and Chan* [1988] showed that variability of OLR has a remarkably similar spatial pattern on the ISO and ENSO timescales. Evidently, it was necessary as part of COARE to gain a data set which would permit researchers to diagnose how these complex multiscale events developed.

There also needed to be a rigorous test of the idea that ocean dynamics, so important for understanding SST changes in the east Pacific, could be ignored for purposes of understanding SST changes in the western Pacific. While earlier workers had suggested that this was probably the case as a first-order description, it was not firmly established.

1.2. Aims of COARE

The stated aims of COARE were given by *Webster and Lukas* [1992, p.1394]:

> To describe and understand (1) the principal processes responsible for the coupling of the ocean and atmosphere in the western Pacific warm-pool system; (2) the principal atmospheric processes that organize convection in the warm-pool region; (3) the oceanic response to combined buoyancy and wind-stress forcing in the western Pacific warm-pool region; (4) the multiple-scale interactions that extend the oceanic and atmospheric influence of the western Pacific warm-pool system to other regions and vice versa.

1.3 History of COARE

The concept of COARE emerged in 1987 at the Western Pacific Air-Sea Interaction Workshop in Honolulu. The design of COARE then developed from international discussions among scientists and science administrators over the years 1987-1992. A key event was the Western Pacific International Meeting and Workshop on TOGA COARE, held in Noumea in 1989. The February 28, 1991, issue of the *Journal of Geophysical Research* was a supplement devoted to papers presented at that meeting. The TOGA COARE International Project Office (TCIPO) was formed in 1990. TCIPO took responsibility for coordinating assembly of all the measuring platforms in the field, according to the TOGA COARE Operations Plan [TOGA COARE International Project Office (*TCIPO*) 1992], and (with advice from the COARE International Science Oversight Team) for determining their deployment on a day-to-day basis, during the intensive observation period (IOP).

Serious students of COARE data should read work by *Webster and Lukas* [1992], the scientific plan for TOGA COARE [WCRP, 1990], the experiment design [TCIPO, 1991], and the TOGA COARE operations plan [TCIPO, 1992]. Here we provide only a brief summary of the plan. It envisaged three components: an interface component, an atmospheric component, and an oceanic component. Specific goals were defined for each of these components. The atmospheric and oceanic components required observations on a range of spatial scales, while the flux component was concentrated within an intensive flux array (IFA). During the IOP of November 1992 through February 1993, observations were collected on all the platforms shown in Figure 1.

Figure 1a shows the upper air sounding stations and integrated sounding systems (ISSs) available, covering the region of strongest convective activity, from Indonesia through the western Pacific. Several stations within this region were installed or upgraded for COARE, including all the ISSs; these consisted of omegasondes, 915-Mhz wind profilers, acoustic sounders, and surface meteorological stations [*Parsons et al.*, 1994]. The COARE sounding network consisted of nested arrays, ranging from the synoptic scale (the LSA, with twice per day soundings) to the subsynoptic to mesoscales (the outer sounding array (OSA) and the intensive flux array (IFA), both with four soundings per day). The OSA and IFA were designed for use in atmospheric budget studies. The ISS and acoustic sounders provide high-resolution (1-hour) vertical profiles of wind and virtual temperature in the lower troposphere. Apart from the value of these budgets in their own right, experience in the Australian Monsoon Experiment (AMEX) [*McBride and Holland*, 1989] and in the Equatorial Mesoscale Experiment (EMEX) [*Webster and Houze*, 1991] showed that data from such arrays also provided valuable consistency checks on aircraft observations. Seven ISS sites were located at Nauru, Kapingamarangi, Manus, and Kavieng and on three ships, the R/V *Kexue 1*, the R/V *Shiyan 3*, and the R/V *Moana Wave* (Figure 1b), to provide more detailed recording of convective events than was possible from conventional soundings. Two C band (5-cm wavelength) Doppler weather research radars were deployed on ships in COARE [*TCIPO*, 1992]. One was the TOGA radar aboard the R/V *Xiangyanghong 5*; the other was the Massachusetts Institute of Technology (MIT) radar aboard the R/V *Vickers* (Figure 1c). These radars provided three-dimensional volume scans, which show the four-dimensional precipitation patterns at high time and space resolution (~2-km horizontal resolution, ~10-min time resolution) within 100 km of the ship. At least one of the ships was present in the IFA throughout all but a few days of COARE. These radars show the pattern of rain over the ocean in great detail and provide estimates of the rain rates. The Doppler velocity information indicated inflow and outflow patterns relative to convective precipitation and, when precipitation was widespread around the ship, allowed for some estimates of the horizontal divergence of the wind. The two shipborne Doppler radars were supplemented for a short time in November by an operational radar aboard the R/V *Keifu Maru*. A pair of X band (3-cm wavelength) Doppler radars operated at Manus Island (Figure 1b) for two and a half months beginning November 12, 1992 [*Uyeda et al.*, 1995; *Takahashi and Uyeda*, 1995]. Several moorings are also indicated on Figure 1c, including a number of acoustic Doppler current profiler (ADCP) and Proteus moorings for measuring currents and the "improved meteorological instrument" (IMET) mooring with comprehensive and redundant meteorological instrumentation. These moorings were in addition to western Pacific enhancements of the regular Pacific-wide Tropical Atmosphere-Ocean (TAO) array (Fig. 1d). The TAO array as a whole was one primary tool for COARE, for documenting the large-scale oceanographic effects of

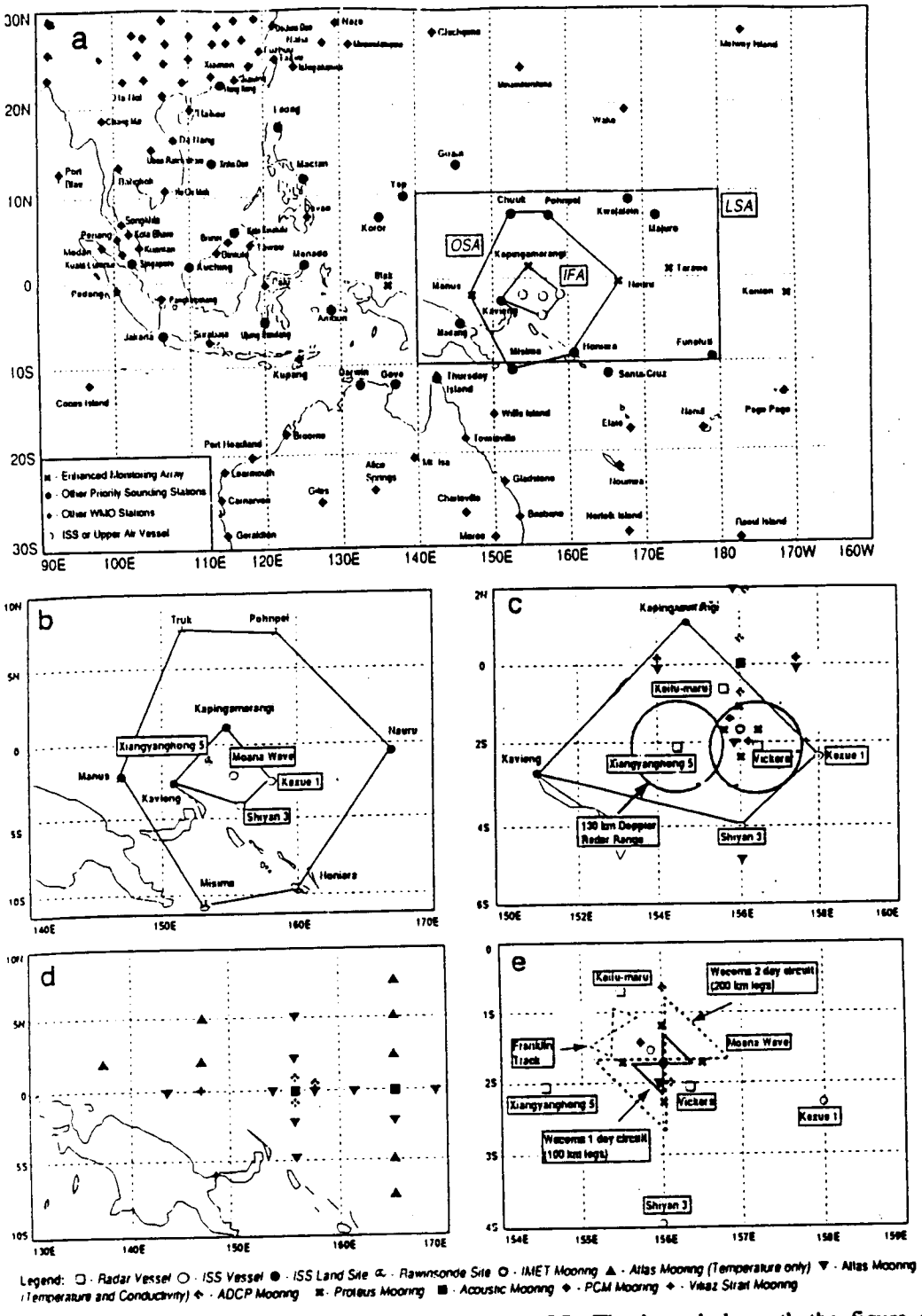

Figure 1. Observational network for the COARE IOP. The legends beneath the figure give symbols for the observational platforms. (a) The entire COARE domain. The large-scale array (LSA), the outer sounding array (OSA) and the intensive flux array (IFA) are outlined. ISS and upper air sounding stations near the warm pool region are shown. (b) Observational components within the OSA. The OSA had five rawindsonde systems and an ISS on Nauru. Within the OSA were six ISS sites: three shipborne on the R/V *Moana Wave*, the R/V *Kexue 1*, and the R/V *Shiyan 3* and three land based on Kapingamarangi, Manus, and Kavieng. (c) The IFA and locations of the shipborne radars on the R/V *Xiangyanghong 5*, the R/V *Vickers* and the R/V *Keifu-maru* relative to the oceanographic moorings. The radars provided near-continual estimates of precipitation over the moorings and the oceanographic survey ships. (d) The large-scale oceanographic moorings comprised of the TOGA TAO and COARE moorings. Additional current moorings were located in Vitiaz Strait (6°S, 149°E). The semipermanent TAO array also stretches across the Pacific Ocean, providing far-field coverage of the equatorial waveguide during (and outside of) the COARE IOP. (e) Oceanographic survey cruises within the IFA. The patterns refer to tracks and circuits of the oceanographic ships as described in the text. Adapted from *Webster and Lukas* [1992].

westerly wind bursts; a second was the enhanced deployment of surface drifters during COARE.

Several research vessels devoted their efforts to documenting changes in the upper ocean, mostly near the IFA (Figure 1e). R/V *Le Noroit* performed 18 SeaSoar sections between 5°S and 5°N during the IOP, along 156°E. All the ships shown in Figure 1e performed regular conductivity-temperature-depth profiles (CTDs) or SeaSoar deployments while within the IFA; *Moana Wave* undertook turbulence measurements near the IMET mooring, while detailed subsurface radiation measurements were made from R/V *Vickers*. R/V *Wecoma* followed a butterfly-shaped track centered near the IMET mooring while R/V *Franklin* periodically deployed a drifting buoy and made similar butterfly patterns around the drifter, the aim in both cases being to quantify advection past the center of the pattern. R/V *Hakuho Maru* and R/V *Natsushima* carried out surveys and eddy-correlation flux measurements near (0°, 156°E), while R/V *Alis* measured biological parameters. R/V *Kaiyo* performed expendable bathythermograph (XBT) measurements, while R/V *Malaita* and R/V *Onnuri* conducted CTD measurements. R/V *Malaita* also performed air-sea flux measurements.

Seven research aircraft participated in COARE: two P-3s and an Electra based at Honiara; an ER-2, a DC-8, and a C-130 based at Townsville; and a Cessna based at Rabaul. Coordinated flight plans for these aircraft were devised beforehand, for each of five classes of meteorological conditions, from class 0 (undisturbed conditions) to class 4 (cloud systems > 60,000 km^2). The aircraft program in COARE and an atlas of all the flights relative to satellite and radar data are described by *Yuter et al.* [1995]. Three of the seven COARE aircraft, the two National Oceanic and Atmospheric Administration (NOAA) WP-3D aircraft and the National Center for Atmospheric Research (NCAR) Electra, were staged out of Honiara (Solomon Islands) for the entire 4 months of the field phase of COARE. These three aircraft were instrumented for airborne radar measurements of deep convection and for flight-track measurements of thermodynamic, radiation, and cloud microphysical parameters. During the last 2 months of the project these three turboprop aircraft were joined by two National Aeronautics and Space Administration (NASA) jet aircraft, the DC-8 and the ER-2, which were staged out of Townsville (Queensland, Australia). The DC-8 provided cloud physics and radiation coverage in the upper portions of the convective cloud systems, as well as carrying "airborne rain mapping radar" (ARMAR), a downward-scanning Doppler radar. The ER-2 provided an array of down-looking radiation measurements from its lower stratosphere flight level. Additional boundary layer data were provided by the United Kingdom Meteorological Office C-130 aircraft on several flights during January 1993. Single aircraft boundary layer flights were flown by the Flinders Institute for Atmospheric and Marine Sciences (FIAMS) Cessna (C-340) aircraft based out of Rabaul, Papua New Guinea.

The objective of the aircraft program was to sample the whole spectrum of convection affecting the warm pool region. Class 0-1 missions (little if any deep convection [e.g., *Chen et al.*, 1996, Figure 5]) mapped the boundary layer by either single aircraft or a multiple aircraft "armada" pattern. While the low-level aircraft were mapping the boundary layer, airborne Doppler radar measurements were made of any small precipitating convection. In some class 0-1 missions, upper level aircraft (DC-8 and ER-2) flew in coordination with the low-level aircraft. For Class 2-4 missions (involving moderate to extensive amounts of deep convection) the turboprop aircraft emphasized airborne Doppler radar documention of the structure of the deep precipitating cloud. Two new techniques were pioneered. The "quadruple Doppler" pattern [*Jorgensen and Matejka*, 1993] was designed to compute more accurate three-dimensional winds in the convection; these data are used to estimate the momentum transports by the deep convection (see section 3.5). The "purl" pattern (Figure 3 of *Yuter et al.* [1995], adapted from *Mapes and Houze* [1995]), was used to collect accurate profiles of the horizontal divergence over areas ranging from 500 to 2500 km^2; these profiles are used to evaluate the effect of the vertical profile of deep convective heating on the environment. The divergence profiles from the purl data allowed for some crude estimates of the heating profiles, based on the assumption that persistent temperature perturbations are prevented by diabatic vertical motions (Section 3.4). Other methods based on rawinsondes and/or Doppler radar data can also be used for this purpose, and the effect of the thermal forcing on the atmosphere is derived from a linearized primitive equation model [*Mapes and Houze*, 1995].

To indicate where the missions were flown, all the flight tracks of the two NOAA WP-3D aircraft are combined in Figure 4 of *Yuter et al.* [1995]. The class 0-1 flights [*Yuter et al.*, 1995, Figure 4a] were all conducted over the IFA, except for one mission associated in Tropical Cyclone Oliver over the Solomon Sea. In contrast, the class 2-4 missions [*Yuter et al.*, 1995, Figure 4b] were spread over a larger area to capture the large convective systems wherever they presented themselves; they occurred too infrequently over the IFA to obtain a reasonable sample if flight operations had been restricted to the IFA [*Chen et al.*, 1996, Figure 2a]. Finally, the GMS, special sensor microwave/imager (SSM/I), TOPEX/POSEIDON, NOAA Polar Orbiting Satellites 11 and 12 and ERS-1 satellites provided a variety of products, not specialized to COARE, but of great value, as will be evident below.

The detailed day-to-day planning of the experiment was carried out from the TOGA COARE operations centers in Townsville and Honiara. Since the aircraft were staged at these two locations, close coordination was required between the two centers. Meteorologists assigned from the Australian Bureau of Meteorology prepared daily briefings at both centers. The principal investigators for the aircraft gathered at both centers for daily briefings and deliberation. The discussions centered on achieving an appropriate balance of sampling among all five classes of convection. Scientists at the two centers conferred by phone and with the Director of the TOGA COARE International Project Office. The Director (D. Carlson) was located in Townsville in November, January, and February and in Honiara during December.

1.4. Data Processing

The immediate result of COARE was the production of a huge and very diverse data set. Bringing it to usable form was a major challenge. An early product was the TOGA COARE intensive observing period operations summary [*TCIPO*, 1993], which contains a day-by-day summary of

meteorological conditions, a midday radar rain map from the IFA, and representative soundings of the atmosphere and ocean in the IFA. Other early products were the electronic atlases summarizing the satellite data over the COARE region [e.g., *Chen et al.*, 1995, Figure 5] and the aircraft missions (*Yuter et al.*, [1995, .Figure 3] adapted from *Mapes and Houze* [1995]). (COARE data as a whole is located at the World Wide Web Site (WWW) http:/www.ncdc.noaa.gov/coare/. The aircraft program electronic atlas may be viewed by visiting the WWW site http://www.atmos.washington.edu/togacoare/summaries.html) The latter atlas contains over 1000 images comprising a comprehensive "road map" of the aircraft program showing the flight tracks of all the aircraft in relation to satellite cloud patterns and radar-observed precipitation patterns.

After the IOP the COARE Project Office moved into a new role, acting as a communications center for interchange and discussion of these data. Richard Chinman became the new Director of the Project Office for this phase. A number of small workshops were organized, on a rather ad hoc basis, to deal with calibration and other problems as they arose. One 10-day workshop, in Toulouse in August 1994, involved nearly all field participants in COARE [*TCIPO*, 1995]; this workshop provided the first opportunity for a comprehensive overview of the data, including an integrated quality control where data sets were cross-checked against one another. The COARE Project Office arranged for a large computer network to be available at this workshop, with new software designed for intercomparison of different data sets. This workshop played a major role in familiarizing COARE workers with results from outside their own disciplines and thus advancing the interdisciplinary aspects of COARE research. However, it was also recognized at Toulouse that in order to achieve reliable accuracy (particularly for flux measurements) over the huge range of platforms and methods involved in COARE, more small workshops were needed. These are continuing. A review of the status of COARE research, as at August 1994, was included in the summary report of the TOGA COARE International Data Workshop [*TCIPO*, 1995].

This paper presents highlights from early results of TOGA COARE researchers, insofar as they exist at this time. This summary is not a review because it is too early to provide the reader with a crosscutting synthesis of results. The summary is of necessity superficial and involves the subjective judgement of the authors. We hope, nonetheless, to give readers the flavor of results emerging from COARE. However, these early results focus on the relatively simple analyses, which can be carried out with limited subsets of the COARE data. These studies tend to be based on single platforms (e.g., satellite data or soundings). The multiplatform analyses based on diverse data sets are still in progress. Because of the interdisciplinary nature of COARE these multi-data-source analyses are the most important, as they are the ones most likely to be crosscutting. Thus a real evaluation, synthesis, and review of COARE results is some years away.

1.5. Plan of This Article

The topics covered in the papers published or in press at this time range through large-scale meteorology, studies of mesoscale atmospheric systems, quantitative studies of air-sea fluxes, observations of the boundary layers of the ocean and atmosphere, and ocean properties and circulation. However, central to the aims of COARE was a concern that strong, two-way air-sea interactions may not be confined to ENSO timescales but may be acting also at the intraseasonal and even the diurnal timescale. If this turns out to be true, it will probably have a major impact on the way coupled modeling and prediction of ENSO evolves over the next one or two decades. No definitive conclusions can be drawn at this stage, but the existence of the COARE data set allows researchers for the first time to consider these questions in a holistic and rigorous way on the basis of detailed observations.

We have therefore tried to organize this article around the theme of air-sea coupling. Together, sections 2, 3, and 4 discuss the phenomenology of the three major ISO episodes during the IOP, with emphasis on the strong December-January windburst. Section 2 describes the large-scale observations in the atmosphere and ocean and the history of convection and associated events within the IFA, as recorded by the IFA sounding array. Factors inhibiting convection and the marine atmospheric boundary layer (MABL) are also discussed. The large body of observations of convection are discussed extensively in section 3, while section 4 describes the lowest-order physics of the SST variations observed during COARE and aspects of the ocean currents generated by the westerly wind bursts.

The phenomena introduced in sections 2 to 4 provide the qualitative framework for considering our theme of air-sea interactions at short timescales. However, in planning COARE it was recognized that quantitatively accurate and consistent sets of fluxes of heat, moisture, and momentum would be essential to further progress. The COARE Flux Group has met several times since the IOP, and they have succeeded in providing the basis for greatly improved accuracy in air-sea fluxes, at least near properly instrumented research ships and planes. Progress is also being made on the two related tasks of (1) using remotely sensed data to provide accurate surface fluxes throughout much of the tropical oceans and (2) developing algorithms to estimate area-averaged turbulent fluxes for a typical grid square of an atmospheric general circulation model (AGCM) under convectively disturbed conditions. Progress in these areas is outlined in section 5. Some important and instructive checks on the flux estimates provided by AGCMs are also discussed in this section.

Modeling activity associated with COARE is increasing (section 6). Real-time outputs from the European Centre for Medium-Range Weather Forecasts (ECMWF), National Centers for Environmental Prediction (NCEP) and Bureau of Meteorology Research Centre (BMRC) weather-forecasting models were used in daily planning operations during the IOP [e.g., *TCIPO*, 1993]. Mesoscale atmospheric modeling is generating valuable insights into processes within and between individual systems. The COARE data set will also provide a very accurate test bed for evaluating the wide variety of ocean mixed layer models now available, and three-dimensional ocean GCMs incorporating sophisticated mixed layer models are now being run [e.g., *Chen et al.*, 1994a, b]. Some simple coupled models are providing preliminary insights into the sensitivity of the ISO phenomenon as a whole to the small ISO-related variations in SST [e.g., *Flatau et al.*, 1997]. The status of COARE-related modeling is considered in

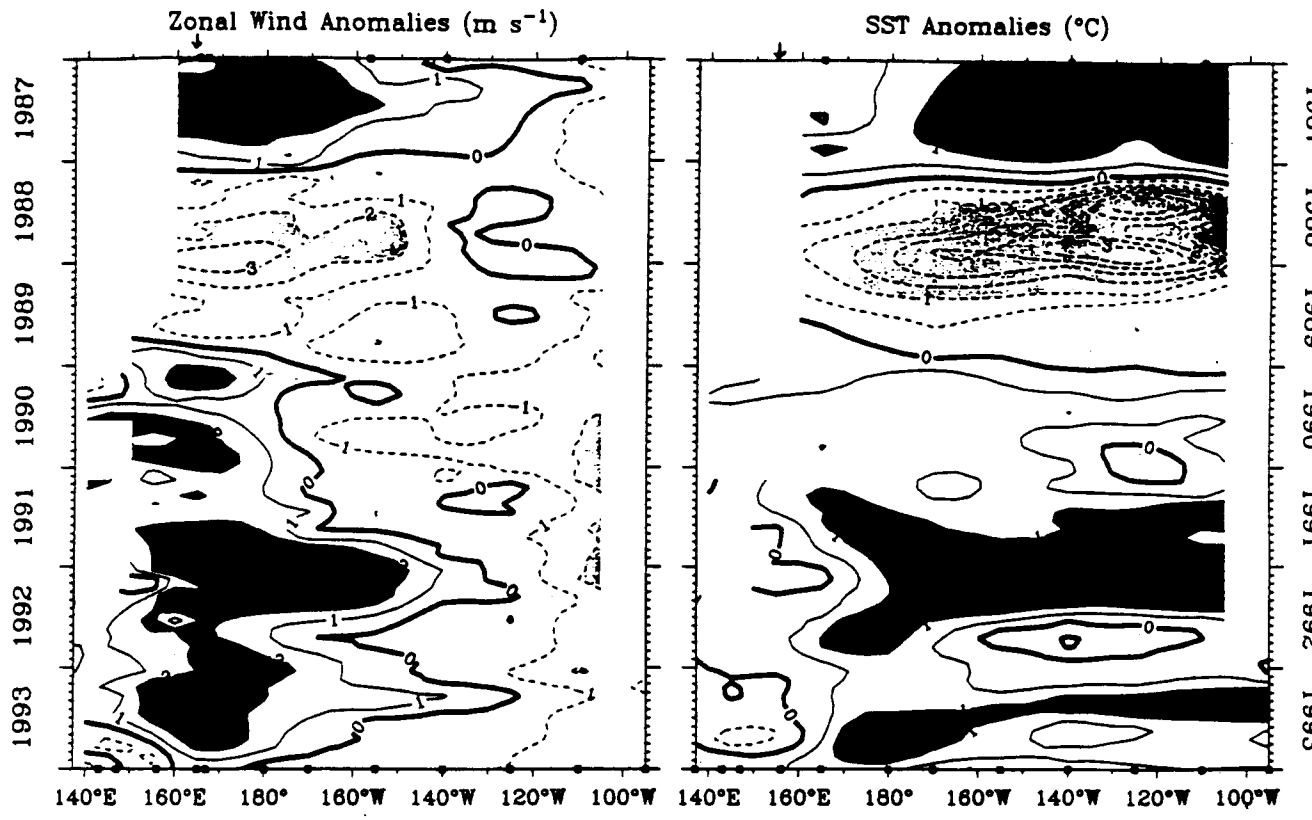

Figure 2a. Monthly mean anomalies of (left) zonal wind and (right) SST along the equatorial Pacific between 1987 and 1993 from the TOGA-TAO array. Data are averaged over buoys at 2°S, 0°, and 2°N. Contour intervals are 1 m s^{-1} and 1°C. Small squares along the abscissa indicate buoy locations, while the arrows indicate the center of the IFA. By courtesy of the TAO Project Office.

section 6. Finally, we summarize our present understanding of air-sea interactions at short timescales in section 7 and outline our view of the tasks ahead. A workshop for numerical modelers and COARE field workers is planned for 1998; it should provide a valuable opportunity for incorporating the field experience of COARE into operational weather and climate models.

2. Large-Scale Behavior

2.1. Global-Scale Observations

Figures 2a,b illustrate aspects of equatorial winds and the ocean response to them, on average over periods of a month and 5 days respectively. Figure 2a shows a Hovmoller diagram of monthly mean zonal wind anomalies and SST anomalies (SSTAs) along the equatorial Pacific, from the TOGA-TAO array [*Hayes et al.*, 1991], for the period 1987-1993. The well-known relationship of SSTAs in the east Pacific with wind anomalies in the west Pacific is apparent throughout Figure 2a. Strong westerlies are seen in 1986-1987 and again in 1991-1992, corresponding to the ENSO warm events in these 2 years. Weaker westerly anomalies are also seen through 1992-1993, i.e., covering the period of the COARE IOP; these westerlies were followed by a few months of positive SST anomalies in the east Pacific. *Ding and Sumi* [1995], *Lukas et al.* [1995], and *Gutzler et al.* [1994] show average environmental conditions for the COARE period, while *Bell and Basist* [1994] give a seasonal climate summary for December 1992 to February 1993. These authors note that in general, and very fortunately for the overall value of the COARE data set, conditions during the IOP were typical of those found near the start of a weak ENSO event. Indeed, the 3-month mean SSTAs for August-October 1992 and December 1992 to February 1993 (Figure 3, adapted from *Gutzler et al.*, [1994]) show strong resemblances to the antecedent and onset phase ENSO composite SSTAs of *Rasmusson and Carpenter* [1982, Figures 17 and 18]. The 1993 ENSO warm event was not well predicted by existing coupled models; it is likely that the COARE data set will prove valuable in diagnosing why the predictions failed. *Lukas et al.* [1995] show pictures of monthly mean SST, OLR, 850-hPa winds, and various other indices at 10, 7, 4, and 1 month preceding the IOP and show monthly means of the same quantities during the IOP. These provide a detailed background of the COARE environment relative to the longer-term sequence of ENSO evolution. Interestingly, *Kessler and McPhaden* [1995] suggest that intraseasonal oscillations played a particularly strong role in the 1993 ENSO event (which in several respects was not a canonical ENSO, such as described by *Rasmusson and Carpenter* [1982]).

Figure 2b shows 5-day running mean equatorial zonal surface wind anomalies for October 1991 through February 1993 from the TAO array. The westerly winds seen in Figure 2a were concentrated in "bursts" occurring at intervals of 30-60 days. Three such bursts are apparent

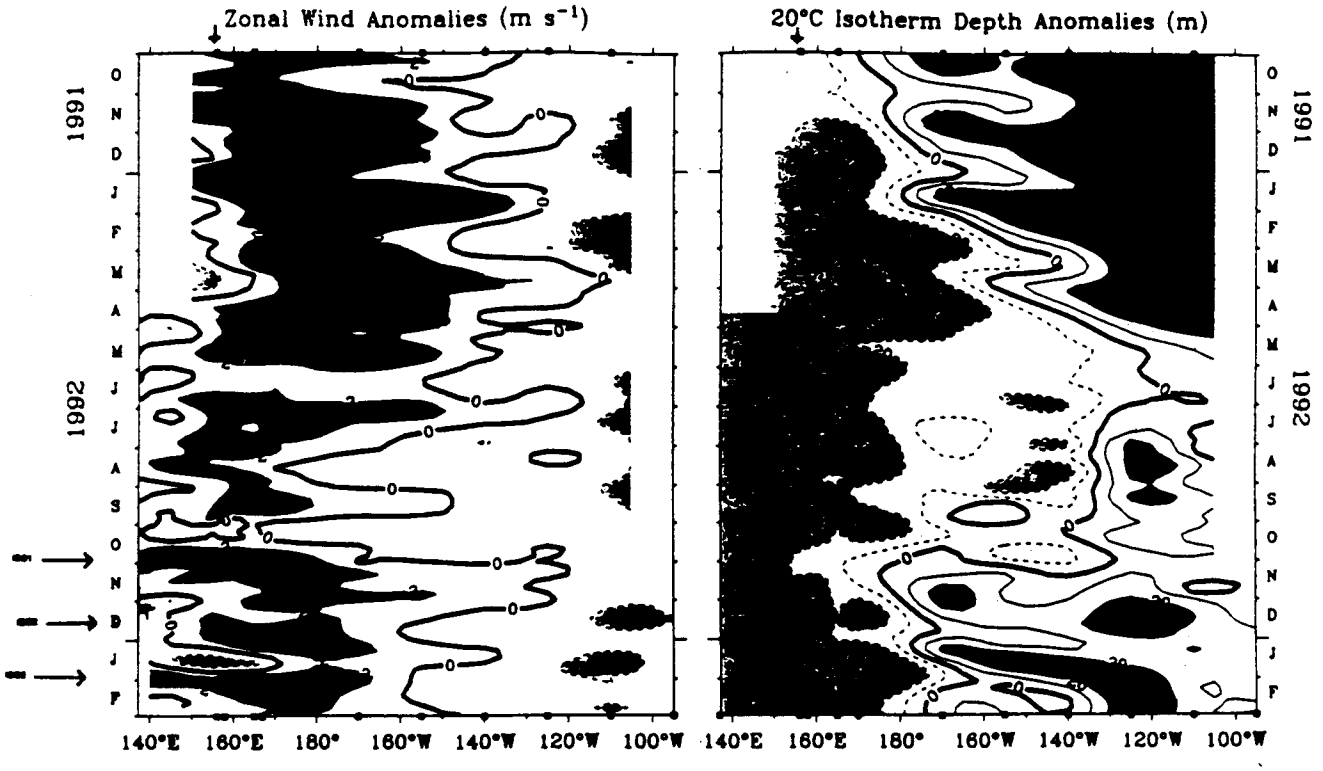

Figure 2b. Five-day mean anomalies of (left) zonal wind and (right) the depth of the 20°C isotherm along the equatorial Pacific between October 1991 and February 1993 from the TOGA-TAO array. Data are averaged over buoys at 2°S, 0°, and 2°N. Contour intervals are 1 m s^{-1} and m, respectively, positive values in Figure 2b (right) indicate that the 20°C isotherm is deeper than normal. Small squares along the abscissa show buoy locations. The vertical arrows indicates the IFA; horizontal arrows indicate ISO1, ISO2, and ISO3. By courtesy of the TAO Project Office.

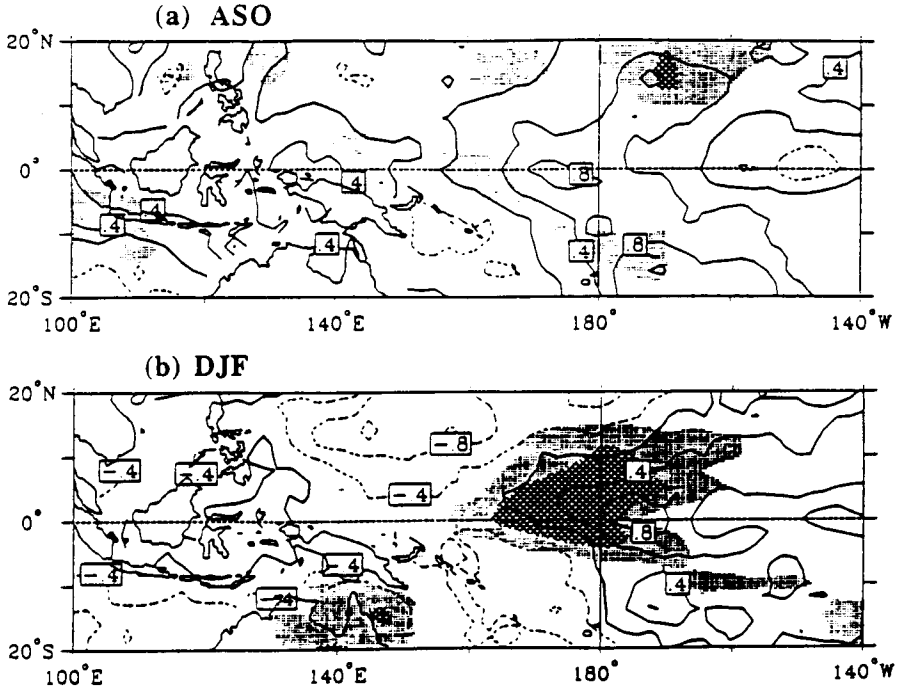

Figure 3. Three-month average SSTAs for (a) the August-October preceding COARE (contours) and for (b) the December-February of the COARE IOP. Light shading is for OLR anomalies < -10 W m^{-2}, and hatching is for OLRAs < -20 W m^{-2}. Adapted from *Gutzler et al.* [1994].

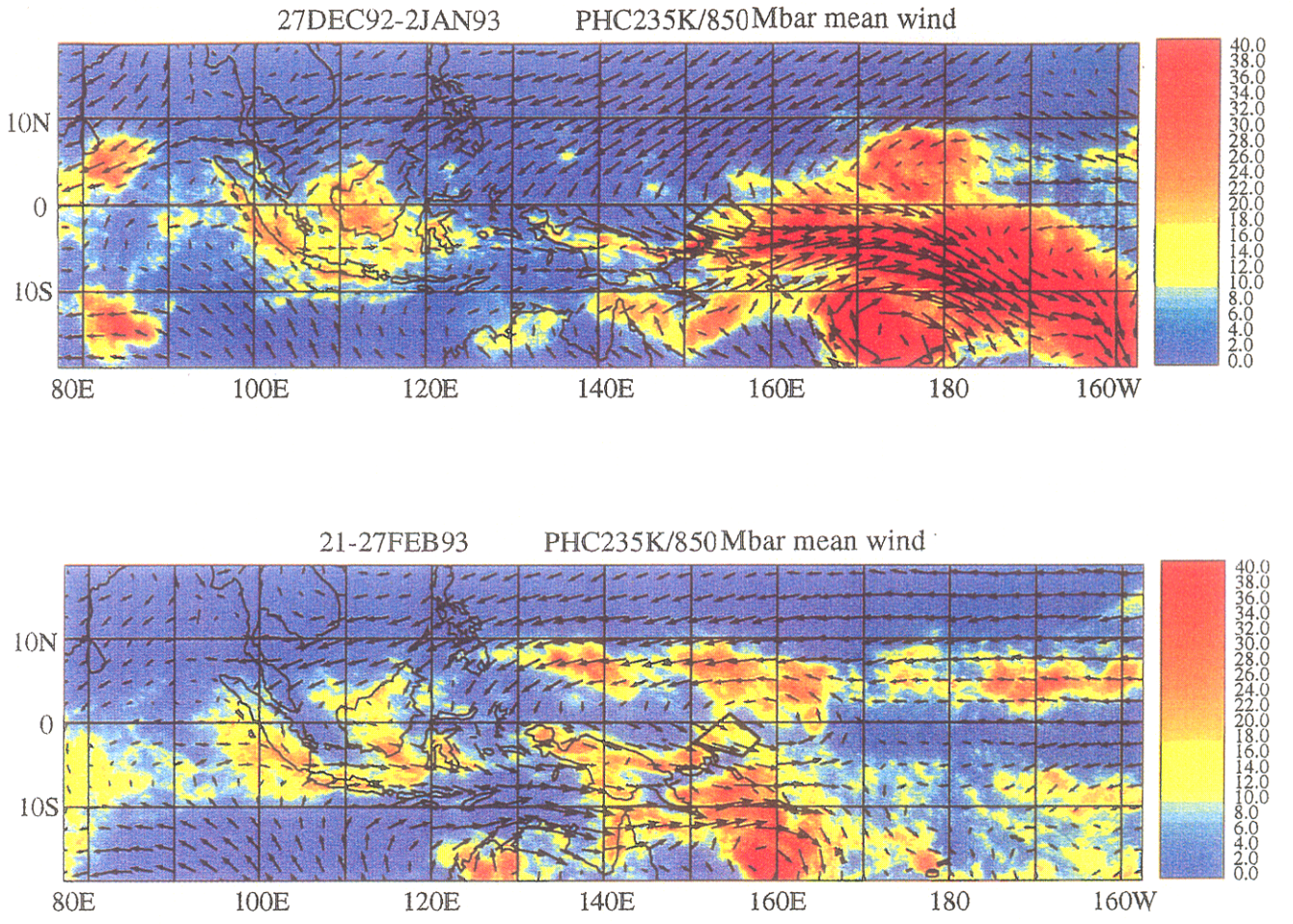

Plate 1. Weekly percent high cloudiness (PHC), calculated as the percentage of time during the week that each 10 x 10 km pixel in the GMS IR image had a value of 235°K or less for (a) December 27, 1992 to January 2, 1993 and (b) February 21-27, 1993. Also shown is the weekly mean wind from the ECMWF global wind analysis at 850 hPa with a 2.5° x 2.5° resolution. Wind vectors are scaled such that a 20 m s^{-1} wind is represented by a vector that would be 2.5° in length on the map. The COARE IFA is outlined. Adapted from *Chen et al.* [1996].

during the COARE IOP, with westerlies in early November 1992 in the IFA, strong westerlies near and east of the IFA in late December 1992, and in late January through February 1993. These three events are referred to below as ISO1, ISO2, and ISO3, respectively. Also shown in Figure 2b are the anomalies of the 20°C isotherm depth from the TAO array. These depth anomalies are evidently related to the winds in the west Pacific, and depth anomalies lag winds by about the amount expected from internal Kelvin wave propagation [e.g. *Kessler et al.*, 1995].

Note that Figures 2a and 2b show surface winds averaged over the narrow band 2°S-2°N, because oceanic equatorial Kelvin waves are driven primarily by winds in this band. WWBs are not tied this closely to the equator. The typical centers of WWBs show a clear annual cycle, appearing near 10°N, 130°E in July and progressing steadily southeastward until they disappear near 10°S, 170°W in May or June; they cross the equator southward around November [*Hartten*, 1996]. These seasonal movements of WWBs and the ISO cloud ensemble follow the center of highest SST southward in conjunction with the annual march of the solar heating of the ocean surface. They are also closely related to the seasonal movements of the monsoons. The full extent of the zonal and meridional variability of convective disturbances within the ISO can be seen by plotting the total high cloudiness and 850-hPa vector wind on horizontal maps at selected intervals of time. *Velden and Young* [1994] provided selected "snapshots" of OLR from the GMS satellite, while *McBride et al.* [1995] describe synoptic events through the COARE IOP, using the Tropical Analysis and Prediction Scheme (TAPS) winds from the Australian Bureau of Meteorology. *Chen et al.* [1996] provide weekly average maps of PHC235, which is the percent coverage by infrared pixels with infrared temperatures < 235°K, and the 850-hPa vector wind from the ECMWF wind analyses. Two examples of these maps are shown in Plate 1. They depict the mean wind and extent of cold cloud top at the end of the active phase of ISO2 (Plate 1a) and near the end of ISO3 (Plate 1b). In both cases the week average wind pattern had a Rossby wavelike structure. Cyclonic gyres straddled the equator. The WWB was the zone of strong westerly wind lying between the

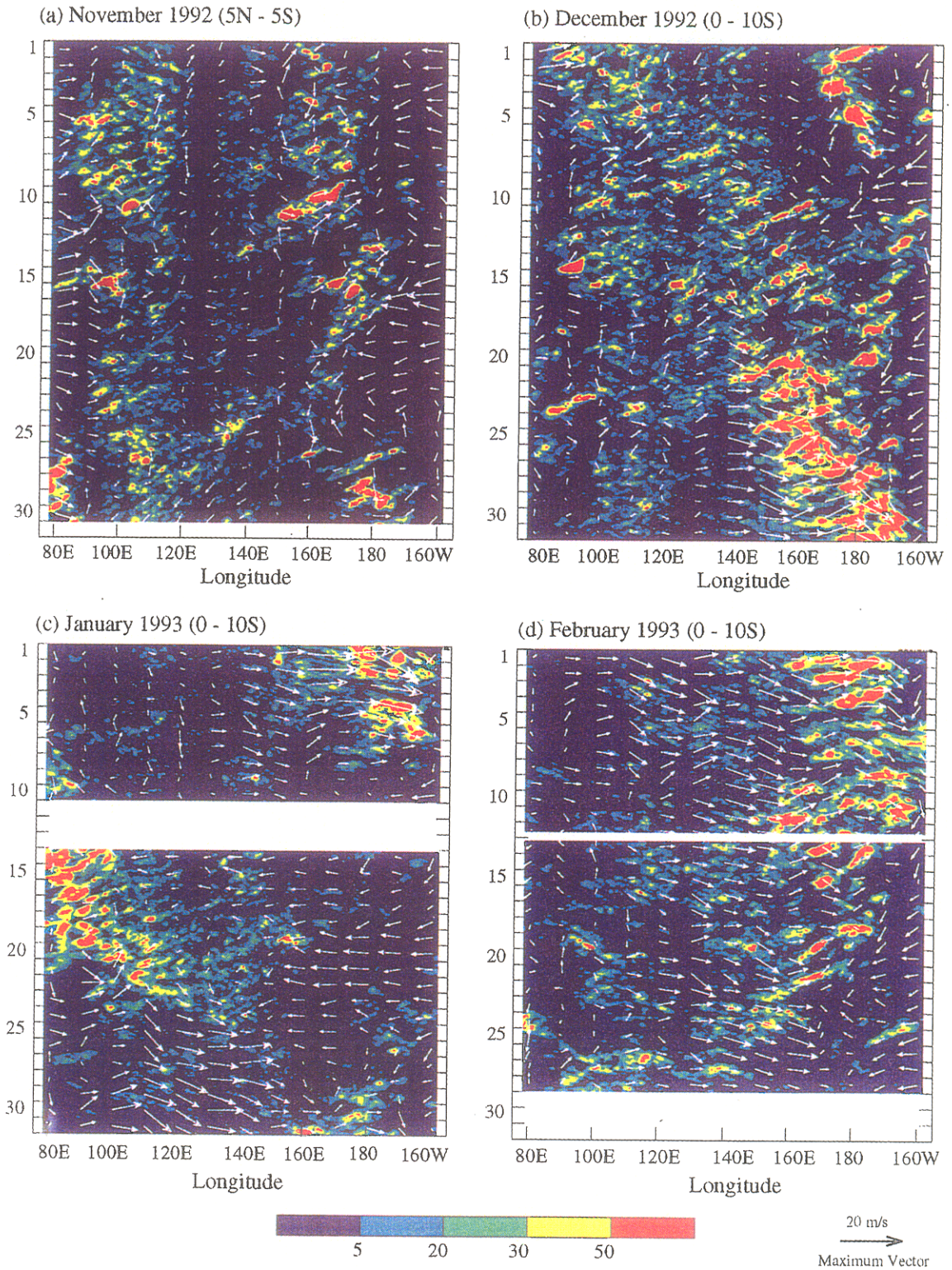

Plate 2. Time-longitude sections of deep convection with cloud top temperature < 208°K for each month from (a) November 1992, (b) December 1992, (c) January 1993, and (d) February 1993. The contours are the number of pixels colder than 208°K in a 10° latitude band at each longitude grid (5°N-5°S in November; 0°-10°S thereafter). The vectors are 850-hPa total wind (m s^{-1}) averaged over the 10° latitude band. From *Chen et al.* [1996].

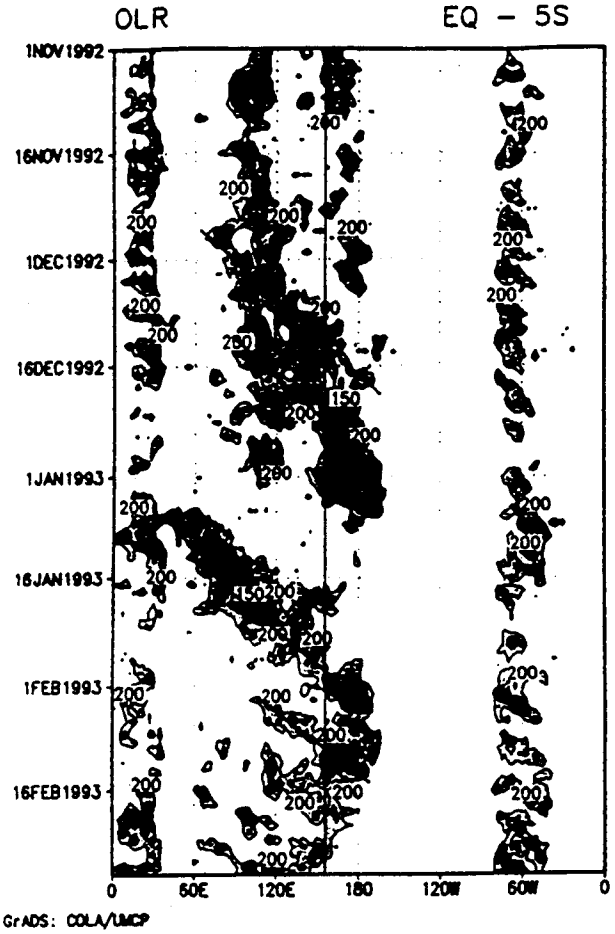

Figure 4a. Outgoing longwave radiation (OLR) from NOAA polar orbiting satellites, averaged between the equator and 5°S during the COARE IOP. Contours are only drawn where the value is < 200 W m^{-2}, with a contour interval of 25 W m^{-2}. The slanted lines show subjectively determined center longitudes of super clusters. From *Nakazawa* [1995]. Vertical line denotes center of IFA.

northern and southern hemisphere gyre. High cloudiness tended to be strongly enhanced in the gyres and in the enhanced westerlies lying between the gyres. The WWB did not lie along but rather a few degrees to the south of the equator. In both Plates 1a and 1b the 2°S-2°N average zonal winds are evidently quite weak compared to the maximum winds; that is, these wind bursts will not drive equatorial Kelvin waves efficiently. ISO1 was weaker, but its winds lay closer to the equator [*Chen et al.*, 1996, Figures 8b-8d], perhaps accounting for the stronger signal seen in Figure 2b (right).

The winds associated with these bursts are stronger than, but spatially very similar to, those associated with the seasonal mean monsoon [e.g., *Wyrtki and Meyers*, 1975, Figure 1; *Hendon and Liebmann*, 1990]. The mean monsoon winds appear to be largely an average over ISO activity. There were no cases of tropical cyclone pair formation during the IOP, though several cyclones did occur in both hemispheres during the IOP; see Table 1 of *McBride et al.* [1995].

Meridional averages that follow the seasonal shifts in ISO activity display a slow eastward propagation over the warm pool [*Madden and Julian*, 1971]. This is seen in *Nakazawa's* [1995] pictures of outgoing longwave radiation (OLR; Figure 4a) and zonal winds at 850 hPa (Figure 4b) during the IOP, averaged between the equator and 5°S. Nakazawa found that the maximum zonal winds lagged slightly behind the centers of depressed OLR. *Nakazawa* [1995] also shows 200-hPa velocity potentials, indicating that a fast atmospheric Kelvin wave continued from the mid-Pacific after the end of ISO2. More detailed study of ISO2 and ISO3 showed that while there were differences between bursts, SST anomalies rather clearly led (or were in quadrature with) the OLR by 12-13 days. Total precipitable water (TPW) led convection by 5-10 days. ISO1 does not show clearly in Figures 4a and 4b because its zonal winds mostly lay north of the equator.

Chen et al. [1996] provide higher-resolution time-longitude sections (Plate 2) of 850-hPa ECMWF winds and total high cloudiness at 1-hour intervals through the IOP, averaged over 5°N-5°S (November) and 0-10°S (December-February). At each time and longitude the color indicates the fraction of a 10° latitude band (5°N-5°S for November; 0-10°S for December, January, and February) that was

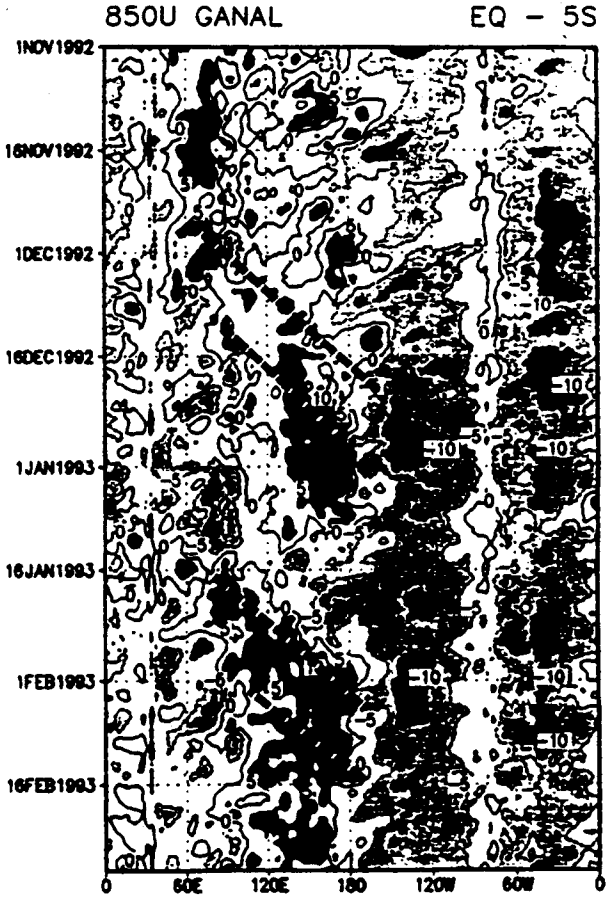

Figure 4b. Zonal winds at 850 hPa from the Japan Meteorological Agency global analysis data set, averaged between the equator and 5°S. Light shading denotes areas of < -10 m s^{-1}, while dark shading denotes areas of > 0 m s^{-1}. The slanted lines are as in Figure 4a. From *Nakazawa* [1995].

covered by cloudiness with IR temperature <208°K. The wind vectors are the daily (average of 0000 and 1200 UTC) ECMWF wind analysis at 850 hPa averaged over the same 10° latitude band. The considerable overlap of the strong westerlies and deep convection is not entirely consistent with existing theories, which place convection either in the easterlies [e.g., *Emanuel*, 1987; *Neelin et al.*, 1987] or in between easterlies and westerlies [e.g., *Lau et al.*, 1991]. However, *Nakazawa's* [1995] lag of maximum winds behind convection is also evident in Plate 2.

The presence of mesoscale westward moving regions of high cloudiness spawned by deep convection within the eastward moving envelope of the ISO activity [*Nakazawa*, 1988] is also clearly apparent from Plates 2a-2d. These features have a periodicity (at a given latitude and longitude) of about 2 days, and they are especially apparent throughout December (Plate 2b) and from late January to late February (Plates 2c and 2d).

850-hPa winds are not necessarily a good proxy for the surface winds that affect the ocean (compare also with Figure 6a). Using TOGA TAO data of 3 years (August 1991 to September 1994), *Zhang* [1996] examined intraseasonal variability at the surface in the warm pool and the phase relations between the surface intraseasonal variations and the ISO signals in the deep troposphere. The intraseasonal variability at the surface is more closely related to the intraseasonal variability in atmospheric deep convection than is the low-tropospheric zonal wind. The three ISO events during the COARE IOP showed the typical ISO-surface relationships as in the 3-year record. *Zhang* [1996] (like *Weller and Anderson* [1996], see section 4) concluded that the SST increases because of a lack of deep convection and cloud cover; in other words, the convection may not have been the result of the increase of SST. However, it was clear that the SST decreased because of the strong surface wind and convection-induced reduction in shortwave radiation.

Kiladis et al. [1994] and *Meehl et al.* [1996] examine correlations between OLR anomalies over the COARE region and anomalies of the large-scale atmospheric circulation for the 7-year period, 1986-1992. The result is something like a "composite" analysis of ISO events over this period for comparison with COARE. The analysis was confined to the November-February period only and was conducted in two frequency bands. First, the data were band-pass filtered for 30-70 day periods and, secondly, for the 5-30-day periods. The circulation patterns are very different on the two timescales. On the 30-70-day scales the 850-hPa stream function contemporaneous with OLR anomalies in the COARE region shows westerly anomalies over the entire tropical Indian Ocean and west Pacific and easterly anomalies over the east Pacific, associated with a steady equatorial surface pressure drop from the western Indian Ocean to 150°E (this gradient moves east along the equator at about 15 m s^{-1}). Off-equatorial flow shows broad low-pressure centers near 10°N and 20°S, at 850 hPa, both extending from the eastern Indian to the west Pacific Oceans.

On the 5-30-day scale, maps from *Kiladis et al.* [1994] (Figure 5) show strong northerly anomalies converging on the equator in the 140°-160°E longitude band toward the convection, emanating from a cold surge over Japan; weaker flows enter from the Coral Sea. The associated zonal pressure gradient along the equator is confined to 110°-150°E at the time of convection; westerly winds lag the pressure gradient by 2-3 days, indicative of the time needed to accelerate this zonal flow. *Meehl et al.* [1996] found that the December 1992 wind burst conformed generally with their composites, both near the equator and at higher latitudes.

Lau et al. [1996] identified an east-west pressure dipole and pointed out the importance of lateral forcing from midlatitudes, i.e., cold surges over east Asia, convection over the Indian Ocean, and SST in the central Pacific as factors controlling the westerly wind burst over the COARE domain. The interaction of the large scale flow and surface fluxes in affecting short-term SST variations was studied by *Lau and Sui* [1997]. They proposed a mechanism by which the SST variations may enhance the amplitude of the Madden-Julian Oscillation (MJO).

In earlier studies, *Lau* [1982] and *Chang and Lim* [1985] described cold surges affecting equatorial convection. These equatorial and off-equatorial events are to be considered part of a dynamical whole; that is, the off-equatorial events "cause" flows on the equator and vice versa.

2.2. Broadscale View of Winds, Surface Fluxes, and Rainfall Over IFA

Prior to TOGA COARE, atmospheric sounding data had not existed over the warm pool, except for several brief periods in the 1950s [e.g., *Nitta*, 1972]. The COARE data set provides high-resolution time series of fields such as the zonal wind (Figure 6a from *Lin and Johnson* [1996a]). The three westerly bursts seen in Figure 2b are apparent in the near-surface winds of Figure 6. ISO1 shows fairly strongly, because its generally weak winds south of the equator happened to be strongest over the IFA [*Chen et al.*, 1996, Figure 8d]. Westerly wind bursts are accompanied by easterlies aloft. The magnitude and vertical extent of the effect is surprising. Figure 6 shows 5-day means; unfiltered zonal winds show a vertical difference of nearly 60 m s^{-1} between 850 and 100 hPa around January 1. Westerlies extend to 200 hPa.

Figure 6 also shows the relationship of westerly wind bursts and the occurrence of rain, as estimated by IFA budget. (Intercomparisons of rainfall estimates from various platforms are presented in section 5.2.) Figure 6 indicates that the surface winds become westerly on about December 10, 1992, and that the rainfall increases sharply at this time. Buoy data in the IFA (not filtered to a 5-day running mean) show rain in ISO2 starting on December 9; surface westerlies started 3 days later [see *Chen et al.*, 1996, Figures 4b and 4f]. Figure 6 suggests that the westerlies were very shallow at that time. The layer of westerly wind then deepened and was strongest and deepest at the end of December and beginning of January. The peak of ISO2 winds was preceded by about 3 weeks of heavy rain. Figure 6 shows that ISO3 was preceded by a shorter, sharper rain event from January 15-21, with no coincident westerlies, either at the surface or at 850 hPa; this is also confirmed on daily timescales by *Chen et al.*, [1996, Figure 4]. ISO3 surface westerlies did not start until January 26.

The rain events of ISO2 and ISO3 were in turn preceded by a moistening of the middle troposphere; thus the 64%

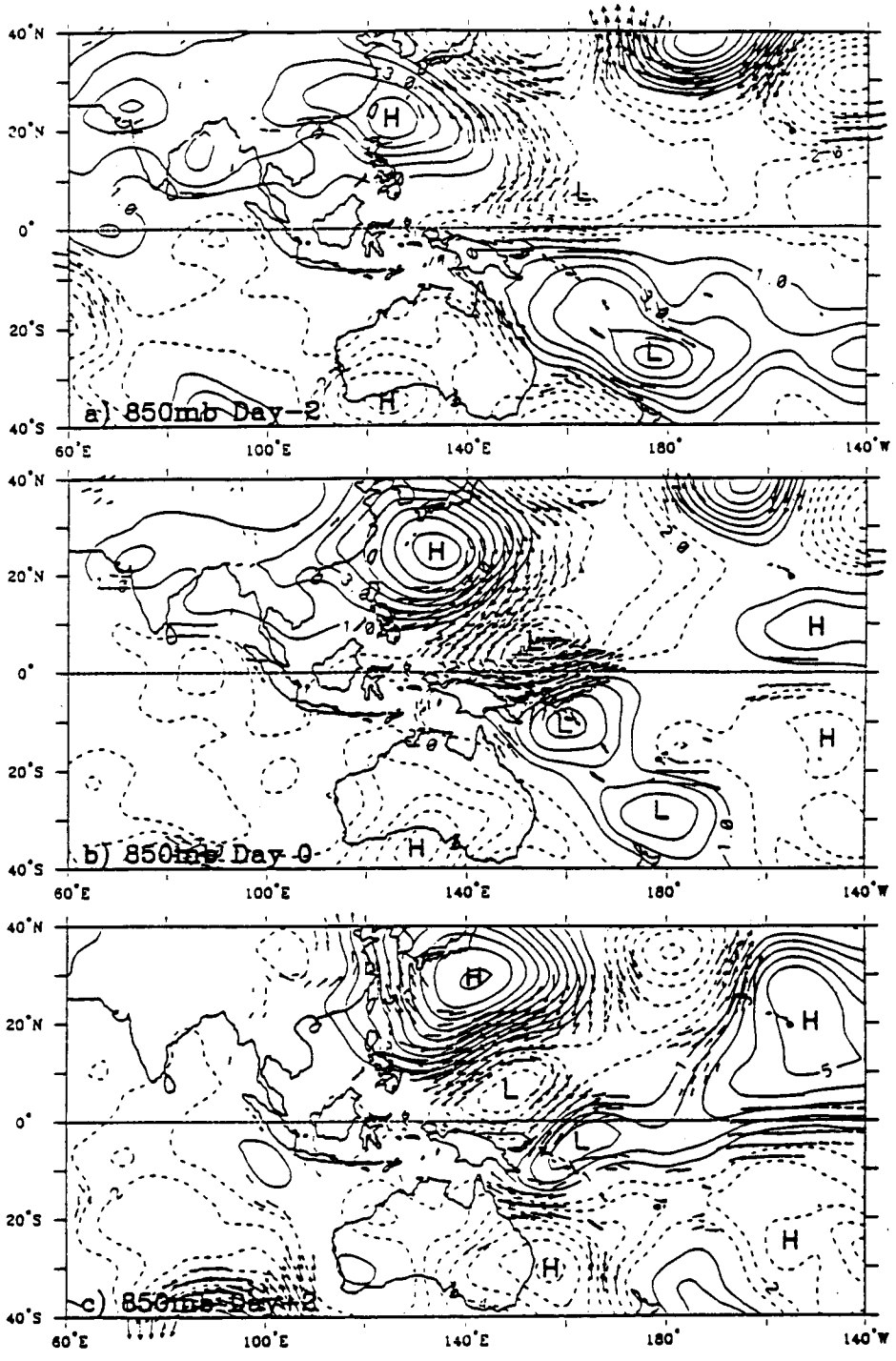

Figure 5. Composite OLR, 850-hPa stream function, and wind vector anomalies for November-March, associated with an area-averaged OLR anomaly of -1 standard deviation in the region 5°S-5°N, 150°-160°E, after band-passing all data for the period range 5-30 days. (a) Circulation leading OLR by 2 days, (b) 0 days, and (c) -2 days. From *Kiladis et al.* [1994].

humidity contour rises steadily from 850 hPa around November 11 to 550 hPa on December 10 (Figure 6c, from *Lin and Johnson* [1996a]), by which time strong, deep convection has set in. *Lin and Johnson* [1996a] show that the deep convection in mid-December and mid-January is accompanied by strong upward vertical motion over the IFA, centered near 500 hPa, with moisture convergence being the main contributor to the rain (Figure 6b).

During these periods, precipitation P exceeds evaporation E (estimated from mooring data and bulk formulae) by 3 to 5 times, implying significant large-scale transport of water vapor into the IFA (moisture storage is small). On the other hand, at other times (e.g., light-wind periods) there appears to be a near local balance between P and E.

It was well known prior to COARE that the IFA was at a local climatological minimum in rainfall. Such was the

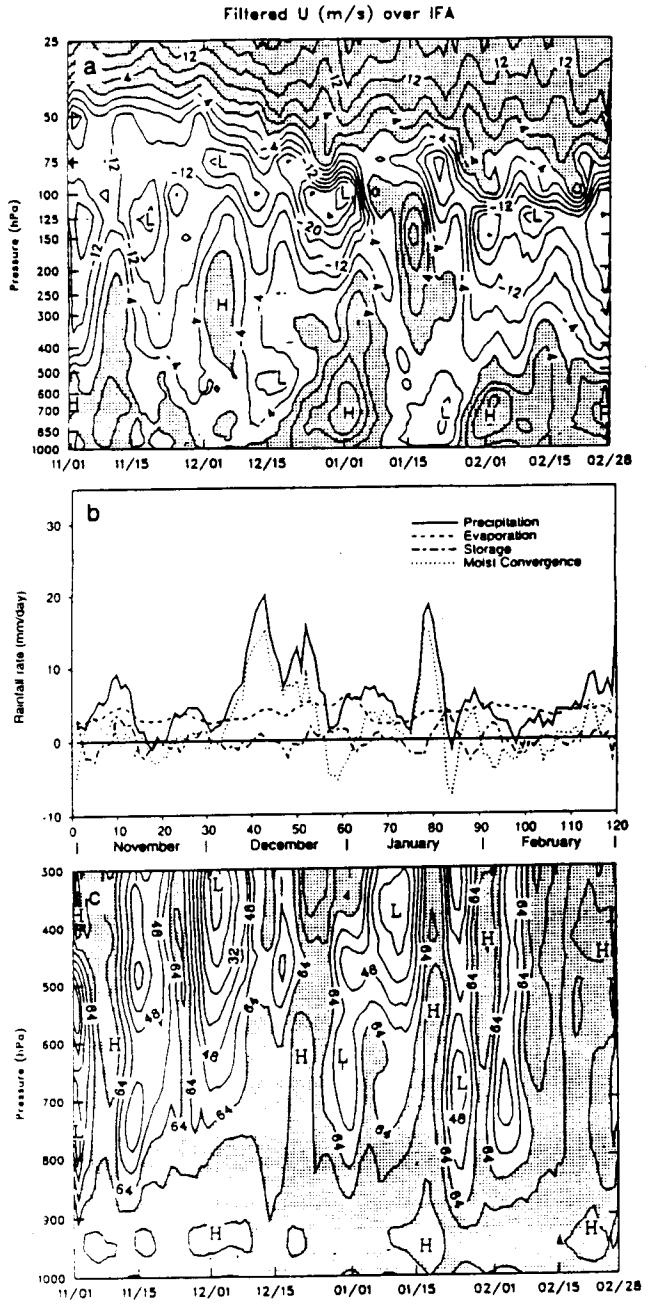

Figure 6. Five-day running (a) mean zonal wind (m s^{-1}) and (c) daily-mean relative humidity (%) averaged over the intensive flux array. Contour interval in Figure 6a, is 4 m s^{-1}; westerlies are shaded. Shaded areas in Figure 6c indicate relative humidity (RH) > 64%. From *Lin and Johnson* [1996a]. (b) The IFA-mean evaporation, moisture storage, and moisture convergence estimated from soundings around the IFA; the surface precipitation rate (solid line) is estimated as their sum. From *Lin and Johnson* [1996b].

case during the IOP, as is evident from the mean north-south cross sections of Q1 and Q2 over the IOP (Q1 and Q2 are the "apparent heat source" and "apparent moisture sink," respectively, after *Yanai et al.* [1973]) averaged between 150° and 160°E (Figure 7, from *Lin and Johnson* [1996b]). The vertical integrals of these quantities are proportional to surface rainfall; hence the heaviest rainfall can be seen in the Intertropical Convergence Zones (ITCZs) north and south of the equator. The vertical distributions of Q1 and Q2 in the ITCZ bands very closely resemble those determined in previous studies of the western Pacific [*Reed and Recker*, 1971; *Nitta*, 1972; *Yanai et al.*, 1973] and in the COARE-domain results of *Ding and Sumi* [1995]. However, near the equator over the IFA the vertical distributions are quite different. Particularly noteworthy are the negative values of Q2 in the lowest 2 km in the vicinity of the equator. These represent a moistening effect presumably associated with vigorous, shallow cumulus that transport moisture upward from the surface during the westerly wind bursts [*Lin and Johnson* 1996b].

2.3. Convection: Inhibiting Factors and Effects on Boundary Layer

The special feature of the warm pool region is that it is so weakly stratified that convection can penetrate, at times, to the stratosphere. Nevertheless, even within the warm

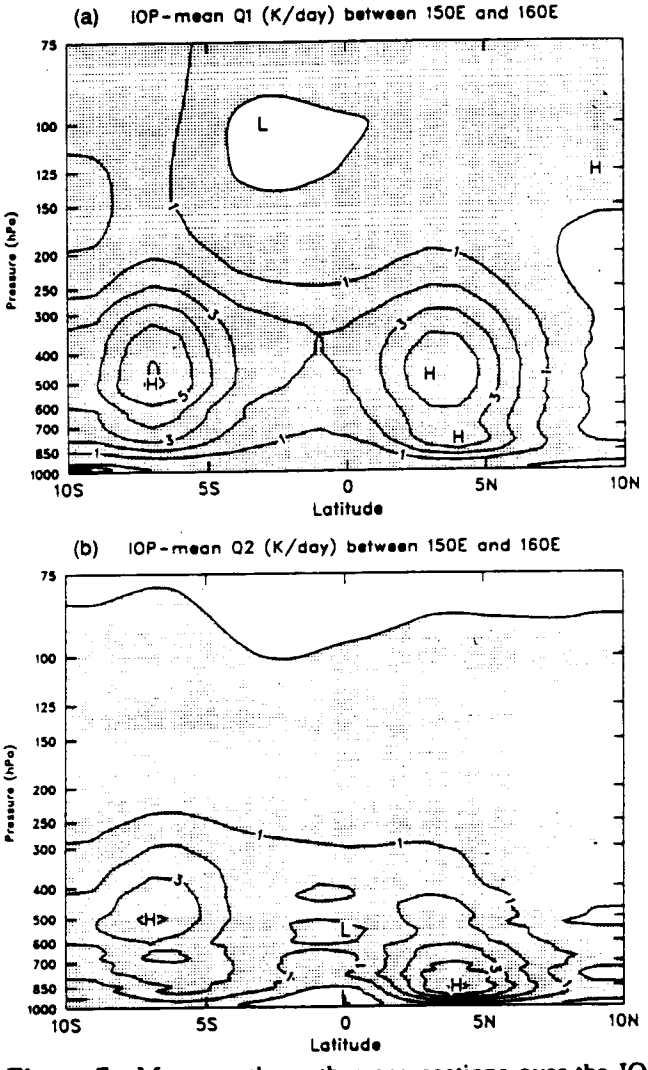

Figure 7. Mean north-south cross sections over the IOP of (a) Q1 and (b) Q2 (°K d^{-1}) between 150° and 160°E. Contour intervals are ±1°K d^{-1}, and areas with positive values are shaded. From *Lin and Johnson* [1996b].

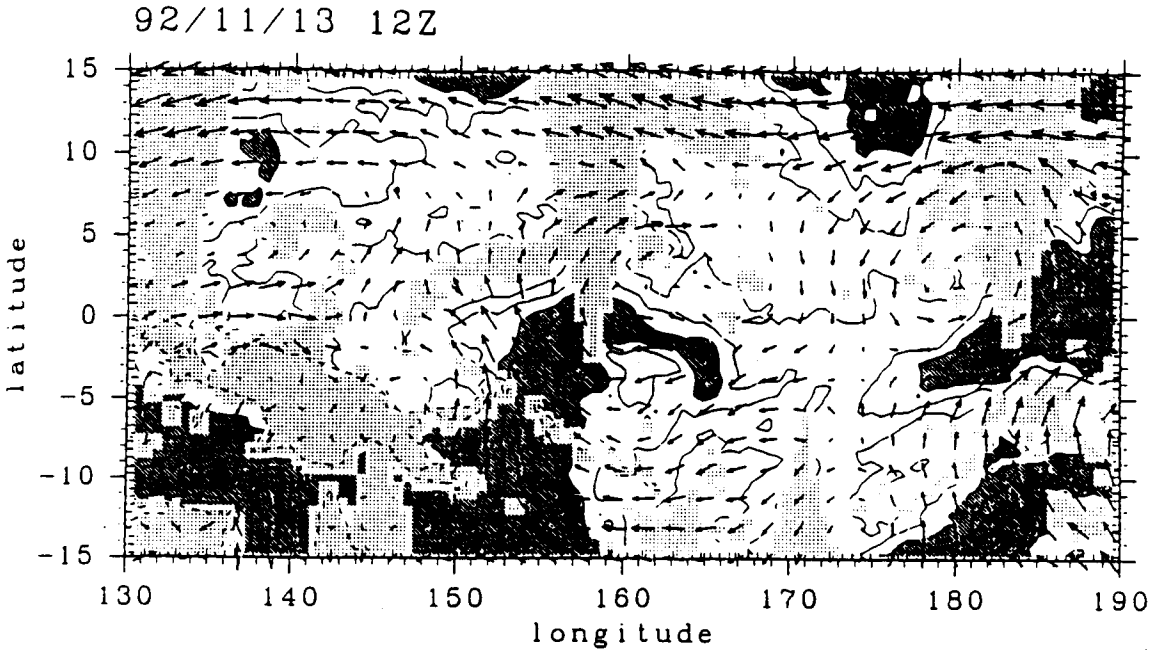

Figure 8. Horizontal distribution of special sensor microwave/imager (SSM/I) precipitable water and 850-hPa horizontal wind on November 13, 1992. Areas of < 40 kg m^{-2} are shaded. Areas of missing observations are denoted by stippling. The unit vectors correspond to 20 m s^{-1}. From *Numaguti et al.*, [1995].

pool it is evident from Figure 6 that deep convection events (times when moist convergence dominates the rainfall rate) only occur for a small fraction of the time. Most of the time there is enough stratification to prevent diurnal rain showers, which are ubiquitous throughout the warm pool region even in calm conditions [Rickenbach 1995], from penetrating beyond the midtroposphere.

Two major causes of this stratification have been identified. The first is the advection of drier air from subtropical latitudes. *Numaguti* [1995] documents vigorous meridional wind fluctuations on the 4-20 day timescale. These appear to be responsible for advecting dry air from the subtropics into the COARE region, near the 700-800 hPa level; the advection carries air masses some 2000 km. They are visible in SSM/I imagery of the atmospheric total water vapor content. Figure 8, from *Numaguti et al.* [1995], shows a tongue of dry air extending from near 15°S to the equator near 155°E; the 850-hPa winds clearly indicate its southern hemisphere origin. This advection is clearly responsible for the dry air above 850 hPa seen in Figure 6c, around November 13. Two other dry air intrusions of this kind (both from the northern hemisphere) were seen in the intervals November 11-27, 1992, and February 5-14, 1993 [see also *Yoneyama and Fujitani*, 1995]. Dry intrusions appear to have a significant impact in suppressing convection in the COARE region in two ways. First, dry-air entrainment can reduce parcel buoyancy [*Mapes and Zuidema*, 1995; *Lucas et al.*, 1996]. Secondly, it has been shown by Mapes and Zuidema that radiation can act upon dry tongues to create stable layers, which can then directly inhibit convective cloud growth.

Two prominent stable layers are frequently found, which do not require the advection of different air masses from elsewhere [*Johnson et al.*, 1996]. One, near 550 hPa or the 0°C level, is largely due to the melting of ice within precipitation systems, though other effects such as radiation acting on intrusions of dry air may sometimes be responsible. The second, near 800 hPa, is associated with the trade wind inversion [see also *Schubert et al.*, 1995]. It is well known that the trade wind inversion restricts cloud growth [e.g., *Riehl*, 1954], but the 0°C stable layers may also impact cloud fields through inhibiting growth or enhancing detrainment and producing cloud layers, as suggested by the humidity data of *Mapes and Zuidema* [1995, Figure 18]. There is some evidence of effects of 0°C stable layers on tropical cloud populations and structure. For example, *Rickenbach* [1995] reports a bimodal population of precipitating clouds at several times during the IOP, with one peak of radar echo tops near the tropopause and another in the midtroposphere. Also, *Uyeda et al.* [1995] and *Hildebrand et al.* [1996] report bimodal distributions of radar reflectivity and vertical velocity in convective cores over the warm pool with minima near the 0°C level. More recent analyses [*Rickenbach and Rutledge*, 1998] actually reflect a trimodal distribution of precipitating tropical convection, the third peak in echo tops occurring near 2-3 km. Apparently, some of the shallow cumulus associated with the trade-like stable layer are actually precipitating, owing to an efficient collision-coalescence process over the warm pool.

Johnson et al. [1996] found that the marine atmospheric boundary layer (MABL) (consisting of the mixed layer and shallow cumulus layer above) over the warm pool is very similar to the MABL in the trade wind regime in several respects. In addition to the commonly occurring stable layers near 800 hPa, the average mixed layer depth (500-600 m) is very close to that observed in the trades. The curious fact that the MABL is not especially deep in the warm pool

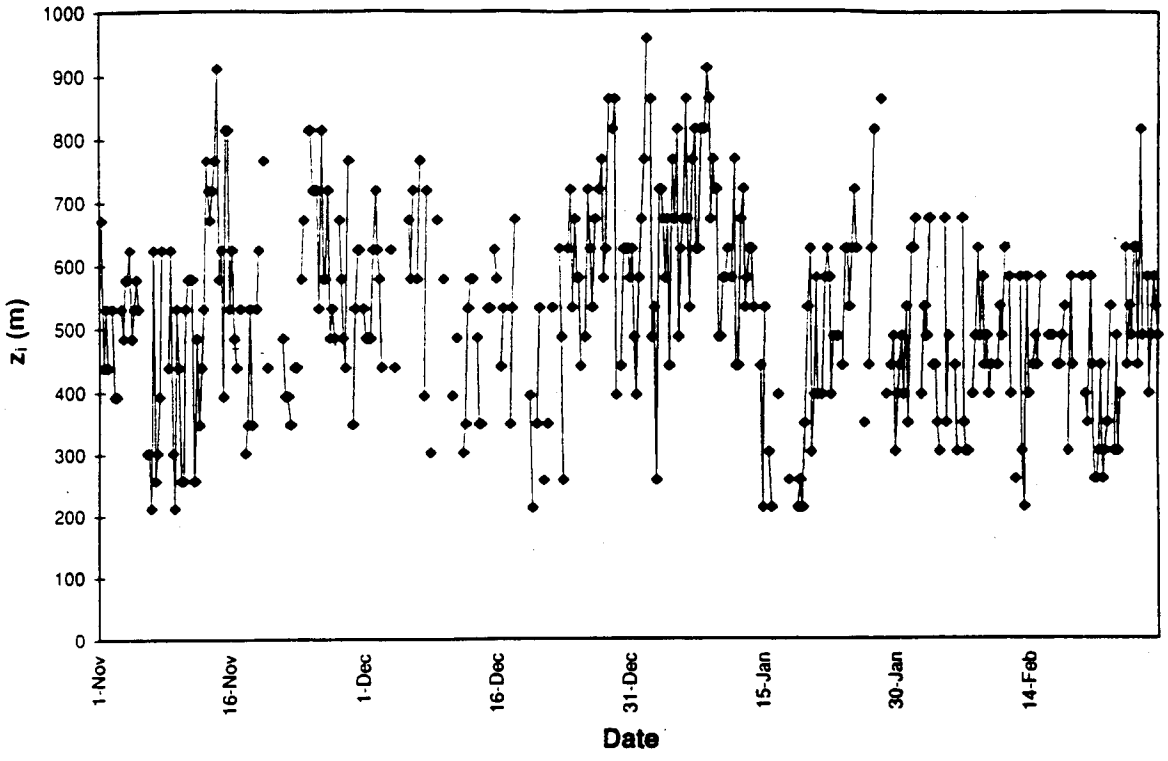

Figure 9. Time series of mixed layer depth (meters) at Kapingamarangi. Line segments connect consecutive 6-hour values, when observed. Mixed layer tops were determined subjectively by examining individual profiles of potential temperature and specific humidity and locating sharp increases in stability and coincident, sharp drying atop a well-mixed layer [*Johnson and Dickey*, 1996]. Seventy-four percent of the soundings exhibited a mixed layer structure.

but is, in fact, similar to the rest of the trade wind zone, is believed to be due to the fact that downwelling of dry air occurs over a wide range of conditions (e.g., westerly wind bursts, light winds, or in the environment of surrounding deep convective cores), and is just as vigorous over the warm pool (at times even more so) as in the rest of the Tropics. Although the mean mixed layer depth is typically between 500 and 600 m, there is considerable variability on both long and short timescales, as can be seen by the time series of MABL mixed layer depth at Kapingamarangi (Figure 9 from *Johnson and Dickey* [1996]). The mixed layer was shallowest (and frequently disrupted) during the mid-December and mid-January heavy rain periods as a result of precipitation downdrafts and recovering boundary layer wakes [*Parsons et al.* 1994; *Young et al.*, 1995]. The latter studies have shown that the recovery of the mixed layer following deep convection, where surface temperature drops of up to 4°-5°C are observed, can take as long as ~10 hours with wakes spreading over areas as large as several hundred kilometers on a side, implying a significant impact on the air-sea exchanges during disturbed conditions. During the westerly wind bursts of ISO2 and ISO3 and in late-November/early-December and early-January light-wind periods, the mixed layer was deepest. This behavior is a result of the lighter amounts of rainfall during these periods (Figure 6b). At other times, when rainfall was greater, the boundary layer was modified extensively by cool downdrafts. When mixed layers existed, they were often shallow, as is characteristic of recovering convective wakes [e.g., *Parsons et al.* 1994; *Young et al.*, 1995]. Note also the considerable high-frequency variability in Figure 9, likely due to intermittent convection and diurnal effects. The remarkable heterogeneity of the MABL is seen in the very long, 20-70 m aircraft legs of *Williams et al.* [1996].

An important aspect of the MABL is its stability to small disturbances, which is measured by convective available potential energy (CAPE) [*Moncrieff and Green*, 1972]. *Petersen et al.* [1996] suggest that CAPE was correlated with the mean wet-bulb temperature θ_w of the MABL and related to lightning frequency. However, *Lucas and Zipser* [1996] identify critical corrections to the sounding data that could call such results into question.

3. Warm Pool Convection

Clouds are a key link in the interaction of ocean and atmosphere in the warm pool region. One of the objectives of COARE research was to make it possible, by means of special observations, to document the exact behavior of the convection on a higher time and space resolution than possible with standard satellite and synoptic data. Such description of the convective process is a fundamental prerequisite to building parametric representations of convection for use in large-scale models lacking detailed input data on the convective structures. The purpose of this section is to summarize what we have learned so far regarding the structure of the convection in COARE and, insofar as is possible at this early stage of the research,

relate the observed temporal and spatial structures to the large-scale behavior described in Section 2.

3.1. Ship and Aircraft Sampling

Figure 10a is a histogram of the infrared temperature values detected over the warm pool region during the entire period of COARE. The *y* axis is expressed as an area, but it is directly proportional to the number of pixels in each 5° interval of the temperature range 187°-307°K. The greatest number of pixels registered values of ~295°K. The number of occurrences of lower-infrared values drops off at first rapidly then gradually with decreasing temperature. Fig. 10b is a histogram of the subset of infrared values observed over

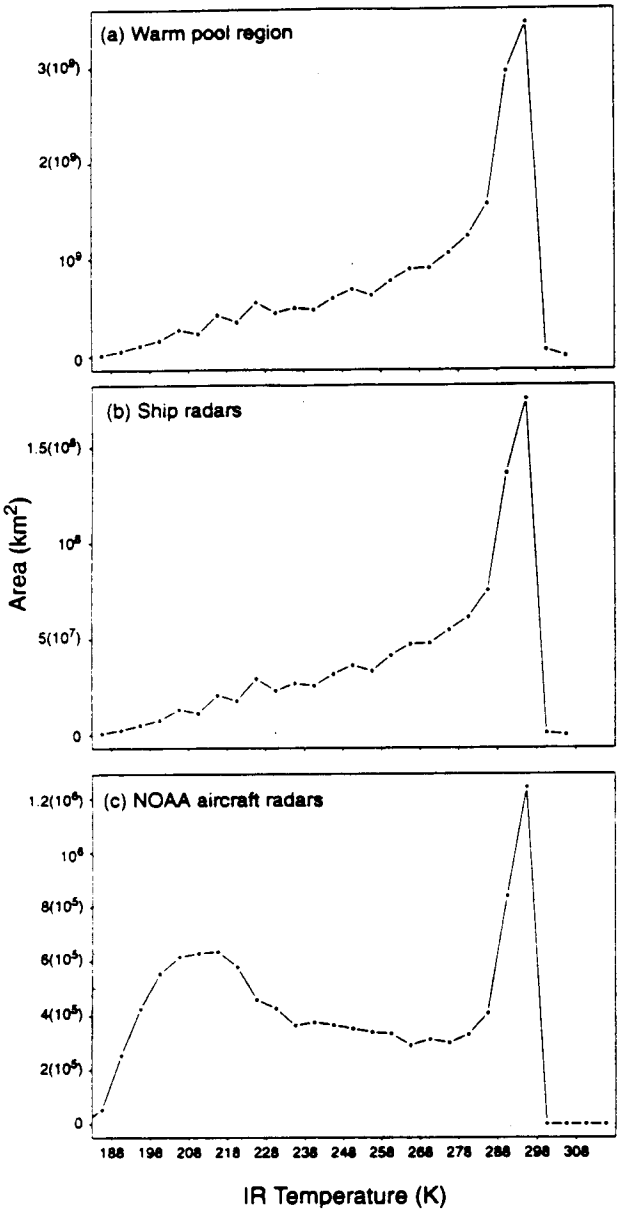

Figure 10. Histograms of the GMS infrared temperature for (a) the warm pool region, (b) the TOGA COARE shipborne radar region, and (c) the sampling by NOAA WP-3D aircraft during TOGA COARE. Histogram bin size is 5°K. From *Yuter and Houze* [1998].

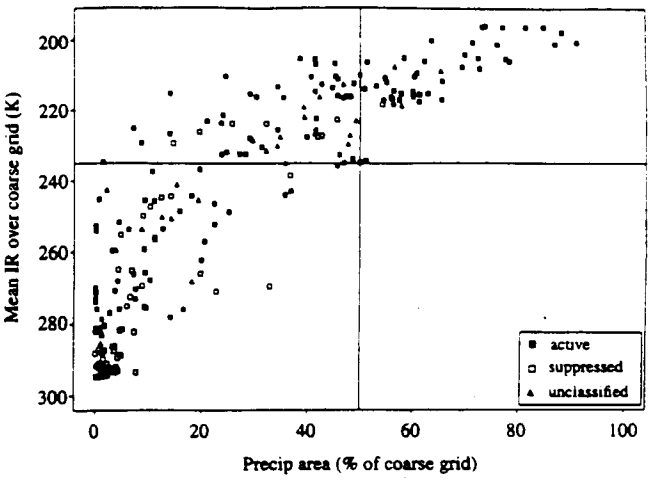

Figure 11. Mean infrared temperature versus the size of the area covered by precipitation in a region ~240 km diameter centered on the aircraft's location for all the NOAA WP-3D aircraft missions in TOGA COARE. Fom *Yuter and Houze* [1998].

regions surveyed by the ship radars. This distribution is very close to the climatology in Figure 10a. This result is reasonable since the ships were stationary and their on-station times were set long before COARE. They thus obtained an unbiased sample of the cloud population. However, the relative rarity of the deeper (colder) clouds means that the ship radars probably did not obtain a significantly large sample of the deeper convection. Figure 10c shows the subset of infrared temperature values surveyed by the airborne radars. It has the peak near 295°K, similar to that in the other two histograms. However, it has a second peak at very low infrared temperatures. Thus the population of clouds sampled by aircraft differed from climatology in an important way. The aircraft radar program, by design, aimed to spend equal numbers of flight hours in different parts of the cloud population. The aircraft radars thus oversampled the deep (cold-topped) convection relative to climatology and thus obtained a large sample of deep convection.

3.2. Joint Variability of Cloud and Precipitation

The advantage gained by the radar measurements in COARE (both ship and aircraft) is that they tell us exactly where the precipitation is located within the cloud regions identified in infrared satellite imagery. This information is not routinely available, and it is important to determine as much as we can about the joint variation of the cloud (satellite-observed) and precipitation (radar-observed) fields. Plate 3 shows three examples of radar data (two from aircraft, one from ship) overlaid on the satellite data. These cases illustrate how large the contiguous rain areas can sometimes be; essentially all the cold cloud top seems to overlie rain in these (extreme) cases. *Yuter and Houze* [1998] have examined every data sample in which the COARE aircraft radars and the GMS satellite obtained data simultaneously. They determined the mean infrared temperature and the size of the area covered by precipitation

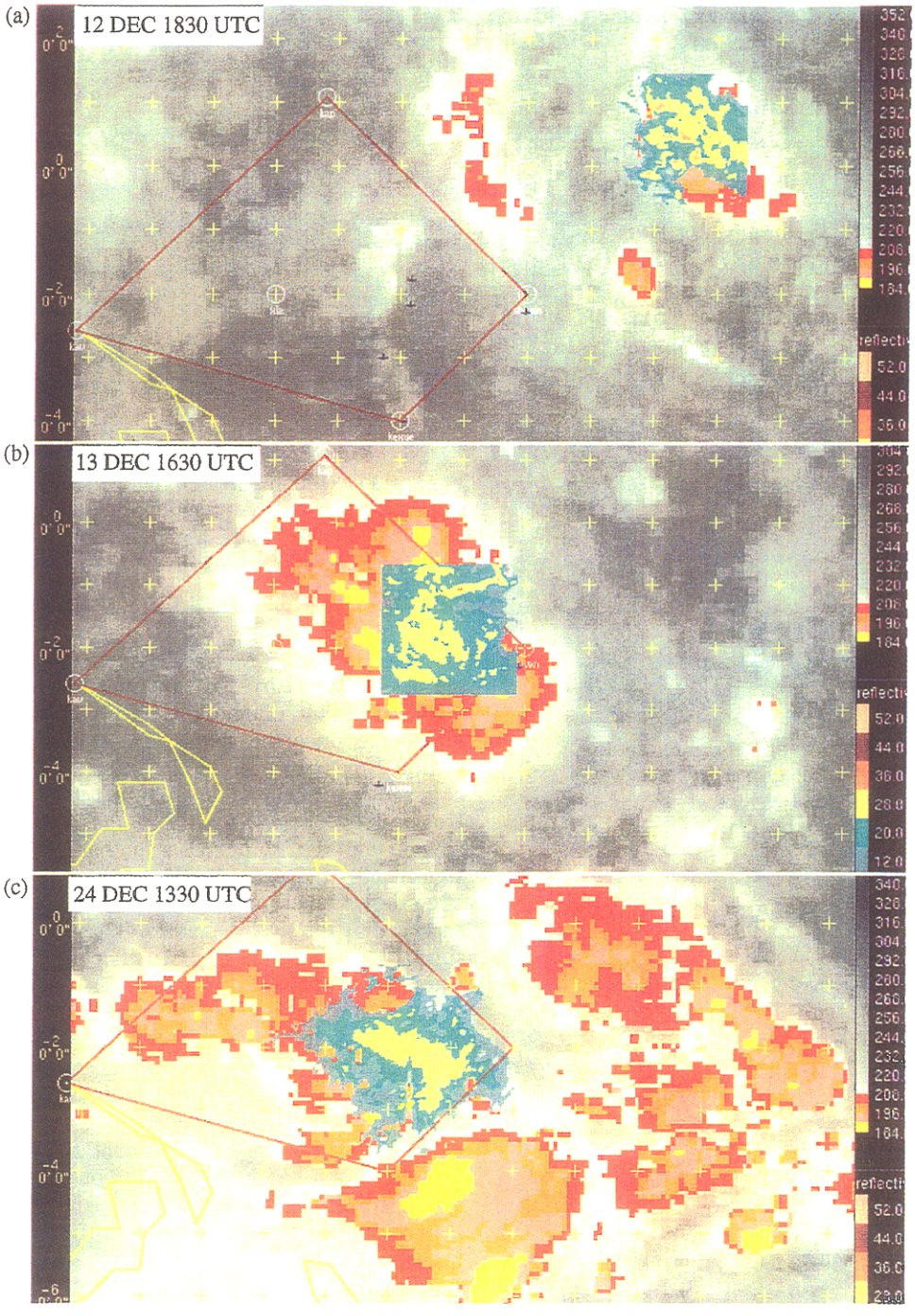

Plate 3. Three examples of NOAA WP-3D N43RF aircraft lower fuselage radar image overlaid on GMS infrared images at (a) 1830 UTC December 12, 1992, (b) 1630 UTC, December 13, 1992, and (c) MIT radar image from R/V *Vickers* overlaid with GMS infrared image at 1330 UTC, December 24, 1992. Both radars are C band (5-cm wavelength); the *Vickers* radar range is 145 km. The color scales indicate radar reflectivity (dBZ) and infrared temperatures (°K). The IFA is outlined. Note that in the GMS image, darker grayscale colors indicate warmer temperatures. Adapted from *Chen et al.* [1996].

in a region ~240 km in diameter centered on the aircraft's location in all of these cases (Figure 11). The most noticeable feature of the relationship between the mean infrared temperature and the size of the corresponding rain area is the scatter. The cloud (satellite) and precipitation (radar) variables have a correlation of only 0.05. (The correlation of percent high cloudiness and rain area size is even poorer.) Yet there is information in this graph. The lower right quadrant of Figure 11 is empty; large rain areas (>50% of the 240 km scale region) do not occur under cloud shields warmer than 235°K, these combinations of variables are evidently physically infeasible. We also note from

Figure 11 that when the mean infrared temperature is less than 235°K, the rain area can be any size (0-100% of the 240-km-scale region); that is, temperature < 235°K by no means guarantees the presence of a big precipitation area. However, a somewhat more restrictive threshold (<220°K) nearly assures a large rain area (>50% of the 240-km-scale region). When the mean infrared temperature over the 240-km-scale region is > 235°K, the rain area is likely to cover < 30% of the 240-km-scale region.

Rickenbach [1995] has analyzed the data from the MIT 5-cm wavelength precipitation radar aboard the R/V *Vickers*. He subjectively classified the horizontal morphology of the echo patterns into four groups, which he calls [*Rickenbach*, 1995, Table 2] (1) "isolated, submesoscale unorganized echoes," (2) "submesoscale contiguous lines" (<100 km in length), (3) "mesoscale, contiguous or broken lines" (100 km in length), and (4) "mesoscale, contiguous echo >100 km in longest dimension" (no linear organization at any time). Types 3 and 4, the larger mesoscale features, accounted for the majority of the precipitation observed by the *Vickers* radar. Future work should help relate these mesoscale and submesoscale structure categories to the cloud shield structures seen in satellite data. Also, it will be useful to develop classifications focused on more dynamically relevant features such as mode of line propagation and orientation relative to vertical wind shear, or to develop more objective methods of characterizing the precipitation areas [*Yuter and Houze*, 1998].

3.3. Remote Sensing Tests

The joint variability of infrared cloud top temperature and radar-observed precipitation, discussed in Section 3.2, will be useful in extending the results of COARE by relating them to a routine type of satellite observation. Later this year, the TRMM satellite will begin to orbit the tropics with passive microwave sensors, a precipitation radar, and other instruments aboard. One of the COARE objectives was to use TRMM prototype instruments aboard aircraft in the presence of other COARE sensors to test the performance of the TRMM remote sensors. Analysis of high-resolution (3 km) NASA ER-2 "advanced microwave precipitation radiometer" (AMPR) data [*McGaughey et. al.*, 1996] showed a poor correlation between increasing 10.7-GHz brightness temperatures and decreasing 85.5-GHz brightness temperatures (two of the channels to be used on the TRMM satellite). The poor correlation was associated with increasing integrated rainwater and ice water contents of the atmospheric column respectively [*Adler et al.*, 1991; *Smith et al.*, 1994]. McGaughey et al. interpreted the lack of correlation between rainwater emission and ice-scattering signatures to be related to the variation of ice-scattering within stratiform regions with similar surface rainfall rates, the presence of shallow (warm) rain, and the tilt with height of strong convective lines. Comparison of AMPR data from two stratiform regions differed by 30°K in average 85.5-GHz brightness temperature and highlighted how the 85.5-GHz ice-scattering signature in particular is very sensitive to the life cycle stage of mesoscale convective systems (MCSs) [*McGaughey and Zipser*, 1996]. Further discussion of microphysical properties is found in section 3.6.

3.4. Divergence in Relation to Mesoscale Precipitating Cloud Systems

Mapes and Houze [1995] analyzed the airborne Doppler radar data obtained in all the larger mesoscale cloud systems sampled by aircraft in COARE. Their analysis derives vertical profiles of mass divergence from the radar data. The mass divergence is, in turn, proportional to the vertical gradient of net heating by the cloud system.

In large regions of rain, like those shown by the data in Plate 3, the radar data show that the precipitation consists of convective cells and regions of lighter and more uniform stratiform precipitation. *Mapes and Houze* [1995] found that in the convective subregions of the precipitation areas the mass divergence profiles indicate removal of mass from the lower troposphere and deposition of mass in the upper troposphere (e.g., Figure 12a). *Yuter and Houze* [1998] found that most of the area covered by precipitation in large rain areas was stratiform. *Mapes and Houze* [1995] found that in the stratiform precipitation regions the divergence profiles show removal of mass from the midtroposphere (especially at the height of the melting layer) and deposition of mass at lower and higher levels (Figure 12b). They obtained a net mass divergence profile by combining all the aircraft measured divergence profiles (Figure 12c). The sharp peak of convergence at the 550-hPa level (~5.1 km mean sea level MSL) shows that the influence of melting cooling, which appears strongly in stratiform regions, is a dominant effect in the overall divergence profile. *Mapes and Houze* [1995] found this profile to be consistent with the sounding data over the IFA, and they used the divergence profile as input to a set of linearized, spectrally decomposed primitive equations. The resulting flow is dominated by two modes: one corresponding to the convective region divergence profile and the other to the stratiform region profile [*Mapes and Houze*, 1995]. This result addresses a major goal of COARE, to understand the nature of the feedback of the convection to the large-scale flow. This work shows that the response to the mesoscale cloud system divergence profile, i.e., to the vertical gradient of heating associated with the convection, is in buoyancy bores, a rapidly moving one corresponding to the convective region profile of divergence and a slower one corresponding to the stratiform region profile of divergence. One implication of this result is "compensating upward motion" at low levels in the vicinity of the convective system. This compensating upward motion makes the vicinity of older large mesoscale cloud systems a likely region for the triggering of newer convection. The deep convection is thus gregarious [*Mapes*, 1993], and this gregarious nature may help account for superclustering of the large convective systems in the active regions of the ISO and 2-day waves.

3.5. Updrafts, Downdrafts, and Other Aspects of Convective Circulations

To achieve the COARE objectives of understanding the role of atmospheric convection in redistributing heat and momentum in the ocean-atmosphere system of the warm pool region, a large effort went toward documenting the properties of the air motions within and induced by the clouds. Buoyancy forces drive the air motions. The updrafts

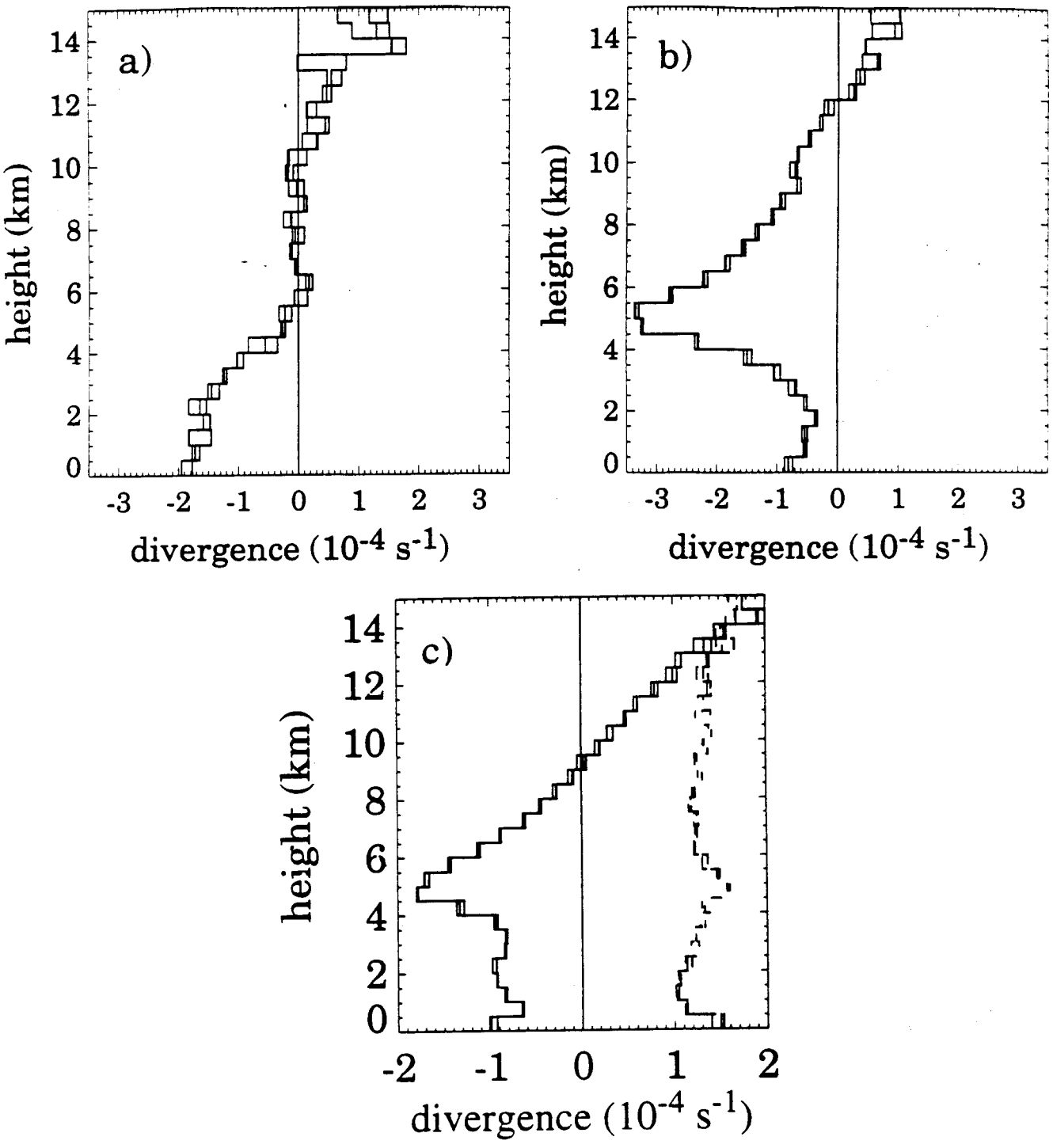

Figure 12. Mean divergence of wind measured by airborne Doppler radar over a 30-km-diameter circle surrounding the aircraft (a) for 13 samples obtained on December 15, 1992, in primarily convective precipitation; (b) for 15 samples obtained on November 6, 1992, in primarily stratiform precipitation; and (c) for all 143 samples obtained in TOGA COARE. From *Mapes and Houze* [1995].

and downdrafts are the basic units of the convective circulations. They have characteristic thermodynamics, microphysics, and horizontal as well as vertical motion. Analyses of these properties are essential to determining the role of the convection in the exchanges of heat, momentum, fresh water, and water vapor between the atmosphere and ocean and between the atmospheric boundary layer and the free atmosphere. Doppler radars on two ships, four aircraft, and on Manus Island documented the updrafts, downdrafts, and related circulations of convection in COARE, and several investigators are intensively using the Doppler radar data to study the

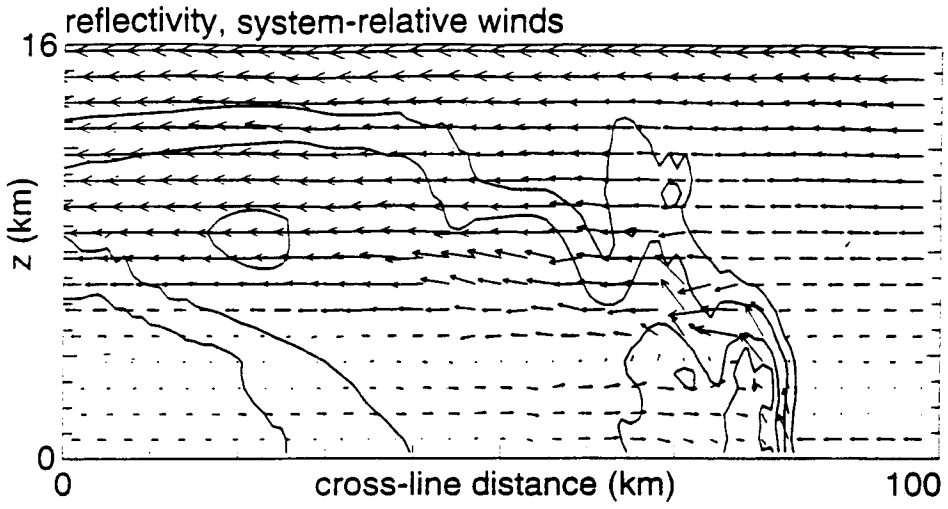

Figure 13. Reflectivity in contours of 10, 25, 35, and 38 dBZ with system-relative wind vectors for a 40-km along-line average at 3 hours of a numerical simulation of the February 22, 1993 TOGA COARE squall line reported by *Trier et al.* [1996].

convective air motions. These studies do not simply document the vertical velocities of the clouds but rather document the entire circulation, thermodynamics, and microphysics of updraft and downdraft circulations. The in-cloud horizontal momentum field is being examined in detail, as are the precipitation reaching the surface, the processes by which the precipitation is produced, and the profound alteration of the atmospheric boundary layer by the downdraft air reaching the ocean surface. Although some of these studies have been published, either in final or preliminary form, and several of these studies are nearing completion, many are as yet not ready for publication, and it is impossible for us to review them comprehensively at this time. We will point out a few of the emerging facts, but the majority of this work and its interpretation in the larger TOGA COARE context must await future reviews.

Trier et al. [1994] simulated the convection observed by TOGA COARE aircraft on February 22, 1993 (Figure 13). This convective system had a leading line of convection trailed by stratiform precipitation. This type of system occurs in the presence of strong low-level shear and has been observed previously over tropical oceans [e.g., *Zipser*, 1969, 1977, *Houze*, 1977]. The model simulation predicts a strongly sloping updraft overlying a sloping downdraft flowing into a cold pool spreading over the ocean surface. *Roux and Bousquet* [1995] and *Jorgensen et al.* [1995] have confirmed the updraft structure of this storm from quadruple Doppler radar data. *Hildebrand et al.* [1996] analyzed the case of February 9, 1993, which was more typical of COARE convection in that it did not have the organization of a continuously propagating squall line with trailing stratiform precipitation. However, it had sloping updrafts and downdrafts. Figure 14 shows an example of a sloping downdraft flowing into the cold pool below a sloping updraft. The multiple-Doppler analyses often do not show the downdraft fully, probably because of difficulties in sampling the lowest altitudes by airborne radar and because of smoothing that occurs in the multiple-Doppler radar data processing. The high- resolution raw single-Doppler velocity data (velocity component of target along the radar

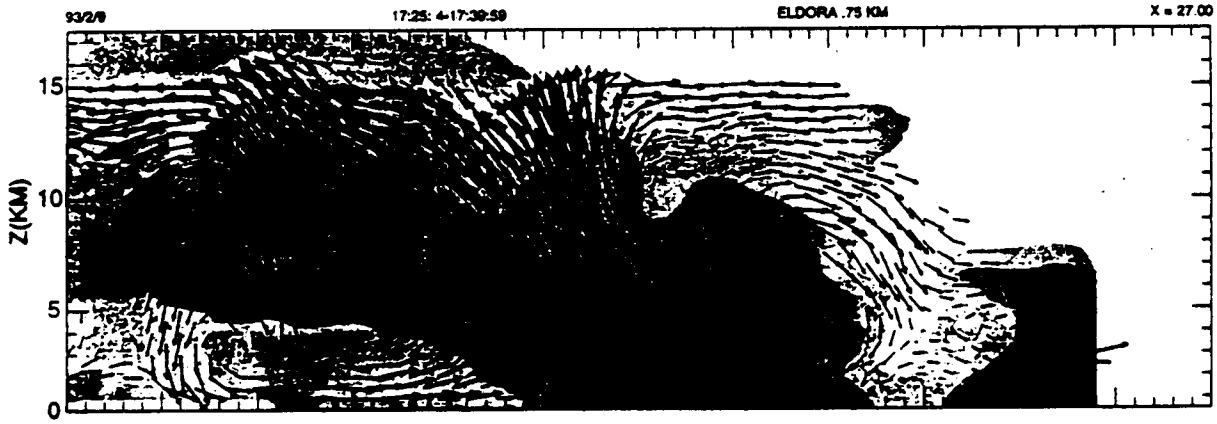

Figure 14. Storm relative airflow derived from dual-Doppler airborne radar observations in the cloud system of 1740 UT February 9, 1993, sampled by NCAR Electra aircraft. From *Hildebrand et al.* [1996].

beam), however, repeatedly show the signature of the cold pool and updraft circulation in fine detail. Making use of the raw single-Doppler tail radar data from the two P-3 aircraft, *Kingsmill and Houze* [1995]; (D. E. Kingsmill, and R. A. Houze, Jr., Inflow and outflow characteristics of convection in TOGA COARE. Part I: Velocity structures, submitted to *Quarterly Journal of the Royal Meteorological Society*, 1998a; referred to below as KH1998a) found that the sloping updraft/downdraft structure and well-defined cold pools were ubiquitous in the TOGA COARE aircraft data.

The convective systems in Figures 13 and 14 occurred in the highly sheared flow at the end of the WWB of late February, and the updrafts sloped upshear. In weaker shear, such as what prevailed in mid-December over the COARE domain, sloping drafts also occurred, but less systematically. However, other aspects of the cloud systems were different. For example, the systems in Figures 13 and 14 have somewhat similar sloping updrafts and downdrafts; however, one of them (Figure 13) was long-lived and moved in a continuous fashion, while the other (Figure 14) had multiple interacting convective bands with evidence of systematic decay and regeneration. Because of its relative simplicity of structure the February 22 case in Figure 13 could be overemphasized in studies of COARE convection. Its place in the overall spectrum of COARE convection awaits the completion of studies of more complex cases and of statistical studies.

The large convective systems in TOGA COARE had large regions of stratiform precipitation adjacent to the deep convective cells. Sometimes the convective cells were in a leading line followed by the stratiform precipitation (Figure 13). This type of organization appears to become long-lasting and to move more or less continuously, maintaining its structure while passing over a large region of ocean. Most of the large convective systems, however, exhibited a more sporadic movement as new areas of convective growth sprang up while others died and turned stratiform. The stratiform regions of these more erratically behaving systems could be as large or larger than the continuously propagating leading-line/trailing-stratiform systems.

In leading-line/trailing-stratiform cases the airborne Doppler radar data show a midlevel "rear inflow" [*Smull and Houze*, 1987]. The midlevel rear inflow plays an important role in both heat and momentum transports by the convection [*LeMone and Moncrieff*, 1994]. *Kingsmill and Houze* [1995] report that midlevel inflows were present in both the continuously propagating leading-line/trailing-stratiform systems and the more discretely propagating, less steady systems. These inflows typically began at the bases of anvil echoes on the periphery of precipitation regions, generally above the melting level. They extended horizontally for great distances (sometimes ~100 km) across the stratiform precipitation area at about the height of the 0°C level. Some of the midlevel inflows extend downward into the cold pool of the convective regions of the systems while others remained elevated. The inflow strengths were as high as 15-20 m s^{-1}. The midlevel inflows enter convective systems from various directions, and Kingsmill and Houze suggest that the concept of "rear" inflow is not always appropriate. Figure 15 shows a typical example of a midlevel inflow in COARE. A shallow layer of easterly momentum begins on the eastern (right-hand) edge of the

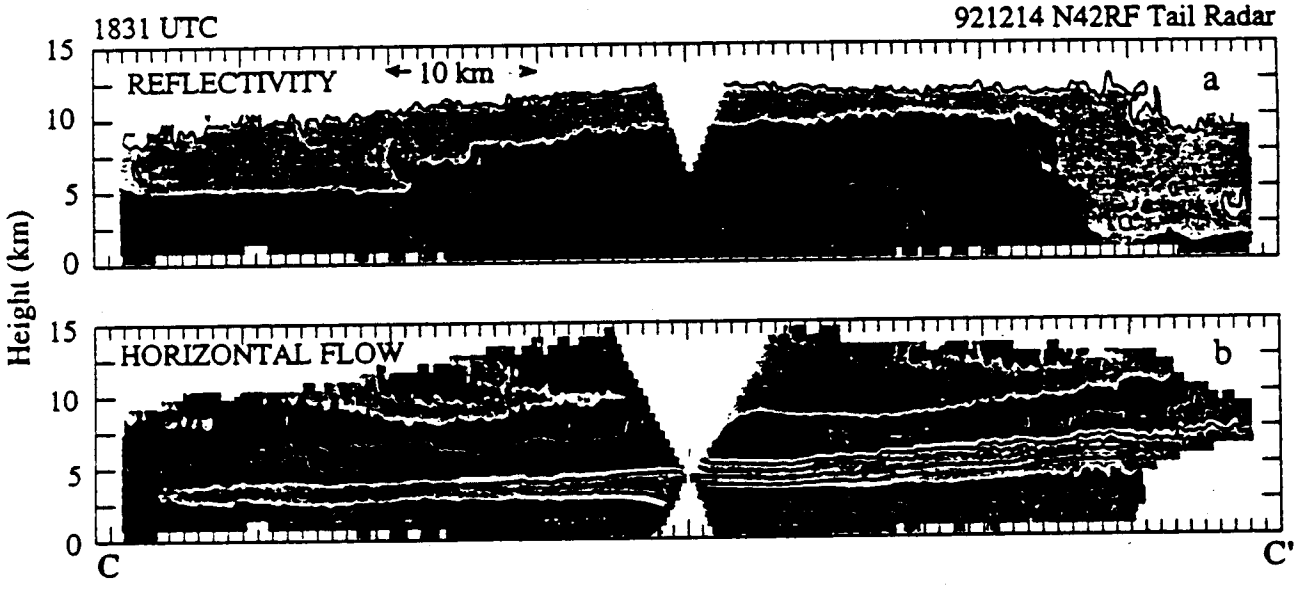

Figure 15. (a) Reflectivity and (b) horizontal wind (Earth relative in the plane of the cross section) determined from individual scans of the NOAA N42RF WP-3D aircraft tail radar for 1831 UTC on December 14, 1992. Reflectivity is contoured at 5, 15, 25, and 35 dBZ. Positive (left to right) horizontal wind is shown in black with white contours; negative (right to left) horizontal wind is shown in gray with black contours at 4 m s^{-1} intervals. The horizontal wind was calculated by dividing the measured Doppler radial velocity by the cosine of the angle measured clockwise from the center of the antenna beam and a horizontal axis extending rightward from the aircraft's position in the cross section (the point of the V at about the 5-km level midway between C and C'). From *Kingsmill and Houze* [1995].

precipitation region at ~6 km altitude and, proceeding westward, gradually descends through the bright band to ~3 km altitude.

Several studies are examining the updraft and downdraft structures in some of the less-organized large, medium, and small convective systems in TOGA COARE [*Smull et al.*, 1995, *Protat et al.*, 1995, *Lewis et al.*, 1995, *Hildebrand and Lee*, 1994, Hu and Barnes 1994; *Hildebrand et al.*, 1996]. It is hard to generalize on these very preliminary results because of the complexity of the patterns and structures. These efforts are nonetheless important, as these complex structures are the norm over the warm pool.

One of the objectives of COARE investigators was to determine the role of convection in the large-scale momentum balance and surface momentum fluxes. The above described studies of updraft and downdraft structures are laying the groundwork for quantitative studies of the feedbacks of COARE convection to the large-scale momentum budget.

Uyeda et al. [1995] used X band (3-cm wavelength) radar data obtained over a 2.5-month period on Manus Island to analyze the convective clouds forming over and near the island. Despite the fact that such radars are heavily attenuated and that the clouds were not necessarily representative of the oceanic convection over the warm pool, they obtained some potentially useful insights into the dynamics of convection in this region of the tropics. They suggest that the heaviest instantaneous surface rainfall rates occur during the earliest stage of cloud development, before the cloud extends much above the 0°C level, and that moderate but more widespread rain continues as the cloud grows above the 0°C level and develops a broad (~200-300 km wide) upper level cloud shield and a region of stratiform precipitation with a bright band at the melting level. These results await verification by the more extensive COARE ship and aircraft radar data, still under analysis.

3.6. Cloud Microphysics

Only a few investigations of the cloud microphysical data collected in COARE have been carried out so far. *Takahashi et al.* [1995] released 13 precipitation particle image sensors, balloonborne instruments that provide visual images of precipitation particles, over the period November 20 to December 9, 1992, into a range of selected convective events. *Pueschel et al.* [1995] have examined images of ice particles observed aboard the NASA DC-8 aircraft in a tropical cyclone over the Coral Sea, which is south of the warm pool. The largest ice particles were aggregates of dendrites, reminiscent of the ice particles observed in a Bay of Bengal depression during the Global Atmospheric Research Program's Summer Monsoon Experiment in 1979 [*Houze and Churchill*, 1987]. Images of raindrops measured aboard the NCAR Electra aircraft have been examined by *Willis et al.* [1995] and *Yuter and Houze* [1997]. The latter show that the raindrop size distribution in the stratiform region is heterogeneous and that the variability in the size distribution is probably related to the presence or absence of the large aggregates of ice particles above the 0°C level, consistent with the result of *McGaughey et al.* [1996] discussed in section 3.3. Further studies of the raindrop size distributions are aimed at developing relations between radar reflectivity and rain rate in order to calibrate radar rain maps (see section 5.2).

3.7. Boundary Layer Near Convection

The NOAA WP-3D and NCAR Electra aircraft obtained a large sample of flight-level data in the atmospheric boundary layer. D. E. Kingsmill, and R. A. Houze, Jr., (Inflow and outflow characteristics of convection in TOGA COARE. Part II: Thermodynamics, submitted to *Quarterly Journal of the Royal Meteorological Society* , 1998b; referred to below as KH1998b) have compiled the boundary layer data in the vicinity of precipitating cloud systems simultaneously observed by airborne radar. Equivalent potential temperature (θ_e) was, on average, ~2-4°K less in rainy regions than in the regions of inflow to the mesoscale cloud system updrafts (Figure 16). The lower mean values of θ_e in the rainy regions is the result of downdrafts, which are systematically associated with the precipitation areas. The θ_e values in the rain areas indicate that the downdraft air reaching the sea surface was coming from relatively low altitudes (~1-2 km). *Zipser* [1977] also found a low altitude of origin of downdraft air reaching the surface in GATE.

Zipser and Caesar [1994] examined in detail the low θ_e air in the cold pools of two TOGA COARE cases. They computed surface latent and sensible heat fluxes and found that the latent heat fluxes depended less upon the changes in atmospheric specific humidity than upon the absolute values of sea surface temperature and wind speed. *LeMone et al.* [1995] calculated the boundary layer recovery time for air moving away from a convective outflow (Figure 17). They found a recovery time of only 3 hours, but they also found that the cold pool was maintained for a long time and over a large area by a continual infusion and spreading of downdraft air from above.

Raymond [1995] has attempted to codify the behavior of warm-pool convection on the basis of the exchange of boundary layer air flowing up into updrafts and downdraft air coming down into the boundary layer from the low to

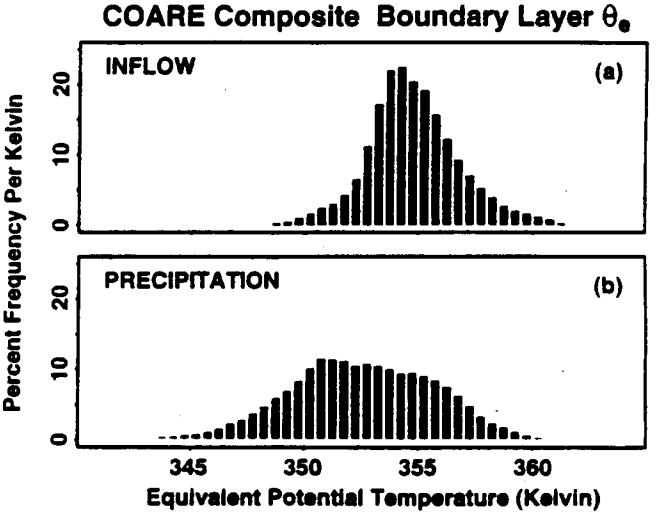

Figure 16. Histograms of equivalent potential temperature measured by COARE aircraft flying in the boundary layer at altitudes ranging from 30 to 350 m above the sea surface. The data are stratified into data collected when the aircraft was flying in regions of (a) inflow to convection and (b) precipitation. From *Kingsmill and Houze* [1997].

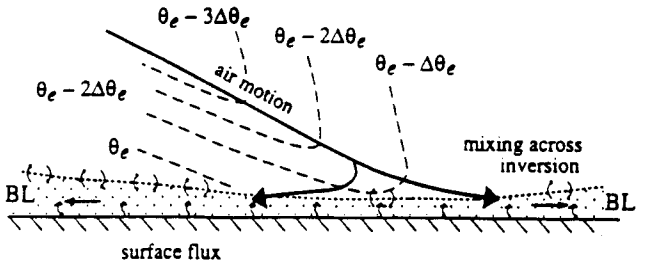

Figure 17. Schematic of airflow contribution to cold pool of a TOGA COARE convective cloud system. From *LeMone et al.* [1995].

middle troposphere. He postulates that this exchange constitutes a self regulation, which he calls "boundary layer quasi-equilibrium," and which holds on timescales greater than half a day. This equilibrium implies a mean mass flux at the top of the boundary layer, which is a function of the ratio of updraft to downdraft mass flux at the top of the boundary layer and the deficit of θ_e in the downdrafts. He notes that these quantities are likely to be highly variable.

Indeed, KH1998b analysis of measured values of θ_e encountered along horizontal flight tracks in the boundary layer shows a very broad spectrum of θ_e values in both the updraft-inflow and downdraft-rainy regions (Figure 16). Updrafts were thus drawing on a wide range of boundary layer θ_e values. The broad spectrum of θ_e values in the rainy regions also indicates that the boundary layer in the rain areas was not composed entirely of downdraft outflow; high values of θ_e, characteristic of unprocessed inflow regions, were also found in the precipitating regions.

3.8. Tracking of Satellite-Observed Features: Time Clusters and Superclusters

One of the main goals of COARE is to relate the details of convective structure (sections 3.1-3.5) to the large-scale view of the satellite-observed clouds, synoptic wind fields, and ocean (Section 2). To help establish this relationship, *Chen et al.* [1996] and *Chen and Houze* [1997] have used an automated method to track cloud areas in the hourly infrared satellite imagery. They define a "cloud cluster" as a region of cold cloud tops surrounded in a satellite image by a single closed contour of a specified threshold infrared temperature (they use 208°K, but this is a user selection).

Chen et al. [1996] applied the tracking method introduced by *Williams and Houze* [1987], and used also by *Mapes and Houze* [1993], to the 4 months of satellite infrared data (November 1992 to February 1993) over the entire GMS domain. The tracking technique identifies a "time cluster," which is a set of cloud clusters that exhibit temporal and spatial continuity across at least two successive frames of satellite imagery. A single time cluster may consist of several cloud clusters in any given frame. To qualify as a trackable time cluster, the overall group must exhibit a specified amount of close proximity in space and continuity in time; namely, if the area of overlap of any two cloud clusters from one satellite image to the next (typically 1 hour apart) exceeds 5000 km^2 or if it exceeds 50% of the area of either cloud cluster, then the time continuity is established. These criteria are set by the user. Note that a time cluster may consist of one or more cloud clusters at a given time, and the members of the time cluster may form, dissipate, merge, or split during the lifetime of the time cluster. The time cluster identified in this automated way corresponds reasonably closely to an entity one would follow subjectively by eye when viewing a loop of satellite images. However, this tracking technique does not take into account changes of cloud top temperature (e.g., vertical growth or decay) in the lifetime of the convective system, and more work is needed to improve the methodology in this respect.

Figure 18 shows the frequency distribution of lifetime versus the maximum size achieved by the time clusters tracked by *Chen et al.* [1996]. The maximum dimension is proportional to the square root of the net horizontal area of infrared temperature < 208°K, the net area being the sum of the area of all the individual clusters making up the time cluster, at the time of the maximum areal extent of the time cluster. The tendency for convective systems with greater horizontal dimension to have a longer lifetime is evident. In Figure 18 the most commonly occurring lifetime of time clusters increases more or less linearly with increasing maximum size; however, the distribution has a considerable spread (breadth of the envelope of contours in Figure 18). The spread is largely a result of the erratic and discontinuous nature of the merging and splitting process, which forms and terminates many of the time clusters.

Figure 18 shows that the overwhelming majority of the time clusters with small maximum size lasted only 3 hours or less. Most of the largest time clusters (>300 km in horizontal dimension) had a lifetime between 8 and 20

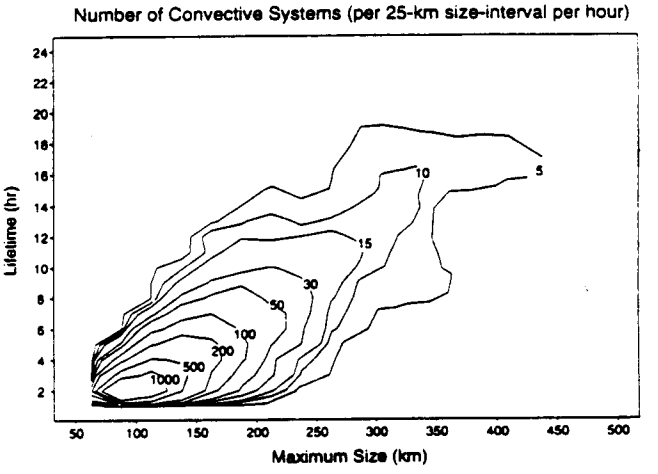

Figure 18. Frequency distribution of time cluster (convective system) occurrences as a function of the maximum size (abscissa) reached by a convective sytem during its lifetime for all of the time clusters that occurred over the warm pool (entire GMS domain) during TOGA COARE. The maximum size is the square root of the net horizontal area of infrared temperature < 208°K, the net area being the sum of the area of all the individual clusters making up the time cluster, at the time of the maximum areal extent of the time cluster. The distribution will vary depending on the choice of infrared temperature threshold. From *Chen and Houze* [1997].

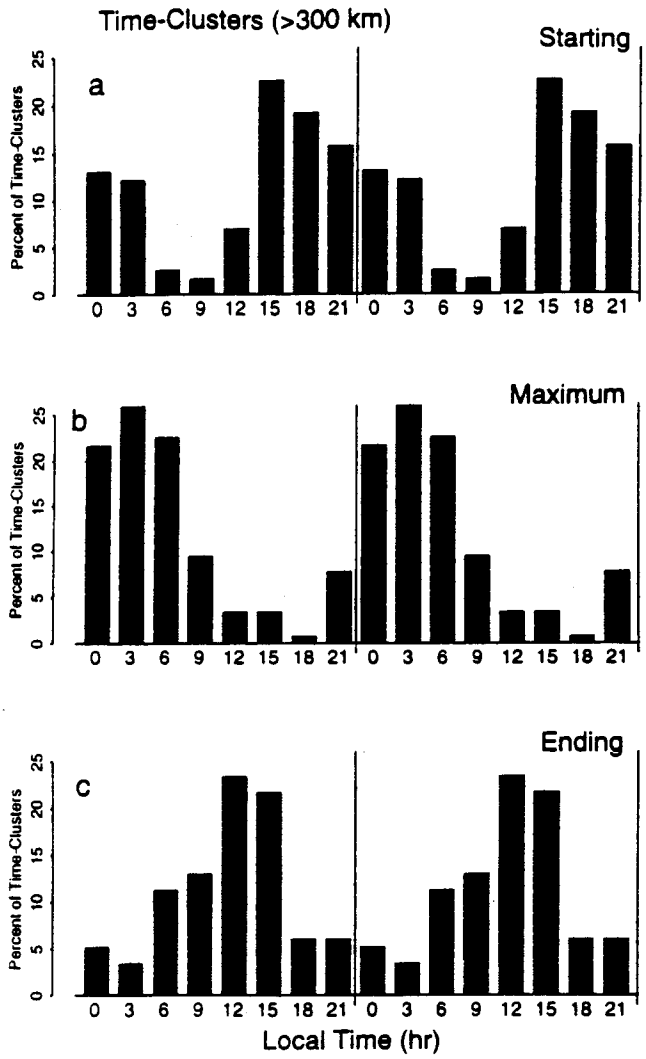

Figure 19. Diurnal frequency distribution of time clusters (convective systems) in TOGA COARE at the time of (a) starting, (b) maximum, and (c) ending of their life cycle for time clusters > 300 km in horizontal dimension at the time of maximum areal extent. Two complete diurnal cycles are shown. From *Chen and Houze* [1997].

hours. This behavior evidently reflects the tendency for convective clouds over tropical oceans to be lognormally distributed in size and lifetime [*Lopez*, 1976, 1977, 1978; *Houze and Cheng*, 1977; *Williams and Houze*, 1987]. Some time clusters lasted more than a few days, and the few time clusters with very long duration and very large maximum size contain a sizable fraction of the total 208°K and colder cloud top area. In particular, time clusters lasting over 48 hours (including five tropical cyclones) constituted some 15% of the total time cluster cloud coverage. *Mapes and Houze* [1993] termed these longlived (>2 days) trackable entities "superclusters" (one word); their definition was an attempt to quantify objectively the features subjectively identified as "super clusters" (two words) by *Nakazawa* [1988, 1995]. Time clusters lasting over 24 hours constituted ~30% of the total time cluster cloud coverage analyzed by *Chen et al.* [1996]. Note that small cloud clusters with the 208°K area <5000 km^2, which constituted about 20% of the total 208°K cloud coverage, are not included in the cloud coverage of the time clusters in Figure 18.

In the case of time clusters with very large horizontal dimension (>300 km) the times obtained from Figure 18 (8-20 hours) are a considerable underestimate of the cloud system lifetime since the peak sizes of time clusters, as defined by the area of cloud top < 208°K, are reached about dawn, and after the Sun rises the cloud tops warm. The cloud top remains but is no longer tracked by the tracking algorithm since its temperature increases to >208°K.

Chen and Houze [1997] used the results of the tracking algorithm to determine the times of day for beginning, maximum areal extent, and ending time of time clusters. Figure 19 shows results for time clusters whose maximum size (as defined above) exceeded 300 km. Most of these large cloud systems first appeared in the afternoon (Figure 19a), at the time of maximum effect of solar heating at the sea surface and atmospheric boundary layer. They generally started out as horizontally small, but deep, convective clouds in the afternoon. They continued to develop and reached their maximum areal extent during the night and early morning hours (Figure 19b). Most of them experienced a rapid decay right after sunrise and died out during the daytime (Figure 19c).

3.9. Diurnal and Bidiurnal Variability: Interaction of Ocean, Clouds, Radiation, and Large-Scale Waves

Chen et al. [1996] showed that the amplitude of the diurnal cycle varies strongly with cloud cluster size. Figure 20 shows the diurnal variation of area covered by cloud tops with infrared temperatures < 208°K in four cluster-size categories. Curve 4 in Figure 20 shows that the largest cloud clusters account for most of the diurnal variation in area of cloud top temperatures <208°K.

Chen and Houze [1997] looked at the frequency of occurrence of all infrared temperature values in the GMS data. In Figure 21, they show the frequency of the infrared cloudtop temperature over the IFA as a function of time of day for convectively suppressed and active periods of the ISO. The suppressed periods included November 13 to December 9 and February 1-9. Figures 21a and 21b contain data from 35-40 days, covering two passages of the ISO in TOGA COARE. The two active periods included December 10-31 and February 10-25. Examination of Plate 2 at the longitude of the IFA (156°E) confirms that these time periods were suppressed and active periods of the ISO.

During the convectively suppressed phases of the ISO, clouds tended to be shorter-lived. Figure 21a shows that the frequency of occurrence of these cloud systems followed the solar cycle very closely. The coldest tops tended to be 200°-220°K and occurred at about 1200-1500 local standard time (LST), when the ocean surface and/or overlying atmospheric boundary layer was at its warmest as a result of solar heating. The maximum cloudtop height dropped off after that time. The warmer cloud tops (>240°K) occurred most of the time throughout the day.

During the convectively active phases of the ISO the frequency of occurrence of infrared cloudtop temperature over the IFA as a function of time of day also exhibited a strong diurnal variation; however, it was a more complex

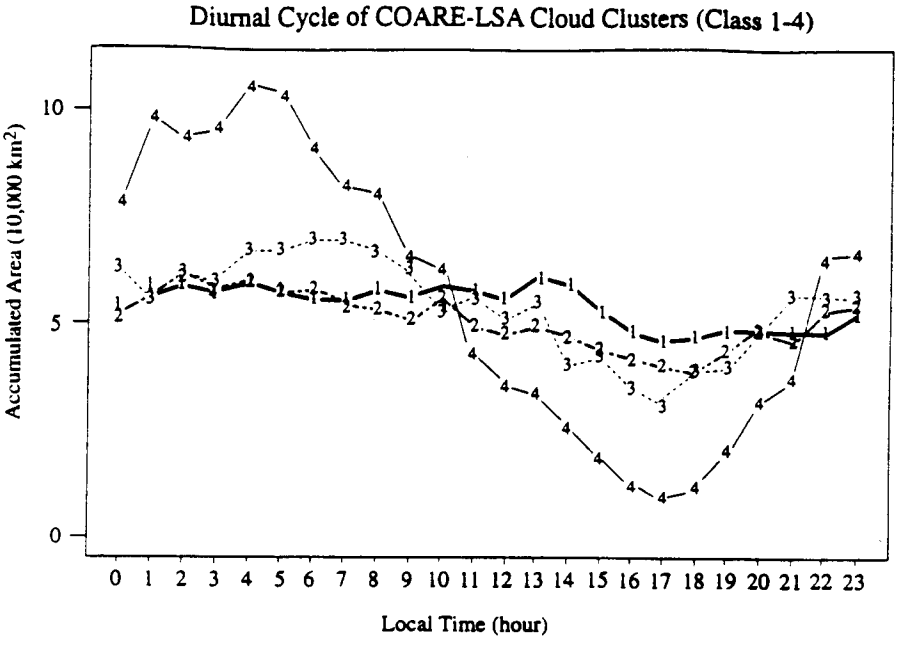

Figure 20. Diurnal cycle of the accumulated area covered by cloud tops with infrared temperature < 208°K over the domain 152°-180°E and 10°N-10°S for each of four size classes. Each closed contour of infrared temperature < 208°K is assigned to a size category as follows: class 1 (<6800 km^2 in area), class 2 (6800-28,300 km^2), class 3 (28,300-92,800 km^2), and class 4 (>92,800 km^2). Each category accounts for one quarter of the total area covered by cloud tops < 208°K. From *Chen et al.* [1996].

and less intuitive variation than that seen during the suppressed phases. The high cloudiness was dominated by larger cloud systems (those with cold tops larger than ~90,000 km^2, as defined by the 208°K cloudtop temperature contour; see the curve labeled as class 4 in Figure 20). These large cloud systems were longer-lived and generally occurred only in the active phases of the ISO. The long lifetimes of these large systems are crucial to understanding the diurnal variation of cloud top temperatures during the active phase of the ISO (Figure 21b). The highest (coldest) cloud tops (~190°K) produced by these systems tended to occur during the predawn hours (0000-0600 LST). The most frequently occurring cloudtop temperature was 200°-220°K during these hours. After 0600 LST the most frequently occurring temperature value increased steadily, reaching a peak of 240°-260°K between 1800-2000 LST.

Chen and Houze [1997] suggest that this gradual increase in the most frequently occurring cloudtop temperature was the result of the warming, decaying, or collapsing of the predawn cloud shields of the large cloud systems. Formation and rapid dissipation of smaller, short-lived cloud shields occurred in the afternoon, at the time of maximum warmth of the atmospheric boundary layer and sea surface, and evidently account for the secondary peak at 1400 LST of the highest cloud tops shown in Figure 21b. At the same time, during the afternoon, some of the cloud systems, starting out small, were developing into larger systems. The difference between the convectively suppressed periods (Figure 21a) and the active periods (Figure 21b) is that these large systems occurred very rarely during the suppressed periods. In fact, no time clusters (defined by the 208°K contour) exceeded 170 km in horizontal extent during the suppressed periods, whereas many such cloud systems exceeded 300 km in dimension during the active periods over the IFA.

Petersen et al. [1996] have examined the diurnal variability of ship-radar-estimated rain amount, cloud-to-ground lightning strikes, and the frequency of infrared brightness temperature <205°K (Figure 22). The lightning shows a peak near 0200 LST, with both rain amounts peaking about an hour later [see also *Lucas and Orville*, 1994]. The satellite brightness temperature < 205°K shows a rather broad peak near 0500 LT in agreement with Figure 21. The lag of the high cloud maxima relative to the rain and lightning is probably related to cloud system lifecycle. *Maddox et al.* [1986], *Heymsfield and Fulton* [1988], and *Zipser* [1988] have shown via case studies that the lowest infrared brightness temperatures do not generally overlie the convective cell region but rather are over the stratiform region, which evolves subsequent to the most convective phase of the storm. *Ushiyama et al.* [1995] used radar data from Manus Island to determine that rain over the island's mountains followed a strong diurnal cycle with little evident relation to ISO events.

Rickenbach and Rutledge [1998] have examined the diurnal variability of their four subjective precipitation-morphology categories (discussed in section 3.2). Recalling from Figure 10 that the ships sampled best the frequently occurring submesoscale convective systems, we can assume that their "isolated, submesoscale unorganized echoes" were quite well sampled. They found that the rain from these smaller isolated systems exhibited a semidiurnal cycle, with maxima of rainfall at 0300 and 1600 LST (Figure 23). *Chen and Houze* [1997] found a similar behavior among the smallest category of time clusters (those whose 208°K cloud shields did not exceed 80 km in maximum dimension;

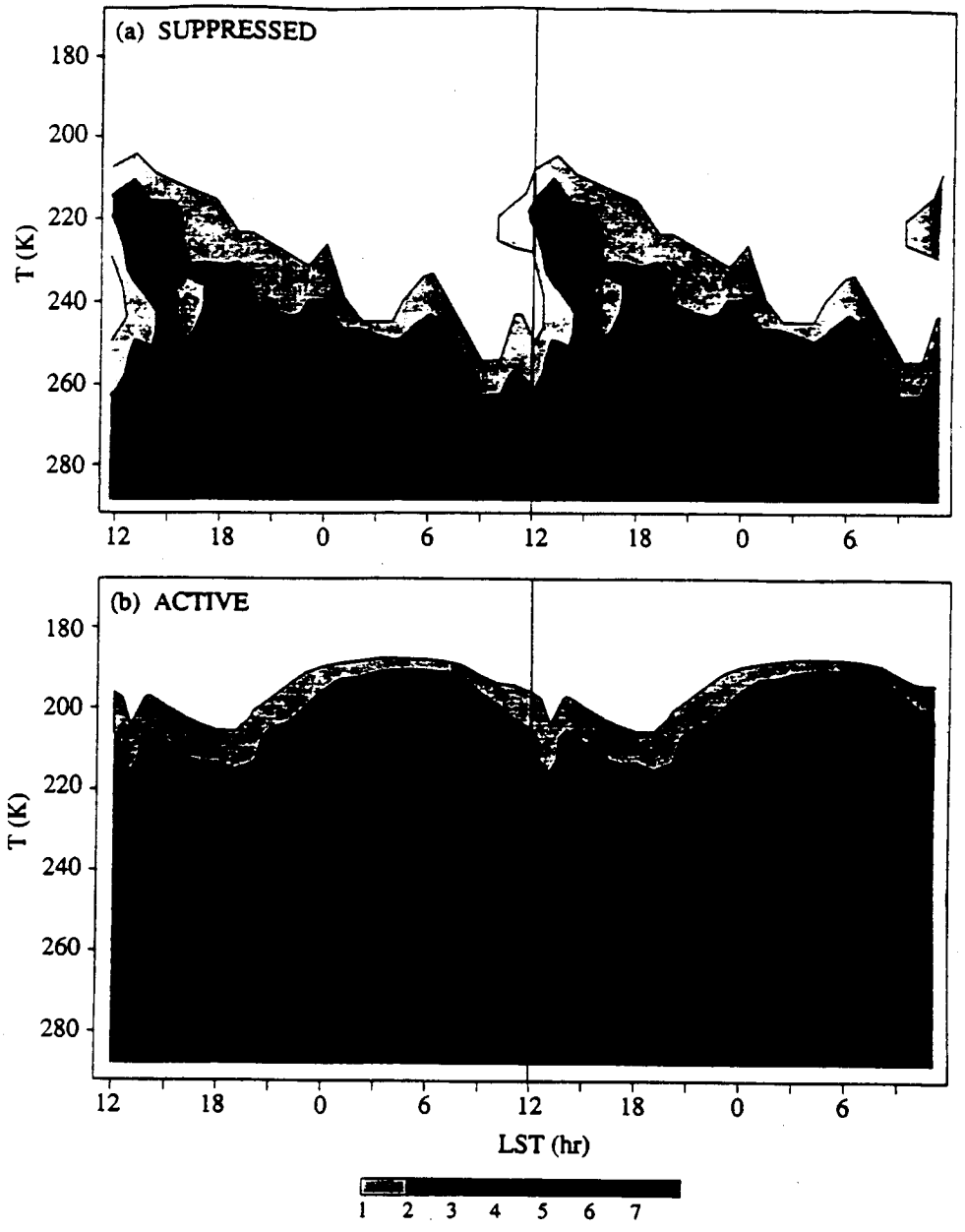

Figure 21. Diurnal variation of infrared temperature (percent area of cloud top temperature within each 5°K interval) over the TOGA COARE IFA for (a) suppressed periods (deep clouds rare) and (b) active periods (deep clouds common) of the ISO. From *Chen and Houze* [1997].

see *Chen and Houze* [1977, Figure 10]). They hypothesized that the afternoon peak results from cumulonimbus forming in conjunction with the diurnal heating of the ocean surface, while the predawn peak is the result of small systems forming by either splitting off from large systems or being triggered by downdraft cold pools of large systems during the night and early morning hours, when the large convective systems are most active (Figure 19). *Sui et al* [1997] showed that the diurnal variations in rainfall/convection over the TOGA COARE region can be classified into three distrinct stages: warm morning cumulus, afternoon convective showers, and nocturnal convective systems. They suggest that the primary cause of the nocturnal rainfall maximum is associated with the increased available precipitable water at night due to radiative cooling and the resultant change in tropospheric relative humidity.

The diurnal timescale is commensurate with the timescale of the large cloud systems. According to Figure 18, the lifetime of the 208°K time cluster is 8-20 hours when the maximum size of the cold cloud region is over 300 km, and since the cloud shield does not disappear but merely warms up, the lifetime of the large time clusters is actually much greater than 8-20 hours. That is, they last over a day. We also noted from Figure 20 that the large cloud clusters dominate the diurnal cycle. From Figure 19, we noted that the large time clusters systematically start at the same time of day (midafternoon). *Mapes and Houze* [1993] and *Chen and Houze* [1997] therefore conclude that the diurnal cloudiness cycle reflects to a great extent the life

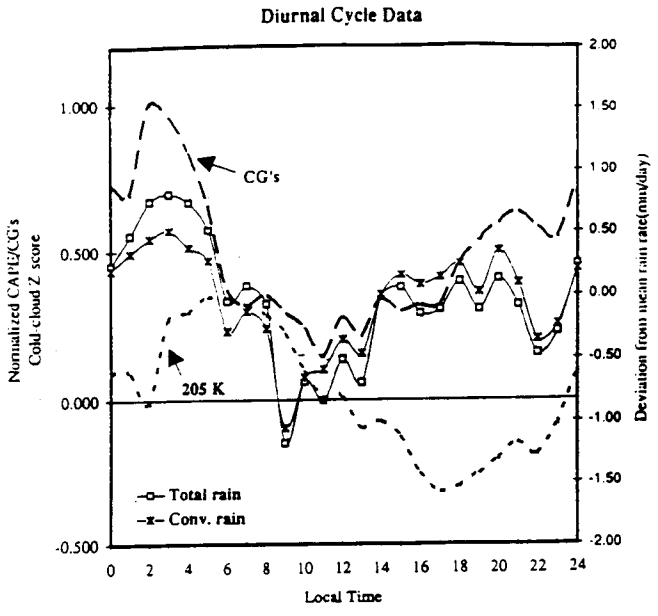

Figure 22. The diurnal cycle of cloud-to-ground lightning (dashed line), cold cloud area with brightness temperatures < 205°K over a 30-day period (dotted line; plotted as a function of the number of standard deviations from the 30-day mean); and total and convective rainfall (plotted as a deviation from the mean in mm d^{-1} over a 90-day period) over the ocean ending February 27, 1993. Local time is indicated on the abscissa. The left ordinate indicates a normalized value for both CAPE and CG lightning and a "Z score" for the cold cloud coverage. The right ordinate indicates the deviation of rainfall from the mean in units of mm d^{-1}. Adapted from *Petersen et al.* [1996].

cycle behavior of the large cloud systems. Figure 24 shows schematically the life cycle of a large convective system and its interaction with the surface air temperature. The time period of the schematic is 2 days rather than 1 day because the occurrence of a large convective system on 1 day affects (suppresses) convective development on the second day at that location over the ocean. The tracking technique shows that it usually takes about 6-12 hours for the large convective systems to grow and reach their maximum areal extent of cloudtop temperature < 208°K. The predawn cross section sketch on the second day schematically illustrates the mature stage of these large systems, which are most likely to occur before dawn (Figure 19b). The large systems usually decayed after sunrise (Figure 19c). As the large cloud systems aged, the cloud top continued to expand; however, it became warmer as a result of absorbing solar radiation and/or collapsing [*Lilly*, 1988]. The cross section for the afternoon of the second day in Figure 24 illustrates the increased cloudtop temperature of the cloud deck generated during the previous night. This warming of the widespread cloud tops accounts for most of the maximum frequency of warmer cloud top temperatures in the afternoon during the active phases of the ISO (Figure 21b).

While the maximum area of cold cloud tops develops during the night, low moist static energy downdrafts from the widespread nocturnal cloud systems spread over the ocean surface and radically change the character of the atmospheric boundary layer. The boundary layer is slow to recover to its undisturbed condition. *Houze* [1977] found the boundary layer recovery time to be > 9 hours in GATE. *Parsons et al.* [1994] found the recovery time to be up to 18 hours in TOGA COARE. As noted in section 3.5, *LeMone et al.* [1995], found the Lagrangian recovery time for elements of boundary layer air moving away from a cold source to be only 3 hours, but they also noted that the cold pool could be maintained for a long time and over a large area by a continual infusion and spreading of downdraft air from above. In addition, the large cloud shield, present during the night, remains during the day and blocks the sunlight and the solar heating is less effective in warming the sea surface and atmospheric boundary layer back up to their undisturbed conditions. This behavior of the surface temperature on the day following a widespread convective event, as a result of cooling by downdrafts and shading by the lingering upper level cloud deck over the open ocean is corroborated by measurements at the TAO buoys [*Zhang*, 1996]. The plot along the lower part of Figure 24 shows the surface air temperature (not SST), and it is based on the analysis of *Zhang* [1996], who shows that on days on which it is cloudy between midnight and dawn, the mean surface air temperature is 1°-2°C cooler than on clear days.

In addition to the modification of the sea surface by the convective system, the shortwave absorption by the long-lasting middle to upper level cloud deck warms the upper troposphere and thus stabilizes the free atmosphere [*Randall et al.*, 1991], further disfavoring new deep convection. Hence the new deep convection does not readily initiate at the same location on day 2 as a result of stabilizing effects in both the boundary layer and the middle to upper level cloud deck. Figure 24 therefore shows cooler surface conditions and no new deep convection formation on the second day.

Does this hypothesized 2-day cloud, precipitation, surface, boundary layer, radiative interaction cycle occur over the warm pool? The data from COARE suggest that it may. Figure 25 from *Chen et al.* [1996], shows the locations of time clusters in time-longitude coordinates for two time periods. The size of the oval indicates the size of the area covered by a time cluster at an instant of time. The first time period (Figure 25a) is during the onset of the westerlies in mid-December (compare Figure 4b); the second (Figure 25b) is during the maximum westerlies toward the end of the active phase of the ISO in late December (Plate 1b). Figure 25a shows that at the longitude of the IFA (156°E) a distinct 2-day alternation occurs in the area covered by time clusters. On December 12, 14, and 16 a large time cluster occurred in the morning hours (LST), while on December 11, 13, and 15 there was no time cluster present. However, this 2-day variation is part of an apparent ~6 deg day^{-1} propagation from east to west, with a 2-day frequency. The westward propagation is not necessarily representative of the continuous motion of individual cloud clusters or their underlying convective precipitation areas; *LeMone et al.* [1994] point out that the apparent motion of convective systems in satellite data is a function of life cycle stage, with new growth and advection by lower level winds predominating in early stages, when convective cells are more active, and advection by upper level winds dominating in the later, more stratiform stages. *Chen and Houze* [1997] postulate that the 2-day variability may be a mutual reinforcement of the cloud-radiative-surface interaction depicted in Figure 24 and a 2-day-frequency

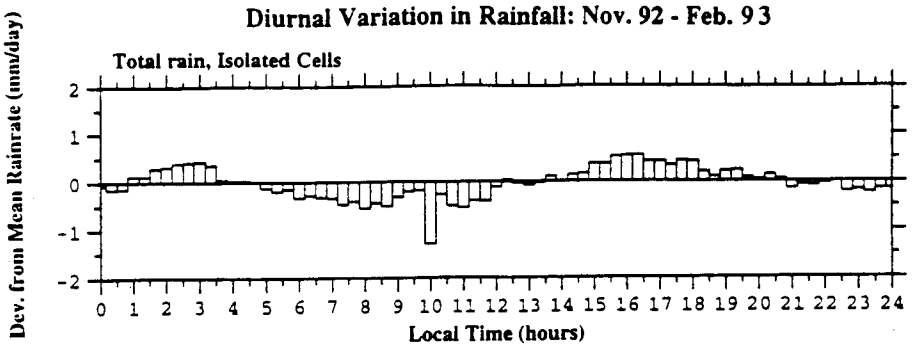

Figure 23. Diurnal cycle of rain from isolated convective cells. Data are from the R/V *Vickers* shipborne C band (5-cm wavelength) radar. The parameter plotted is the deviation from the mean radar-estimated rainfall (T.M. Rickenbach, personal communication, 1996).

westward propagating inertio-gravity wave [*Yoshizaki*, 1991; *Takayabu*, 1994; *Takayabu et al.*, 1996]. Figure 25b shows that when the westerlies became more pronounced in the later part of the active phase of the ISO, the time cluster locations and sizes in time-longitude space began to take on the appearance of the larger-scale ~3 deg day^{-1} eastward propagation of the ISO itself. At this stage the ensemble of time clusters has the characteristics that led *Nakazawa* [1988, 1995] to refer to the whole ensemble loosely as a super cluster. At this stage the 2-day variability is largely obscured by the larger-scale processes.

The complex combination of westward propagation (at the scale of the 2-day variability) and eastward propagation (at the still larger scale of the ISO as a whole) both occur for convective phenomena whose space scales are comparable to or greater than the Rossby deformation radius

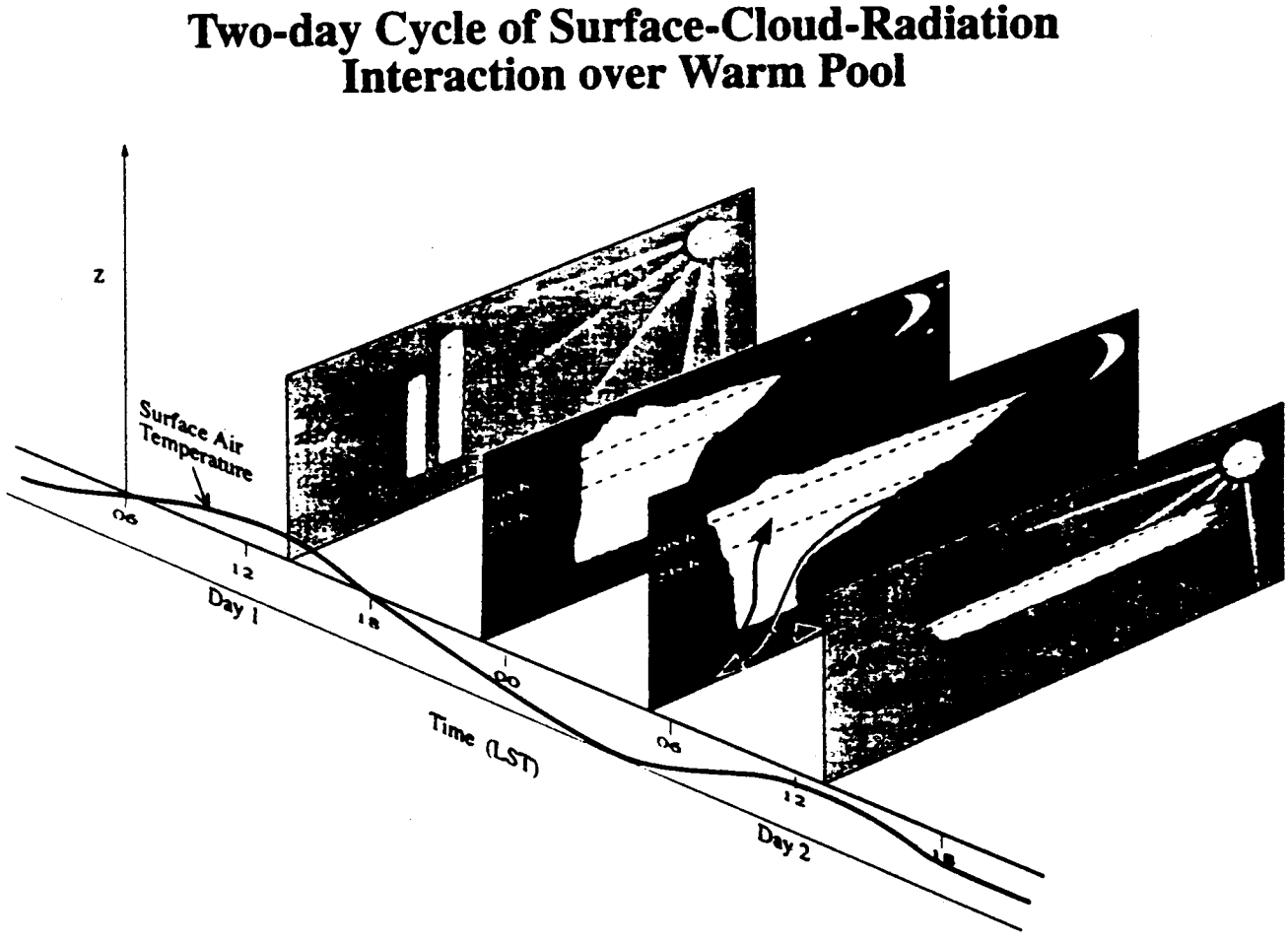

Figure 24. Schematic of the 2-day cycle of surface-cloud- radiation interaction for large convective systems. The surface temperature curve along the bottom axis shows the surface IR temperature, which has a stronger diurnal variation than the underlying water temperature. Adapted from *Chen and Houze* [1997].

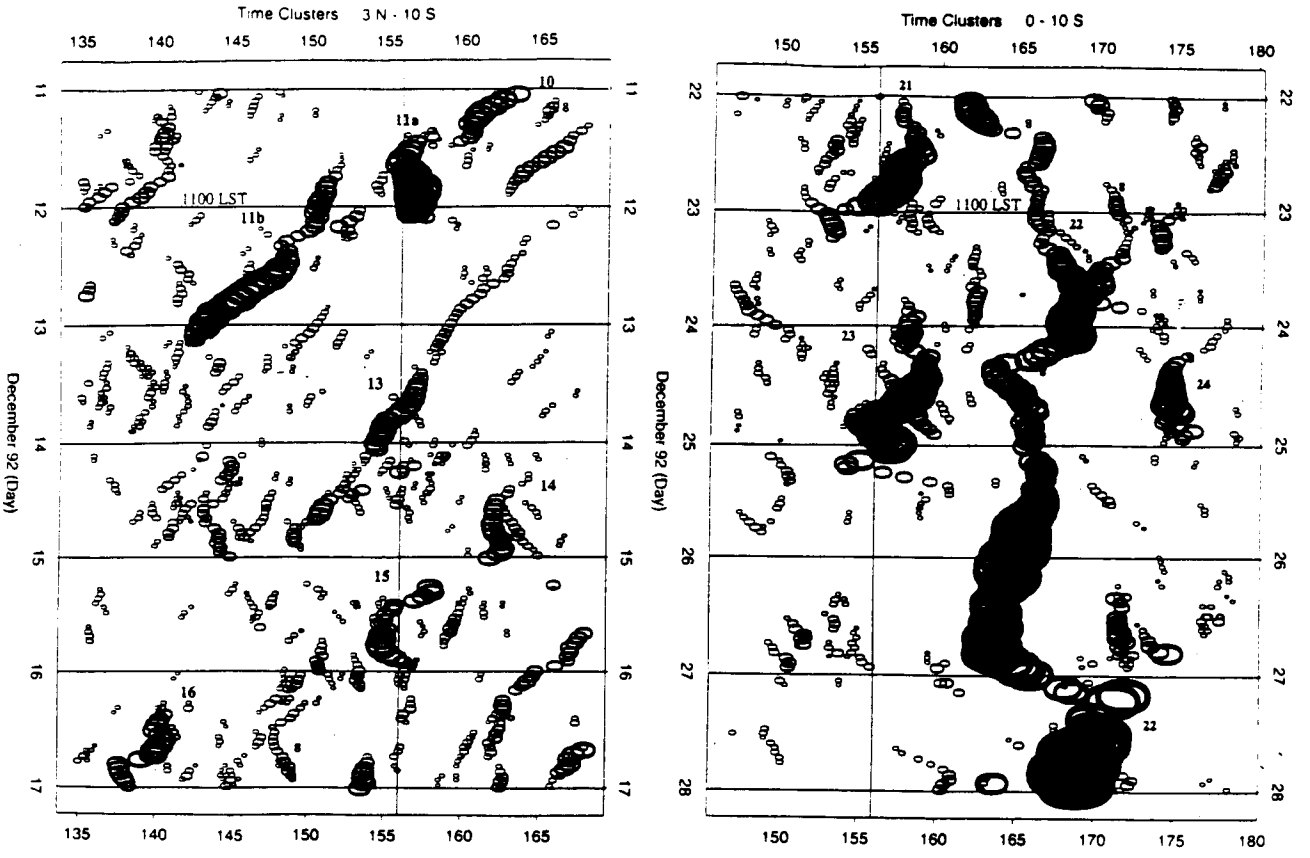

Figure 25. Time clusters (tracked convective systems) in time-longitude space. Times in LST. (a) December 11-17, 1992 (b) December 22-28, 1992. Sizes of each oval are proportional to the sizes of actual time clusters at a given instant. Adapted from *Chen et al.* [1996].

in the equatorial atmosphere (around 2000 km). At the shorter scales where the convective systems develop, geostrophy plays essentially no role. Figure 6a shows that wind shear, recognized as a factor organizing convection, ranged from weak (e.g., early to mid-December) to strong westerly (e.g., late December) to strong easterly (e.g., mid-January). The spectrum of convection observed during COARE has no spectral gaps, with horizontal scales ranging from 10 to 1000 km, and a variety of storm organizations. COARE radar data from aircraft (http://www.atmos.washington.edu/togacoare/summaries.htm) and ships (http://rainfall.atmo.ttu.edu/toga.html) show that convective organization in bands are often observed at scales around 100 km. At these scales the structure and lifetime of convective systems are qualitatively similar to those observed elsewhere (e.g., GATE).

3.10. Wave Motions

Several westward propagating mixed Rossby-gravity waves (Figure 26, from *Pires et al.* [1994]) were detected from ECMWF and the Japan Meteorological Agency Global Analysis (JMA-GANAL) analysis data as well from GMS IR temperatures [*Numaguti*, 1995; *Pires et al*, 1994, 1997]. These waves of 3-6-day period have a dominant wavelength around 4000-5000 km and are able to drive large convective systems along the equator. Analysis of atmospheric rawinsonde data also supports the existence of such westward propagating mixed Rossby-gravity waves [*Haertel*, 1995; *Numaguti et al.*, 1995]. A composite structure of these waves is given in Figure 27 [from *Numaguti et al.*, 1995]. The envelope of the waves was found to be eastward moving by *Pires et al* [1994]. A strong correlation between convection and these waves exist, as shown on Figure 28 [from *Pires et al* 1997]. A one-point lag correlation between IR temperature and 3-6-day wave wind for November 1992 shows a correlation structure that is antisymmetrical about the equator for meridional velocities, as expected for mixed Rossby-gravity trapped waves (zonal and vertical motions are symmetrical about the equator).

Second, gravity waves were detected on the 200-hPa divergence fields of ECMWF analysis and GMS IR temperature [*Pires et al*, 1997]. These waves were previously detected on GMS IR temperature by *Takayabu* [1994] on periods before the COARE experiment. These waves are correlated to the convective activity with typical wavelengths of 1000 km or less. They are more numerous during WWBs.

3.11. Convection and COARE Objectives

COARE observations of atmospheric convection were aimed to elucidate the impacts of convection in several broad, interrelated categories, including (1) large-scale environment interactions expressed through net heating, (2)

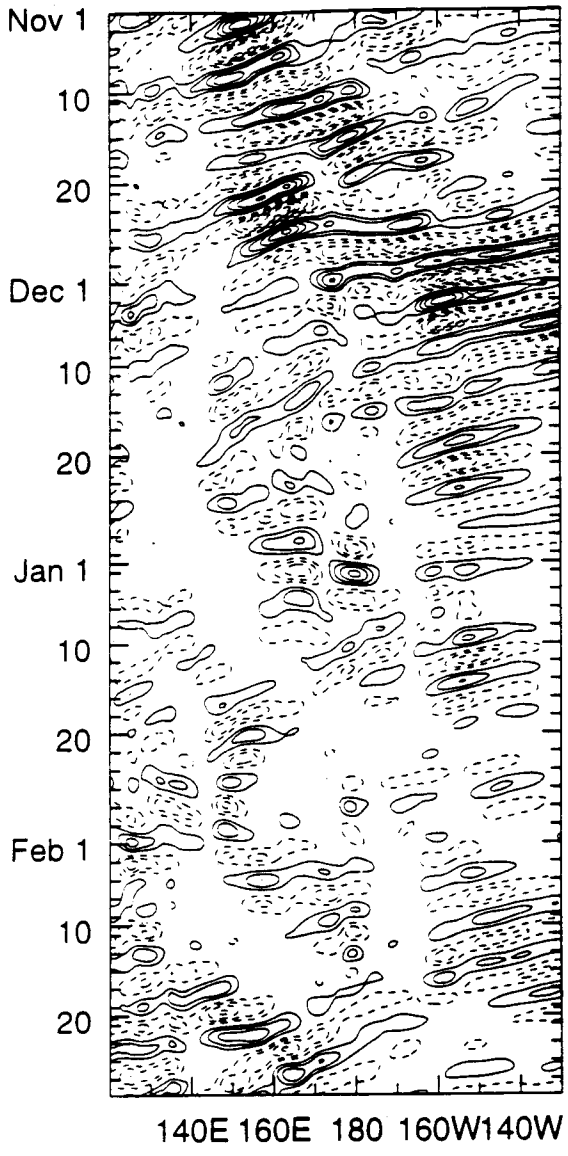

Figure 26. Time-longitude section for the 3-10-day bandpass-filtered ECMWF meridional wind at 850 hPa, averaged between 5°S and 5°N. Contour interval is 1.0 m s^{-1} (zero line skipped). From *Pires et al.* [1994].

large-scale environment interactions expressed through redistribution/ generation of momentum, (3) modification of interfacial fluxes through surface thermodynamic changes, and (4) modification of interfacial fluxes through surface wind changes. The COARE research to date, discussed in sections 3.1-3.7, only partially address these categories of interaction. The studies of divergence profiles (section 3.4) address the manner in which the large-scale circulation responds to the mass field disturbance associated with the vertical distribution of latent heating. The studies of boundary layer thermodyamics (section 3.6) in regions of inflow to and outflow from convection address partially the modification of interfacial fluxes through surface thermodynamic changes. However, studies related to momentum flux estimates and surface stresses, categories 2 and 4 above, have not yet reached fruition. An important reason for this is that the momentum fluxes require high-resolution detailed information on the internal air motions in convective systems. Time-consuming, multiple-Doppler radar synthesis of aircraft radar data must be carried out for these studies. The response to convective heating, on the other hand, can be approached via the integral behavior of the wind field in the vicinity of convective systems, and these studies are more quickly completed [e. g., *Mapes and Houze*, 1995]. A complete picture of the COARE convection must await the completion of a large number of multiple-Doppler studies being conducted by several COARE investigators.

4. Oceanic Phenomena

4.1. SST Variations and Surface Fluxes

Time series from the IMET mooring (Figure 29, adapted from *Weller and Anderson*, [1996]) provide an overview of the temporal variability of the surface meteorology within the IFA. From late October to early November 1992 a series of 3-7-day long southwesterly wind events with speeds between 3 and 8 m s^{-1} were observed (ISO1). Low wind speeds, typically 2 m s^{-1}, persisted from November 14 through December 12. From December 13, 1992, to January 4, 1993, a sequence of moderately strong wind events with flow toward the southeast associated with the December westerly wind burst (ISO2) was observed. A peak wind of 17.2 m s^{-1} was seen at the IMET mooring on December 23. ISO2 was followed by another period of very low wind speeds from January 4 to 15, 1993, after which squalls developed and persisted through February (active phase of ISO3).

The rainfall (Figure 29c) and wind stress magnitude (Figure 29d) agree quite well in timing and magnitude with what one would expect at 156°E from Figures 4a, 4b, and 6 and Plate 2. The suppressed phases of ISO2 and ISO3 are marked by little high cloud cover and low winds, leading to positive net heat flux into the water of order 50 W m^{-2} for several days (first two panels of Figure 32); conversely, they approach -50 W m^{-2} during active phases of ISO2 and ISO3. During the active phase of ISO3, moderate winds with short-lived (several hours to 1 day in duration), higher speed westerly wind events were seen in the IFA rather than sustained westerlies.

Figure 29e shows the observed SST at the IMET buoy. Comparison with Figures 29a - 29d reveals that the amplitudes of the striking diurnal spikes in SST are tightly related to the wind stress magnitude. A dimensional argument given by *Price et al.* [1986] shows that for given time history of Q_{net} the diurnal SST amplitude should be inversely proportional to wind stress magnitude, and the observed SST spikes follow this rule quite well. Occasional downward spikes in SST are associated with rain events, which can place thin layers of fresh, cool water over the sea surface.

Of greater significance for understanding the ISOs are the longer-term trends in SST, which are clearly related to ISO activity as suggested by *Krishnamurti et al.* [1988]. The nighttime minimum SST in Figure 29e shows maxima on December 10 and January 15. These dates agree remarkably closely with the dates of maximum SST found from

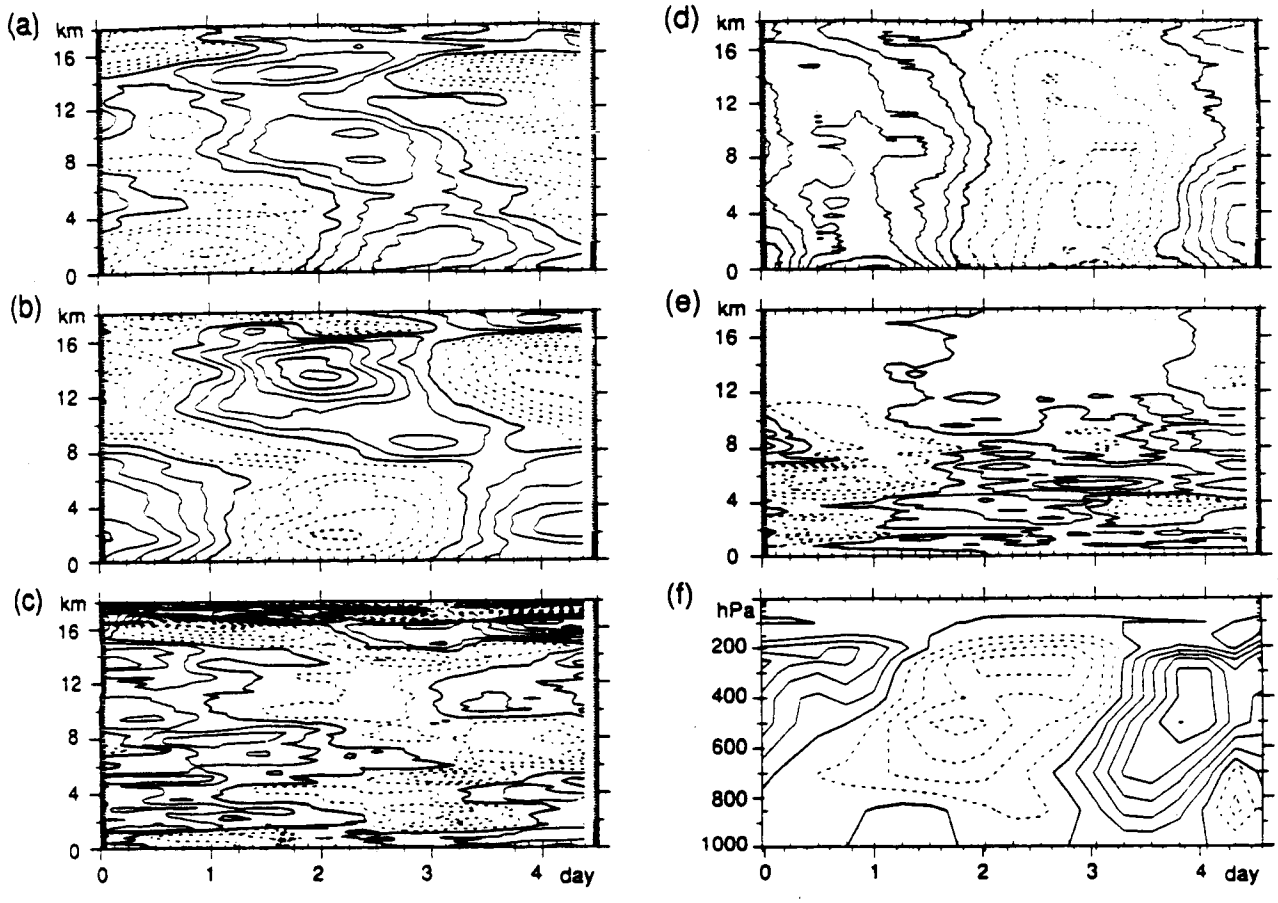

Figure 27. Composite structure of the 4.5-day-period variation observed on the Hakuho-maru (0°N, 156°E). (a) Zonal wind; the contour interval is 1 m s^{-1}. (b) Meridional wind; the contour interval is 1 m s^{-1}. (c) Temperature; the contour interval is 0.2°K. (d) Pressure; the contour interval is 0.1 hPa. (e) Relative humidity; the contour interval is 5%. (f) Vertical p velocity, ω, estimated from GANAL data; the contour interval is 1 x 10^{-4} hPa s^{-1}. A 24-hour moving average is applied and the time average is subtracted. Solid and dashed lines denote positive and negative deviations from the mean respectively. From *Numaguti et al.* [1995].

satellite-derived averages over the 500-km-wide swath, 0°-5°S, at 156°E by *Nakazawa* [1995, Figure 10]. Thus as noted by Nakazawa, maximum SST precedes deep convection by 12-13 days in the two ISO events sampled in COARE. *Velden and Young*'s [1994] SST image for December 10 probably captures the maximum SST before the ISO event, but Figure 29 suggests that their January 10 image may be about 4 days after the SST minimum, near the IFA; so their image pair may somewhat underestimate the SST change across the ISO event.

Inspection of Figure 29 suggests that the IMET-observed SST changes are largely controlled by one-dimensional processes of heat storage in the mixed layer, much as suggested by *Meyers et al.* [1986]. The two major ISO events are preceded by calm sunny conditions when the SST warms up about 1°C; the cooling periods are characterized by net heat flux out of the water (Figure 29a) and strong winds. Both of these effects produce cooling, by direct heat loss and by mixed layer deepening, respectively. However, as discussed below, advective influences can also be strong at times.

On the basis of IMET buoy flux data, *Lau and Sui* [1997] investigated the variation of short-term SST with respect of surface wind and shortwave radiation forcing over the COARE region. They concluded that fluctuations of local SST on timescales of weeks to months over the warm pool of the western Pacific are part of a large-scale dynamic and thermodynamic adjustment to inherent atmospheric low-frequency variability associated with the MJO. On these timescales both surface processes (shortwave radiation and evaporation) and upper ocean processes contribute to the regulation of SST of the warm pool.

4.2. Variations of the Oceanic Mixed Layer, Currents, and Thermocline During the IOP

Eldin et al. [1994] reported results from 18 meridional sections between 5°S and 5°N, along 156°E, on *Le Noroit*. Figure 30 shows results on winds and currents from their work. The wind stress vectors (Figure 30a) clearly show the westerlies associated with ISO2 and ISO3 accompanied by enhanced trades north of the equator. To first approximation the currents in the top 60 m (Figure 30b) follow the surface winds within a few days. They attain quite large magnitudes; for example, winds associated with ISO2

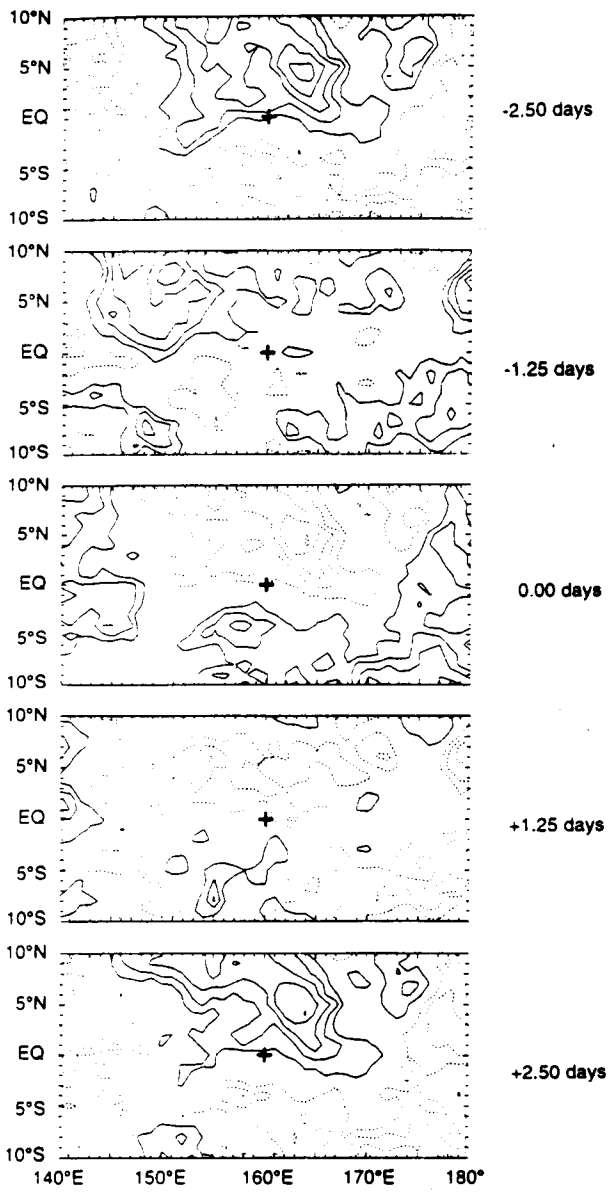

Figure 28. One-point lag correlation between IR temperature and 3-6-day wave bandpass-filtered meridional wind for November 1992, showing an antisymmetrical correlation structure as expected for mixed Rossby-gravity trapped waves. From *Pires et al.* [1994].

(December 10, 1992, to Januarty 2, 1993) generated an equatorial jet with a transport of some 12 Sv (1 Sv = 10^6 m^3s^{-1}), with surface flows nearing 1 ms^{-1}. In the presence of such large currents, horizontal heat advection may be comparable to the one-dimensional processes that were thought before COARE to be the major contributors to the heat budget of the ocean mixed layer. At greater depths, flows were more stable in time, and particularly in the 150-280 m layer they were easily related to classical currents (Equatorial Undercurrent, subsurface countercurrents). There were strong suggestions of nonlocal forcing in the changes occurring at 60-150 m.

Figure 31 shows 1°N-1°S mean zonal winds, SST, and thermal structure from *Eldin et al.* [1994]. The SST is broadly consistent with that shown in Figure 29; the thermal structure shows that the cooling after ISO2 was associated with a deepening of the mixed layer from 30 to 60 m. Restratification occurred in the following 2 weeks but was accompanied by shallowing of the thermocline. *Eldin et al.* ascribe this to the action of upwelling due to the easterly winds in mid-January (Figure 31a); though whether this has a significant effect on SST is not clear.

Huyer et al. [1997] examined the data from over 30 repeats of the butterfly-shaped *Wecoma* survey pattern seen in Figure 1e, centered on the IMET buoy. Horizontal temperature gradients were usually quite weak in the Wecoma survey data; but on January 4, after the westerly winds of ISO2 stopped, the zonal jet created by these winds apparently broke down. An energetic, cyclonic submesoscale eddy (radius about 40 km) developed, centered near the center of the IFA [*Hacker and Lukas*, 1995]. Isopycnals in the eddy center came up from nearly 80 m almost to the surface. However, no surface signature was seen, because of the fresh and very stable layer created by heavy rains on January 4.

The *Wecoma* data are being used to estimate advection relative to the IMET buoy. As the wind stress increased, and horizontal currents increased in the upper ocean (compare Figure 30), horizontal inhomogeneity (and temperature gradients) decreased in magnitude, tending to compensate for the stronger currents in the advective term. *Huyer et al.* [1997] also note the rise in the thermocline, associated with the easterly winds in mid-January (Figure 31).

An important source of SST change is the absorption of solar radiation with depth. *Lewis et al.* [1990] noted that tropical Pacific Ocean water is sufficiently transparent that solar penetration through the base of a typical mixed layer depth (40 m, say) can be of order 10 W m^{-2} or more, so it is certainly significant for SST evolution in the warm pool region. *Siegel et al.* [1995] carried out an intensive study of solar penetration from R/V *Vickers*. Only the blue light penetrates below about 10 m; in pure water its intensity falls exponentially with an *e*-folding depth of about 34 m. In calm conditions Seigel et al. found an "e-folding" depth (in the mixed layer) of order 20-30 m, but after westerly bursts this decreased substantially, because of the upward mixing of nutrients and subsequent phytoplankton growth. The fraction of incoming light in the blue range also varied considerably with cloudiness, time of day, etc. This result raises the interesting possibility that plankton dynamics may have a significant influence on SST in the warm pool region and may need to be allowed for in modeling SST. Measurements of nutrients, chlorophyll-a and zooplankton were made from R/V *Alis* during COARE [*Kaneko et al.*, 1996], so some data are available for such modeling. The importance of penetrative absorption of solar radiation on upper ocean surface temperature was also investigated by *Sui et al.* [1998a].

Figure 32a shows the observed SST at the IMET mooring (See also Figure 29e). Figures 35b, 32c, and 32d show SST as generated by three runs of a one-dimensional mixed layer model driven by observed wind stresses and heat fluxes [from *Anderson et al.*, 1996]. The fluxes were corrected as described in section 5 before application to the model. In runs P0, P1, and P2 the precipitation was given values of zero, the observed precipitation, and twice the observed precipitation, respectively. Overall agreement of

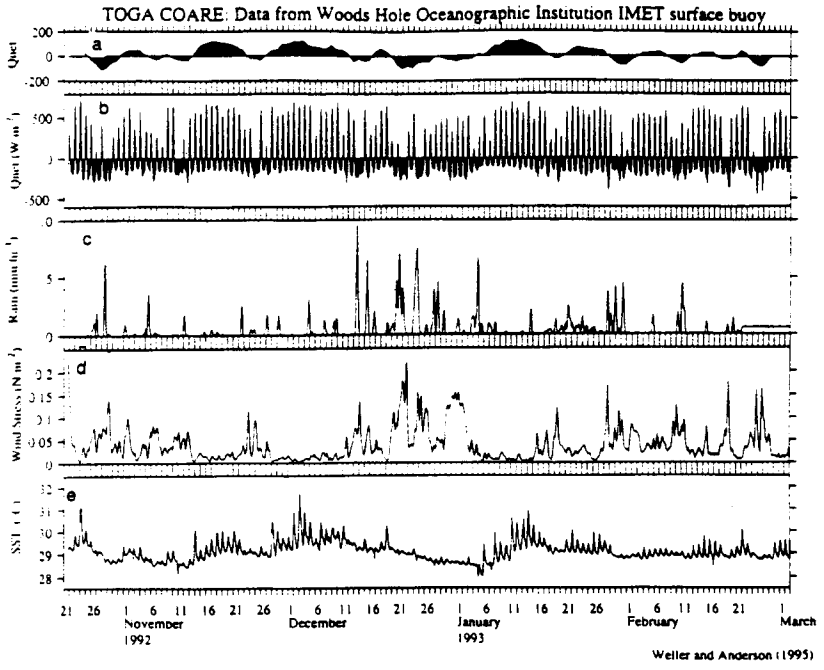

Figure 29. Observations from the Woods Hole Oceanographic Institution IMET mooring, at 1°45'S, 156°E. (a) The 24-hour running mean net heat flux (positive into the water). (b) The 2-hour net heat flux into the water. (c) Rain rate, mm h^{-1}. (d) Wind stress magnitude. (e) SST (measured 0.45 m below the surface). Adapted from *Weller and Anderson*, [1996].

model and observation in Figure 32 is certainly encouraging. Observed SSTs fell from October 26 to November 4; this was not captured by the models and is believed to be due to horizontal advection. The observed SST cooled faster than was simulated in any of the runs between December 10 1992, and January 5 1993; this is also thought to be due to the effect of advection [*Feng et al.*, 1998]. The model used the (time-averaged) vertical transmission profiles obtained by *Siegel et al.* [1995]; these were crucial to the results. For example, increasing rainfall caused the model mixed layer to shoal as expected, but the SST did not necessarily increase as a result the net SST change over the whole period of Figure 32 was (0.25°, 0.23°, and -0.02°C) for runs (P0, P1, and P2); that is, the SST trend decreased with increasing freshwater input despite the fact that the average mixed layer depths shallowed with increasing rainfall. This is apparently at odds with the concept that a salt-stratified "barrier layer" insulates the surface against mixing from below; but it in fact is not. For much of the time, vertical mixing at the base h of the mixed layer can indeed be neglected, so that the mixed layer temperature equation can be approximated by

$$\partial T/\partial t = [Q(0) - R_S(-h)]/\rho C_p h$$

where $Q(0)$ is the net incoming surface heat flux and $R_S(-h)$ is the shortwave radiation penetrating through h. If h is shallow enough, $R_S(-h)$ becomes comparable to or can even exceed the surface heat flux $Q(0)$ (which is the difference between $R_S(0)$ and the sum of latent, sensible and longwave heat losses), so the decrease in the net heating $[Q(0) - R_S(-h)]$ with decreasing depth can more than compensate for the effect of the $1/h$ factor. Thus the warming rate $\partial T/\partial t$ can decrease with decreasing mixed layer depth [*Anderson et al.*, 1996].

The success of the one-dimensional model suggests that horizontal advection is not very important for setting SST in the warm pool region; however, this may not always be true. The first comprehensive estimate of horizontal advection in COARE is due to *Cronin and McPhaden* [1997]; using five TAO moorings centred at 0°,156°E, they found heat advection of order 30 W m^{-2}, though this happened to be reduced during the IOP, and thus does not necessarily conflict with the conclusions of *Anderson et al.* [1996], *Smyth et al.* [1995] and *Li et al.* [1998] that heat advection was small for most of the IOP. Nevertheless, *Feng et al.* [1998] found advection of 43 W m^{-2} during 19 days of IS02, contributing to the cooling at this time in Figure 29. *Godfrey et al.* [1995] documented advection of heat and freshwater for short periods following a drifting buoy; they find that even relative to the buoy, advection of freshwater and heat can be strong on time scales of a few days.

Ralph et al. [1997] used data from drifting buoys released in COARE to estimate advection over much larger areas associated with the equatorial jet generated by ISO2. Like *Cronin and McPhaden* [1997], they found that horizontal advection could amount to several tens of W m^{-2}. Time-averaged currents in the Pacific are in rather accurate geostrophic balance quite close to the equator [e.g., *Lukas and Firing*, 1984]. Y. Yu et al. (An annual cycle of geostrophic currents in the western tropical Pacific from satellite altimeter measurements, submitted to the *Journal of Geophysical Research*, 1997) compared the trajectories of drifters released during COARE with geostrophic currents

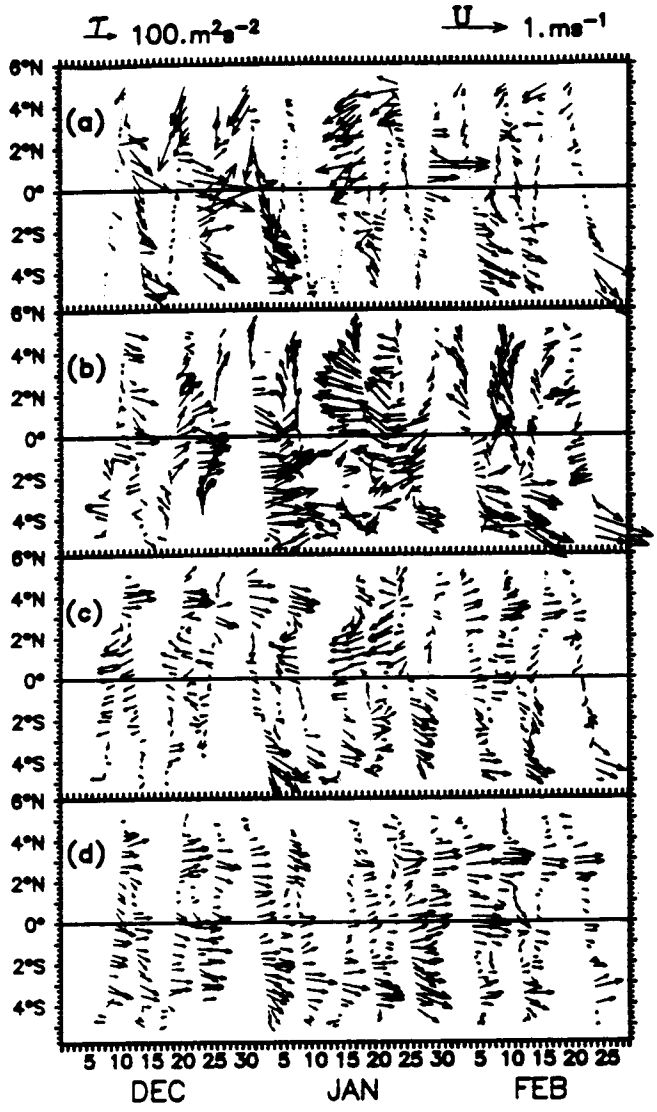

Figure 30. Time-latitude plots at 156°E, along the ship track, from December 1992 to February 1993 of (a) wind pseudostress (i.e., stress calculated with unit transfer coefficient) and current velocity vectors averaged for (b) 16-60 m, (c) 60-150 m, and (d) 150-280 m. Vector scales are shown above. Adapted from the color original of *Eldin et al.* [1994].

estimated from TOPEX/POSEIDON altimeter data; they obtained excellent agreement.

5. Quantification of Air-Sea Fluxes

The scientific objectives specific to the air-sea flux component [*Webster and Lukas* 1992] were, in essence, to provide a high-quality data set of all surface fluxes in the warm-pool region, allowing for all relevant spacescales and timescales, and to develop improved algorithms for them. The warm pool region, with its low mean wind speeds, high tropical insolation, and intermittent, energetic forcing associated with convective systems presented a particular challenge. Radiative heating errors were anticipated in unaspirated sensors. The accuracy in the tropics of the bulk formulae transfer coefficients and parameterizations, which had primarily been developed during midlatitude field programs, was suspect. The use of enough different platforms to capture the space and time variability of the region would require careful intercalibration. Pilot air-sea flux field studies done in the warm pool [*Bradley et al.*, 1993] were, however, encouraging; and a major effort was developed for the COARE field experiment. This section summarizes the air-sea interface field work done during TOGA COARE, the level of success achieved in obtaining accurate fluxes, and the work that remains to be done in the ongoing analysis efforts.

5.1. Observational Approach During COARE

During the planning for COARE it was recognized that success in addressing the objectives of the flux component of COARE would require the coordinated use of multiple measurement platforms, emphasis on comparison and intercalibration across these platforms, and the development of improved bulk formulae. The TOGA Tropical Atmosphere and Ocean (TAO) [*Hayes et al*, 1991] array of surface buoys provided a large scale, longer term context. It was supplemented for COARE by additional "automated temperature line acquisition system" (ATLAS) buoys to improve zonal resolution of westerly wind bursts and ocean response and to measure shortwave radiation and rainfall in the warm pool. Shipboard, ground-based, aircraft, and satellite sampling in the COARE large-scale domain (LSD) and outer sounding array (OSA) also provided large-scale coverage for the air-sea interface work.

During the IOP, surface meteorogical and surface flux fields from satellites and from the analysis cycle of the operational numerical weather prediction models were collected and archived for later use by COARE investigators. GMS, NOAA, DMSP, ERS-1, and

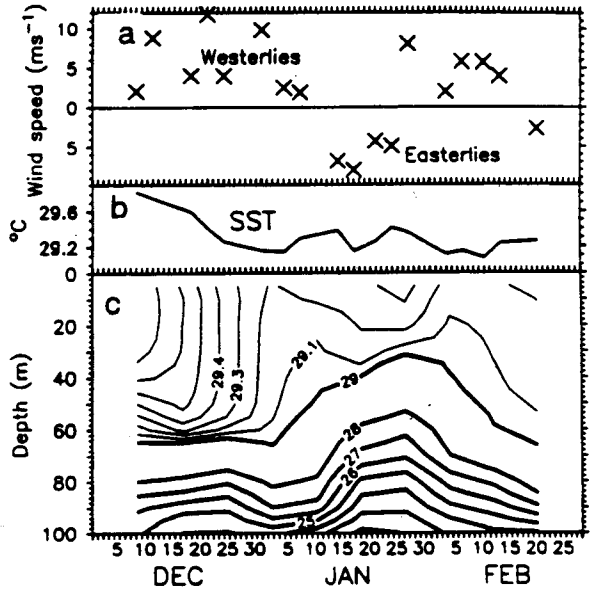

Figure 31. December 1992 to February 1993, 1°S-1°N averages along 156°E. (a) wind speed (b) SST, and (c) temperature structure, 0-100 m (contours every 0.1°C above 29°C; 1°C below). From *Eldin et al.* [1994].

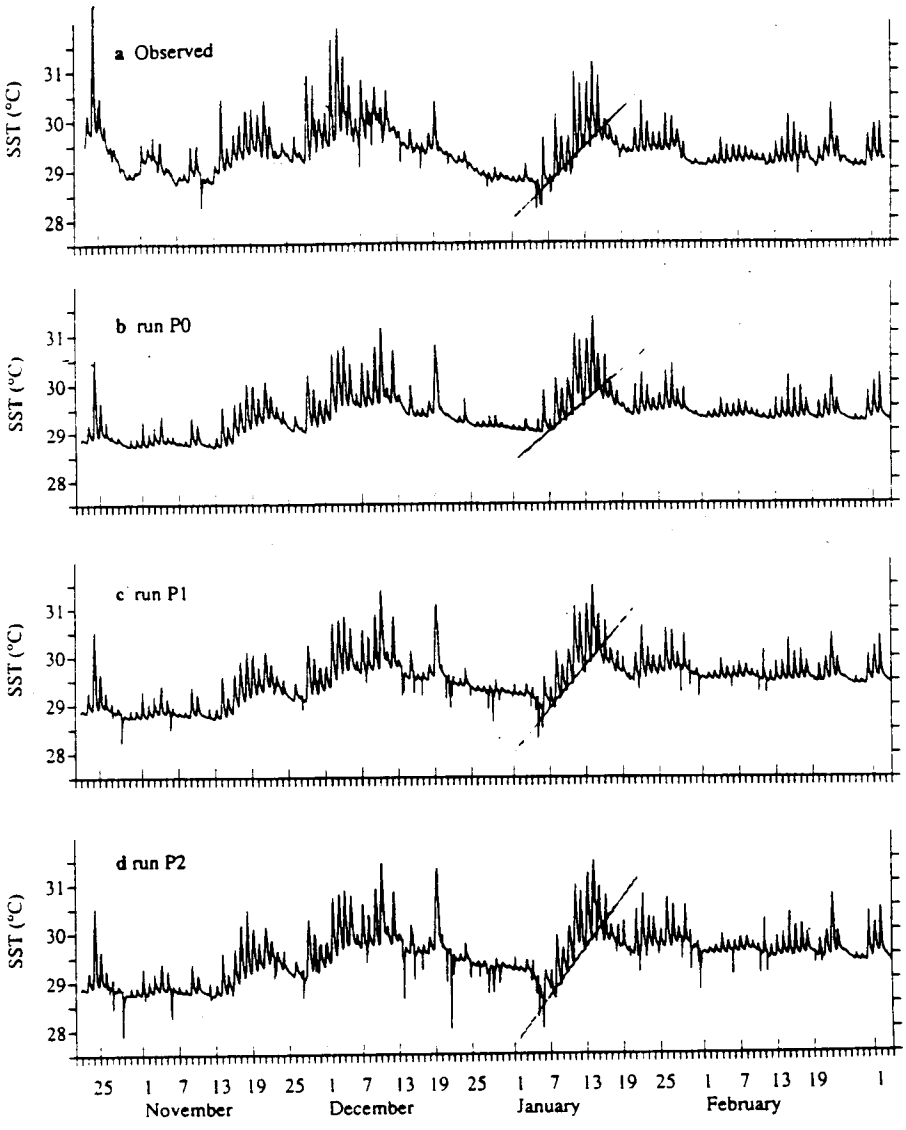

Figure 32. (a) Observed SST from the IMET mooring November 1992 to February 1993. In runs (b) P0, (c) P1, and (d) P2 the precipitation was taken as zero, observed precipitation, and twice observed precipitation respectively. SST simulated with a one-dimensional mixed-layer model, driven by IMET-observed surface heat, evapouration, and momentum fluxes. From *Anderson et al.* [1996].

TOPEX/POSEIDON satellites provided data, including estimates of sea surface temperature, sea level, radiation, wind speed, and rain. Model output was collected from BMRC, NMC (now NCEP), ECMWF, and JMA.

To achieve accuracy and consistency of flux estimates among all these platforms has required a series of international workshops, involving many participants of the air-sea flux field studies. The emphasis has been on attention to instrumental problems (section 5.2), and to developing flux algorithms consistent with the corrected flux data (section 5.3). Reports on these workshops have been prepared [*Bradley and Weller*, 1995a, b; 1996]. Validation of the fluxes by use of ocean budgets and mapping the flux fields over larger areas are considered in sections 5.4 and 5.5.

5.2. Intercomparisons of Basic Observables

It was anticipated that the bringing together of data from the diverse platforms deployed in the field in COARE would only be successful if the field program included dedicated intercomparisons. Shipboard measurements were made close to the surface buoys and in the company of other ships, and the aircraft periodically flew in tight formation and overflew the buoys and ships. Immediately following the field program, analysis of the data from these intercomparisons was a priority activity; and further calibrations and comparisons of sensors were initiated as needed to resolve issues arising from the field intercomparisons. The accuracy of measurements of three of the observables (namely shortwave radiation, sea surface

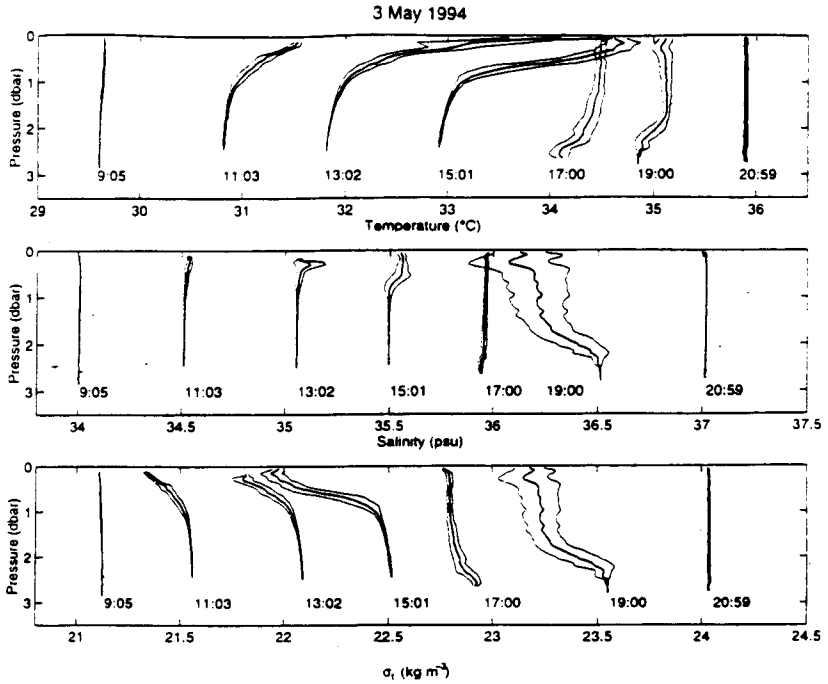

Figure 33. Vertical profiles of temperature, salinity, and density (σ_t) obtained by averaging a bow sensor within 0.1 m range on 10-min segments, during light winds. Each successive temperature, salinity, and σ_t profile is shifted by 1.0°C, 0.5 practical salinity units (psu), and 0.5, respectively. Thin curves represent one standard deviation from the mean. Temperature increases 2°C in the top meter near 1300 LT. A rain event before 1900 LT creates a small temperature inversion, along with freshening in the top 2 m (1 m = 1 db). From *Soloviev and Lukas* [1997a].

temperature and precipitation) have received particular attention.

The R/Vs *Franklin*, *Moana Wave*, *Wecoma*, *Hakuho-Maru*, and *Natsushima* assembled near the IMET mooring for two dedicated meteorology and flux intercomparisons on November 27-28, 1992, and on February 3-4, 1993. Three of the ships steamed upwind from the buoy on parallel tracks separated by ~0.5 km for 3 hours at 1.5 m s^{-1}, returning in 1 hour at 6 m s^{-1} and repeating the process. Up to six upwind legs were completed during the 24-hour intercomparison periods. During the comparison R/V *Wecoma* continued on its sampling pattern at 3.5 - 4 m s^{-1} and passed the buoy twice. In addition to the times of the dedicated intercomparisons, R/V *Moana Wave* operated next to the Woods Hole Oceanographic Institute (WHOI) mooring. The major problem areas found in the raw data as a result of these intercomparisons were radiative heating of passively ventilated air temperature sensors, calibration errors in shortwave radiation sensors, calibration and radiative heating errors in longwave radiation sensors, a lack of understanding of the performance of different rainfall sensors, and the need to correct near-surface ocean temperature measurements to take into account the depths of the various sensors and produce values representative of the true remotely sensed sea surface skin temperature.

Air temperature sensors protected by nonventilated, multiplate shields [*Gill*, 1983] were biased high by as much as 1°C during sunny, low-wind conditions [*Anderson and Baumgartner*, 1998]. Empirical algorithms developed [*Weller and Anderson*, 1996; *Tsukamoto and Ishida*, 1995] to reduce this error reduced the mean daytime biases between nonventilated and aspirated sensors to 0.01°C and standard deviations of the bias of 0.4°C [*Anderson and Baumgartner*, 1998]. Because computation of specific humidity from the relative humidity measured by some sensors required air temperature, radiative heating errors were of concern for the computation of latent as well as sensible heat flux. Without corrections to air temperature, specific humidities across the three platforms had instantaneous differences of as much as 1.0 g kg^{-1}. With corrections, these were reduced to 0.3-0.5 g kg^{-1}. Comparison of winds measured by the surface platforms pointed out the care needed to compute winds relative to the reference frame of the earth on the ships rather than relative to the ship. The difficulty rests, primarily, with developing an accurate time series of ship velocity as, even with GPS navigation, speed and direction errors occur. In particular, when the ship turns quickly relative to the averaging interval used for the navigational fixes, the ship's velocity is difficult to compute accurately. Under ideal conditions, ship and buoy wind speeds were typically within 0.1 m s^{-1} and directions within 10°.

Consistent differences in incoming shortwave and incoming longwave radiation were discovered when comparing raw data from the November 27-28, 1992, and February 3-4, 1993, buoy-ship intercomparisons. Shortwave and longwave sensors from a number of the

platforms were collected after the experiment and mounted together on the roof of a building at WHOI; these comparisons reproduced the differences seen during COARE. As a result, many of the shortwave sensors were sent to F. Bradley at the Commonwealth Scientific and Industrial Research Organisation (CSIRO) in Canberra, where they were intercompared over a few clear days during the southern hemisphere summer. One of the instruments was selected as a secondary reference standard and subsequently sent to Melbourne for calibration against the Bureau of Meteorology pyrheliometer. Corrections to the shortwave radiometer calibrations were as large as 8%. Closer examination of the raw incoming longwave data revealed that the differences among the sensors were due to the sensitivity of some of the sensors to radiative heating of the body and silicon dome of the sensor and also to calibration errors. The radiative heating effects were largely removed using the algorithm developed by *Alados-Arboledas et al.* [1988]. With the heating effects removed first, biases were then identified and removed. Prior to the corrections nighttime differences were often as much as 40 W m^{-2}. After the corrections, day and night instantaneous incoming longwave radiation agreed beween *Wecoma*, *Moana Wave*, and the buoy to ~10 W m^{-2}.

Sea surface temperature comparisons required recognition of and correction for the strong near-surface temperature gradients that developed during low-wind conditions in conjunction with the surface fluxes and the penetrating shortwave radiation. Figure 33 [from *Soloviev and Lukas*, 1997a] shows near-surface temperature profiles during low wind and strong insolation, which included a short period of rain before 1900 (local). Rainfall fell at a temperature close to the wet-bulb temperature, cooler than the sea surface temperature prior to the rain, and produced (with attendant surface latent heat losses) a near-surface layer of cool, fresh water. The penetrating solar radiation resulted in diurnal restratification in low winds. Very near the surface, additional gradients were associated with the cool skin. In comparing sea surface temperature measurements and in preparing estimates of the skin temperature that would be used in the flux calculations, ocean temperatures were extrapolated upward from their measurement depth whenever the fluxes were available using a one-dimensional mixed layer model. During the first intercomparison, without correction for the near-surface profile of temperature, *Moana Wave*, *Franklin*, and IMET buoy sea surface temperature differed by about 0.2°C at night and 0.5°C during the day. During the (windier) second intercomparison, agreement of 0.1°C was seen during the night and the day.

The result of these dedicated ship-ship-buoy intercomparisons was the development of corrections, in the form of algorithms to remove radiative heating errors and changes in sensor offsets and gains, which were applied to the raw data from these platforms. The success of these intercalibrations is indicated in the comparison of the means of the leg 1 (November 14 to December 3, 1992) surface meteorological observables from R/V *Moana Wave*, R/V *Wecoma*, and the WHOI mooring (Table 1). The *Moana Wave* held position close to the mooring. *Wecoma* executed a butterfly pattern around the mooring that was 130 km across, but during this period the meteorology had spatial scales large compared to *Wecoma* separation from the mooring.

Attempts were then made to extend the intercomparison to include other data sets. Sea surface temperature was of particular interest. The skin temperatures were measured by various infrared (IR) sensors on the ships and aircraft while temperatures at a variety of near-surface depths were measured by in situ sensors on various platforms. Under the best conditions, agreement to 0.03°C was seen between different aircraft, but at other times, disagreements of several tenths are found. Spatial variability may be a factor, as there is indication of structure in surface roughness [*Walsh et al.*, 1996] having small-scale variability matching the observed SST variability.

The aircraft flew a number of intercomparison flights and

Table 1. Averages of Corrected Meteorological Variables

Variable	R/V *Moana Wave*	R/V *Wecoma*	IMET Buoy
Air temperature, *°C	...	28.03	28.42
Air temperature, **°C	28.00	27.92	...
SST, °C	29.45	29.55	29.57
U,* ms^{-1}	3.39	3.40	...
U,** ms^{-1}	...	3.43	3.18
Wind direction, deg	88.7	77.2	87.4
Specific humidity,* g kg^{-1}	...	18.23	18.30
Specific humidity,* g kg^{-1}	18.95	18.00	...
Skin temperature, °C	29.28	29.26	29.30
Incoming longwave radiation, Wm^{-2}	409.4	409.2	410.3
Incoming shortwave radiation, Wm^{-2}	237.8	238.1	232.8

Averages are from leg 1 (November 14 to December 3, 1992). IMET buoy data corrected to ship height. SST is sea surface temperature; U is wind speed.

*At 8 m.

*At 15 m.

**At 20 m.

overflights of the buoys and ships to test their IR sea surface temperatures. Comparisons were done of static pressure, total temperature, ambient temperature, and dewpoint temperature from the two P-3s, Electra, and C-130 while flying in the boundary layer, usually at 60 m. P-3-P-3 comparisons had averaged difference magnitudes of 0.056°C in ambient temperature, 0.19°C in dew point, 0.18 m s^{-1} in east wind and 0.07 m s^{-1} in north wind. The agreement between the Electra and two P-3s was similar, with average difference magnitudes of 0.05°C in air temperature, 0.06°C in dew point, and 0.17 and 0.01 ms^{-1} for east and north winds, respectively.

The aircraft measurements were also compared with those from the surface platforms. Comparisons between the *Franklin* and the low-flying Cessna showed an average difference in air temperature of 0.03°C, in humidity of 0.07 g kg^{-1}, in incoming shortwave radiation of 10 Wm^{-2}, in incoming longwave radiation of 2 W m^{-2}, in wind speed of 0.7 m s^{-1}, and radiometric sea surface temperature of 0.03°C. Differences between the larger aircraft and the surface platforms were also examined. When the Electra was within 2.5 km of the Franklin, wind speed agreement was 0.03 m s^{-1}, but air temperature agreement was 0.4°C, specific humidity agreement was 0.5 g kg^{-1}, and incoming shortwave radiation agreement was 0.3 W m^{-2}. The data from the Electra and two P-3s were also compared to that from the IMET buoy. These comparisons led to an ongoing examination of the calibration of the longwave sensors on the aircraft.

Along with sea surface temperature the precipitation measurements made during COARE have received considerable attention in an effort to determine the accuracy that should be associated with various methods. Point rainfall measurements were made on the ships and buoys using volumetric gauges, such as the self-siphoning R. M. Young sensor and optical rain gauges (Scientific Technologies miniature optical rain gauge or ORG). Spatial maps of estimated rainfall were made every 10 min by the Doppler radars on the *Vickers* and *Xiangyanghong 5*. Initial comparisons suggested that rainfall estimates varied by a factor of 2, with various point gauges reporting 10 to 11 mm d^{-1} and the radars reporting 5 mm d^{-1} as the average over the IOP. Even among the point gauges, there were differences, and an initial impression was that the optical rain gauges overestimated the rainfall. However, over the course of the flux workshops, considerable progress was made in understanding how best to compare the diverse measures of freshwater flux available during COARE and the corrections that needed to be applied to each of these estimates [e.g. *Bradley and Walter*, 1996]. Underestimation by the volumetric gauges can be caused by the deflection of rain that should have fallen into the the gauge by airflow around the instrument [*Koschmeider*, 1934]. Correction of the siphoning gauges for wind effects can increase their values by as much as 70%, while correction of optical rain gauges for a lack of cosine response can decrease their reading by 20% or so. The optical rain gauges also have errors associated with calibration bias, variations in drop size distributions, and differences between the performance of individual instruments. Testing of the optical and siphon rain gauges was carried out to investigate these effects, and the optical rain gauges that survived the deployment were recalibrated.

Satellite and shipboard Doppler radar data provide valuable spatial coverage. The accuracy of the satellite rain data has been examined by intercomparison with ship radar rain data. Estimates done using outgoing longwave radiation (OLR) show that correlations increase with averaging area; averages over daily periods and 1.25° squares have correlation of over 0.7 with radar. The radar reflectivity is converted to rain rate by an algorithm which relates radar reflectivity Z to rain rate R. *Short et al.* [1995] and *Tokay and Short* [1996] developed a 2-by 2-km, 10-minute data set using two Z-R relationships, one relation for stratiform and one for convective rain. More recently, range-dependent gain corrections have been determined and applied. While there is little range dependence within 100 km of the radar, beyond that a quasi-exponentially increasing gain factor is now applied. This correction increased mean rainfall by ~12.5%. However, *Yuter and Houze* [1997] analyzed raindrop images obtained on flights of the NCAR Electra aircraft in COARE and found no statistically significant difference in the Z-R relation for radar-detectable convective and stratiform precipitation regions. More remains to be done to clarify the ship radar rain calibration. C. Leary has produced the highest-resolution rain maps (see the World Wide Web site http://rainfall.atmo.ttu.edu/toga.html). For comparison with surface rainfall measurements it was found to be important to take into account the time delay for rain at the height of the radar data (1 or 2 km, depending on the data set) to fall to the surface.

An additional source of information about rain over the IFA has been the estimation of surface precipitation as a residual of an atmospheric moisture budget. Table 2 summarizes various rainfall estimates (including ocean freshwater budget estimates, which are discussed in section 5.4). With the various corrections now applied, Table 2 shows much better agreement among certain estimates, particularly those that sampled the same location(s) for the same period of time. Among all the methods, however, instances of factor of 2 disagreement can be found. At the fourth workshop, there was a breakthrough in understanding this range in various leg-averaged rain rates. Differences were found in different atmospheric moisture budget estimates that could be attributed to the way in which different objective analysis techniques handle sparsely sampled data. Comparison of budget estimates from the IFA with similar estimates from the OSA led to a greater awareness of the spatial and temporal variability of rainfall in the COARE domain. Leg-averaged mean rain maps produced from the radar data by Paul Kucera [*Bradley and* Weller, 1996] showed that spatial differences in mean rain rate within the area sampled by the radar could be as large as an order of magnitude. Taking care to make sure that estimates were based on data from the same time period and location, as, for example, by extracting the radar rain rate from the 2-by 2-km location closest to one of the point gauges for a coincident interval, showed that agreement between the radar rain and the in situ data was much better than a factor of 2; they were typically within 25% of each other.

5.3. The Development of the Bulk Formulae and Intercomparison of the Fluxes

The initial approach to the development of bulk formulae suitable for use in the warm pool was to use coincident

Table 2. Comparison of Rainfall Estimates From Various Methods

Observer	Method	Cruise Leg	Day of Year Start	Day of Year End	Rate, mm d^{-1}
Fairall	*Moana Wave* optical	1	318.25	337.14	3.6
		2	354.49	10.81	17.4
		3	28.36	36.37	13.4
		all			11.3
Paulson	*Wecoma* optical	1	318.24	337.17	3.0
		2	353.8	10.81	16.4
		3	27.25	56.56	6.5
		all			8.9
Paulson	*Wecoma* funnel	1	318.24	337.17	2.0
		2	353.8	10.81	11.5
		3	27.25	56.56	4.4
		all			6.3
Bradley	*Franklin* optical	1	327	333	15.7
		2	336	349	16.2
		3	10	20	7.6
		4	22	35	4.7
		all			10.5
Rutledge et al.	MIT radar z = 2 km	1	317	345	3.7
		2	357	18	5.0
		3	30	54	4.5
		all			4.5
Leary and Doggett	MIT radar z = .85 km	1	316	345	3.2
		2	356.08	19	6.2
		3	29.73	54.81	4.7
		all			4.7
Short and Kucera	MIT/ TOGA radar; z = 2 km	1	310	346	3.6
		2	349	18	6.0
		3	25	53	3.9
		all			4.5
Johnson/ Ciesielski	Atmospheric budget MQD MIT area	1	317	345	5.6
		2	357	18	10.9
		3	30	54	4.2
		all			7.5
Johnson/ Ciesielski	Atmospheric budget MQD MIT/ TOGA area	1	317	345	2.9
		2	357	18	8.5
		3	30	53	2.2
		all			4.7
Feng	Ocean budget	1	323	335.64	4.2
		2	355	7.86	16.5
		3	28	44.35	5.0
		all			9.3

Comparison of rainfall estimates within the COARE inner intensive flux array defined as the region from 1°-3°S, 155°-157°E. The observations were taken during the intensive observation period from November 1, 1992, to February 28, 1993. Measurements were taken with volumetric (funnel) and optical rain gauges (ORGs) on the survey ships R/V *Wecoma*, *Franklin* and *Moana Wave*. The MIT radar was mounted on R/V *Vickers*, and the TOGA radar was mounted on R/V *Xiangyanghong 5*. Radar data were processed to yield rainfall estimates at 10-min intervals within 2-km pixels (MIT data set by Rutledge et al. and a combined MIT/TOGA data set by Short et al. Leary and Doggett produced high-resolution (0.25 x 0.25 km) rainfall maps. Johnson et al. estimated precipitation from atmospheric budgets for the MIT radar area and the combined MIT/TOGA radar area; MQD refers to the multiquadric method of analysis. Feng has analyzed the ocean freshwater budget in the upper 50 m to estimate precipitation minus evaporation, using the Wecoma evaporation measurements to obtain his rainfall estimates. All data and authors from *Bradley and Weller* [1996].

turbulent flux and mean surface meteorological observations made on the same platform to guide revisions to the transfer coefficients and parameterizations in the bulk formulae. *Fairall et al* . [1996a] took this approach and, while doing so, made the developing algorithms available for trial use by flux investigators with data from other platforms. This iterative process took place parallel with the efforts to understand the accuracy of the basic observables. Most recently, the *Moana Wave* turbulent fluxes were compared with the turbulent fluxes available from other ships and aircraft. This led to a final refinement of the algorithms.

The steps taken in the development of the algorithm have been reported by *Fairall et al.* [1996a]. Briefly, they include modifications to the stability dependent computation of the transfer coefficients as described by *Liu et al.* [1979], reduction of surface vapor pressure by 0.98 to account for the effect of the salinity, adding *Webb*'s [1982] corrections to the latent heat flux, multiplication of net radiation by 0.97 to account for emissivity of sea water, use of a surface albedo of 0.04, referencing the surface wind to the surface current, use of the mean wind speed rather than the magnitude of the vector wind, use of *Kristensen et al.*'s [1997] equations to correct for separation of vertical velocity and temperature or moisture sensors, and inclusion of the contribution to the sensible heat flux of fluctuating heat capacity due to variable atmospheric moisture. Correction of ship-measured near-surface temperature up to the surface, using a "warm layer-cool skin" approach with the warm layer determined from a simplified version of *Price et al.*'s [1986] mixed layer model, has also been included [*Fairall et al.*, 1996b]. The modifications to *Liu et al.* [1979] were the inclusion of *Charnock*'s [1955] roughness length, as suggested by *Smith* [1988]; change in the profiles for the stability dependence of temperature, moisture, and momentum in very unstable conditions to agree with the free convection limit of *Panofsky and Dutton* [1984]; use of a von Karman constant of 0.4 and of dimensionless scalar gradient functions with neutral values of 1.0, changes to the form of the neutral transfer coefficients to correct for *Liu et al.*'s [1979] use of a von Karman constant of 0.35, and inclusion of a gustiness algorithm for low wind conditions.

In the latest version, 2.5, of the COARE flux algorithm the exchange coefficients were reduced by 6%. Previously, it was thought to be necessary to account for the physical separation of the velocity, temperature, and humidity sensors, but comparison of the *Moana Wave* turbulent fluxes with aircraft fluxes indicated this correction was not

Table 3. Comparison of Time-Averaged Fluxes and Observables from R/V *Moana Wave*, R/V *Wecoma*, and the WHOI buoy.

Variable	Leg 1			Leg 2			Leg 3		
	Moana Wave	Buoy	*Wecoma*	*Moana Wave*	Buoy	*Wecoma*	*Moana Wave*	Buoy	*Wecoma*
SST, °C	29.45	29.55	29.57	28.88	29.00	29.00	29.06	29.18	29.25
Air temperature, *°C	28.00	27.92		27.38	27.30		27.70	27.86	
Air temperature, **°C		28.03	28.42		27.41	27.54		27.96	27.47
U, *ms^{-1}	3.39	3.40		5.70	5.77		6.27	6.21	
U, **ms^{-1}		3.43	3.18		5.86	5.93		6.31	6.35
Wind direction, deg	88.7	77.2	87.4	127.2	128.8	129.8	122.4	130.4	126.2
Specific Humidity,* g kg^{-1}		18.23	18.30		18.88	18.44		17.88	17.90
Specific Humidity,* g kg^{-1}	18.95	18.00		18.29	18.70		18.19	17.65	
Incoming longwave radiation, W m^{-2}	409.4	409.2	410.3	417.0	417.1	413.9	413.2	416.1	407.8
Incoming shortwave radiation, W m^{-2}	237.8	238.1	232.8	171.5	171.4	177.3	187.6	183.1	204.7
Skin temperature, °C	29.28	29.26	29.30	28.68	28.82	28.77	28.89	28.92	28.96
$\|\tau\|$, N m^{-2}	0.020	0.020	0.017	0.064	0.064	0.064	0.053	0.060	0.057
Q^{lat}, W m^{-2}	-89.7	-92.0	-86.0	-118.8	-113.3	-120.3	-137.5	-146.9	-149.6
Q^{sens}, W m^{-2}	-5.98	-6.96	-4.56	-8.38	-9.83	-9.09	-9.39	-9.11	-13.94
Net shortwave radiation, W m^{-3}	224.7	225.2	223.1	162.0	162.0	168.2	163.9	173.0	192.8
Net longwave radiation, W m^{-2}	-62.8	-63.0	-62.1	-52.0	-52.4	-55.5	-53.5	-54.3	-59.5
Q^{net}, W m^{-2}	66.2	63.0	70.3	-17.2	-11.61	-16.7	-36.6	-37.3	-30.2

Buoy variables at 3.5 m have been corrected to ship heights. Here τ is wind stress, and Q^{lat} and Q^{sens} are latent and sensible heat, respectively.

*At 8 m.

†At 15 m.

**At 20 m.

needed. Surface stress due to rain is also parameterized. Refinement to parameters used in the radiative fluxes, such as albedo and emissivity, results largely from the radiative flux measurements, including upward and downward looking shortwave, longwave, and all-wave radiometers, mounted out on a boom extending forward of R/V *Franklin*.

The means of the fluxes computed with this algorithm from *Wecoma* and the IMET buoy are compared with turbulent flux data from *Moana Wave* in Table 3, which also shows mean values of raw variables. SST was obtained from the ships' thermosalinographs, while skin temperature was obtained by adding a correction obtained from the COARE flux algorithm. The leg-averaged observables and surface fluxes agreed well. During leg 1, under low wind speeds and clear skies, net longwave radiation on the three platforms agreed to within 1.5 W m^{-2}. The sensible and latent heat fluxes and net shortwave radiation agreed to better than 2.5, 4.0, and 2.1 W m^{-2}, respectively. The wind stresses agreed within 0.0031 N m^{-2} or ~15%. The leg-averaged net surface heating agreed to within 4.2 W m^{-2} with the *Wecoma* fluxes on the high side due to the lower observed wind speeds and reduced latent and sensible heat losses. Leg 2 included the end of the December westerly wind burst and then a period of very low wind speeds. The shortwave radiation, longwave radiation and sensible heat fluxes each agreed to better than 6.2, 3.5, and 1.5 W m^{-2}, respectively. Very good agreement of the mean stress (0.0003 N m^{-2}) was observed. The latent heat flux from the buoy during leg 2 was lower than the ship estimates by about 9 W m^{-2} because of higher humidity and lower wind speed. The net heat flux estimates agreed to within 7 W m^{-2}. Leg 3 was the shortest with only 6 days of *Moana Wave* operation in the IFA. The difference in the net heat flux was 7.1 W m^{-2}; the difference observed in the surface wind stress during this leg was 0.0062 N m^{-2} or ~10%. Larger differences were seen in the separate components of the heat flux during leg 3 than during legs 1 and 2.

Comparisons of the fluxes have been done across the various platforms, ship, buoy, and aircraft. Initial differences between turbulent fluxes on other platforms and those on *Moana Wave* led to the revision of the algorithm to version 2.5. Uncertainties in the incoming longwave radiation data associated with calibration of the Eppley pyrgeometers were investigated and compared with estimates from radiative transfer models prior to the fourth flux workshop, where they were discussed in detail [*Bradley and Weller*, 1996]. This led to final corrections of between 0 and 8 W m^{-2} being applied to the various incoming longwave data sets collected in COARE.

All the foregoing has been concerned with flux parameterization at a point. However, AGCMs need fluxes averaged over grid boxes that are large compared to mesoscale phenomena. The mesoscale variability of surface fluxes induced by atmospheric convection has been studied [*Jabouille et al.*,1996a, b] by using three-dimensional cloud explicit simulations of two convective cases (November 26, 1992, and February 17, 1993) corresponding to different ambient surface wind conditions, namely light and moderate winds. Intense wind gusts generated by convective outflow were found mainly responsible for the enhancement of a factor of 2 for the latent heat flux and a factor of 3 for the sensible one, in the rainy regions. At the simulation domain scale (90 x 90 km) corresponding to a general circulation model (GCM) grid box, it was shown that convective activity significantly increased the averaged surface fluxes. Using the TOGA TAO buoy moorings, *Esbensen and McPhaden* [1996] estimated the mesoscale enhancement of monthly averaged surface fluxes. They found that this increase is due primarily to the lack of wind steadiness on subsynoptic time scales. They also confirmed that the flux increase is associated with periods of significant precipitation. The mesoscale enhancement of monthly averaged surface evaporation can reach 30% of the total surface evaporation. *Sun et al.* [1996] examined 27 NCAR Electra flight legs and obtained similar mesoscale enhancements for individual flight legs in the presence of well-organized convective cloud systems.

It is hoped that the good resolution of that variability in COARE will assist the development of better parameterization of the fluxes on the grid scale of the atmospheric general circulation models. Higher-resolution model runs may be done in the future, and both NCEP and ECMWF have expressed interest in collaboration with COARE investigators making use of the COARE data, investigating the use of the COARE bulk flux algorithm in the models, and developing a better understanding of the surface fluxes in COARE.

5.4. Confirmation of the Fluxes: Ocean Heat and Freshwater Budget

Oceanographic data from within the IFA is being used to examine closure of heat and freshwater budgets for TOGA COARE and thus to validate the overall consistency of all the estimates discussed above.

M. Feng's (personal communications 1997) ocean freshwater budget estimates for rainfall based on the *Wecoma* SeaSoar data are included in Table 2 and show an IOP mean rain rate that is within 5% of the *Wecoma* ORG rain rate. *Feng et al.* [1998] have performed complete budget analyses over a 19-day period covering ISO2, using data from the R/V *Wecoma* and R/V *Moana Wave*. The *Wecoma* SeaSoar data [*Huyer et al.*, 1997] were used to construct temperature and salinity gradients using simple linear regression relative to the central point. The gradients were combined with ADCP current data to generate estimates of horizontal advection; ADCP estimates of divergence were used for estimating vertical advection. The R/V *Moana Wave* measured ocean microstructure and surface meteorology while maintaining a station within 10 km of the IMET mooring. Measurements from the *Moana Wave* were used to construct estimates of radiant, turbulent, latent, and sensible heat fluxes as well as turbulent and surface salt fluxes. The total heat budget closed to better than 10 W m^{-2}, but rain rates needed to be reduced by 25% to achieve closure. E. Antonissen (personal communication, 1997) is performing similar analyses for the other cruises during COARE.

This work was complemented on several occasions by R/V *Franklin*. In each case a drifting buoy was deployed for a few days, with meteorological instruments on top and two current meters below the surface. The methodology was somewhat different from *Feng et al.* [1998], though the preliminary conclusions are that heat budgets do not always close to within the 10 W m^{-2} accuracy desired. There are a

number of possible causes; one is that near-inertial oscillations with vertical length scales of a few tens of meters complicate the estimation of vertical advection. Small-scale horizontal structure in salinity and temperature [e.g., *Tomczak*, 1995; *Soloviev and Lukas*, 1996, 1997b] can also create serious problems in estimating gradients.

5.5. The Remaining Challenge: Mapping the Flux Fields

Work to date has focused largely on assuring the accuracy of the mean and turbulence measurements, on developing the COARE bulk formulae, and on air-sea interaction studies using data from single platforms. Considerable progress has been made toward the air-sea interface-specific goals of providing a high quality flux data set, understanding the physics and thermodynamics of the interfacial exchange processes in low wind speeds, improving the formulae used to estimate net heat fluxes in the warm pool, and determining the magnitude of short time-scale variability of the fluxes. However, the final goal of the flux component of COARE, that of understanding the impact of the range of wind structures, from trade-wind regime through westerly bursts, on the ocean-atmosphere fluxes of heat, moisture, radiation, and momentum over the warm pool, will require that the flux fields be mapped in space and time. For the further analyses of data from the COARE IOP, this mapping is needed to bring together data from the multiple platforms and to consider the integrated influence of the fluxes on the ocean and atmosphere in the warm pool region. In addition, it is hoped that this work will provide the basis for improved accuracy in future maps of the air-sea flux fields for the region that might be produced by combinations of numerical weather prediction (NWP) models, mesoscale atmospheric models, and remote sensing methods.

The data available from the COARE field program is not evenly distributed in space and time, and recognition of the energetic spacescales and timescales is an important prelude to mapping the fields. Perhaps the most energetic spectral peak in the heat fluxes was at the diurnal period, and some of the work has focused on describing the diurnal cycles in convection, precipitation, and the heat fluxes. At the low end of the frequency spectrum, three intraseasonal oscillations (ISOs) were sampled during the IFA. A wide range of spatial scales was seen. *Chen et al.* [1996] identified a range of convective systems, ranging from the scales of 100-200 km or less of isolated convective systems to the 10,000-km scale of the ISO.

The resolution sought in the maps varies with application. The large-scale maps of fluxes will provide the context for work within the IFA. It will also be used in atmospheric heat and moisture budget studies, for forcing three-dimensional ocean models, and to study large scale air-sea interaction, and it will be compared with fluxes from atmospheric and coupled atmosphere-ocean models. Some of the most demanding requirements for mapping are those posed by ocean models that seek to replicate the response of the upper ocean. For these the diurnal cycle must be well resolved, and to capture the response to locally heavy rain and squall-like forcing events, the spatial gridding may need to be as fine as 1 km. Work is now underway, for example, using fluxes from a cloud-resolving atmospheric model [*Trier et al.*, 1996] to examine oceanic response to squalls. These fluxes were provided at 3-km spatial and 5-min temporal sampling.

The initial approach to the mapping will be one of building outward from the center of the IFA. Spatial domains to be addressed will include an array defined by the R/Vs *Wecoma and Moana Wave* and the IMET buoy; the region within 100 km of each of the ships with Doppler radar, *Vickers* and *Xiangyonghang 5*; and, finally, the IFA. In the time domain, work will address selected case studies of one to several days, individual ship legs (roughly 3 weeks in duration), and, ultimately, the duration of the IOP. At the smaller spacescales and timescales the surface observations; aircraft, shipboard radar, and satellite data; and fields from mesoscale atmospheric and NWP models will be used. At the larger scales, objectively analyzed surface data, satellite data, flux estimates from budget studies, and NWP fields will be used.

Clayson and Curry [1996] are investigating the development of flux estimates based on satellite data. Progress has been associated with the development of physical models for determining flux components from satellite-sensed quantities, the use of data from more than one sensor, the use of models of the atmosphere and upper ocean to determine parametric relationships, and the availability of the high- quality in situ flux validation data collected during COARE. A major source of error in the method remains the difficulty in accurately determining surface radiative fluxes from satellite; biases in the satellite incoming shortwave are as high as 44 W m^{-2}. Spatial variability in optical depth resulting from biomass burning in New Guinea is a major source of the error in satellite incoming SW radiation. Work also continues on refining satellite estimates of sea surface temperature. *Wick* [1995] has compared the AVHRR with radiometric sea surface temperatures from various aircraft and ships, finding the differences with the Cessna to be 0.4°C, with the *Vickers* to be -0.3°C, with the Jet Propulsion Laboratory (JPL) sensor on the Electra to be -0.4°C, and with one of the P-3 aircraft to be 0.05°C.

The COARE data set provides an important calibration point for existing satellite-based estimates of net shortwave radiation into the ocean [e.g., *Rossow and Schiffer*, 1991, *Bishop and Rossow*, 1991], which presently differ from one another by as much as 40 W m^{-2} on annual mean [*Chen et al.*, 1994b; *Seager and Blumenthal*, 1994]. *Waliser et al.* [1996] have used shortwave radiation data from the IMET mooring to estimate clear-sky shortwave radiation, a source of much of the error. Their COARE-average values from two methods were 310 and 315 W m^{-2}. These imply a mean reduction of shortwave radiation by clouds of -103 to -107 W m^{-2}. *Chou and Zhao* [1997] estimated the surface solar fluxes and cloud radiative forcing over the TOGA COARE domain showing that the fluxes for COARE may provide a useful database for climate process studies involving surface fluxes and SST changes.

In addition to satellites, numerical models offer the ability to provide large-scale coverage. The European Centre for Medium-Range Weather Forecasts (ECMWF) TOGA COARE special data set provides gridded surface meteorology and fluxes. These are compared to IMET observations in Table 4. Modeled 10 m winds were often

Table 4. Comparison of the Means From the Observations and ECMWF Analysis and Forecast Fields

	Westerley Wind Bursts		January Low-Wind Event		Squalls	
Variable	ECMWF	WHOI IMET	ECMWF	WHOI IMET	ECMWF	WHOI IMET
Air temperature, °C	28.78	27.71	27.74	27.64	28.57	27.95
SST, °C	29.34	28.99	29.09	29.42	29.33	29.18
$U10m$, ms^{-1}	6.32	7.38	2.33	2.19	5.13	6.17
Wind direction, deg	108.1	128.0	353.2	248.0	109.3	126.1
Specific humidity, g kg^{-1}	19.37	19.04	18.40	19.43	19.07	18.38
Barometric pressure, hPa	1008.0	1007.3	1009.5	1008.9	1009.5	1009.4
$\|\tau\|$, Nm^{-2}	0.0796	0.0919	0.0089	0.0109	0.0452	0.0626
τ_{east}, Nm^{-2}	0.0725	0.0658	-0.0010	-0.0029	0.0387	0.0468
τ^{north}, Nm^{-2}	-0.0242	-0.0486	0.0031	0.0001	-0.0170	-0.0319
Rain rate, mm h^{-1}	0.7	1.2	0.6	0.2	0.4	0.9
Q^{lat}, Wm^{-2}	-207.6	-142.79	-85.5	-56.0	-158.4	-145.1
Q^{sens}, Wm^{-2}	-11.7	-11.5	-7.9	-7.0	-10.2	-10.3
Q^{lw}, Wm^{-2}	-54.5	-51.6	-53.3	-57.9	-57.0	-51.8
Q^{sw}, Wm^{-2}	213.2	156.5	196.0	202.1	250.0	161.9
Q^{net}, Wm^{-2}	-60.6	49.3	49.3	81.3	24.4	-45.4

Wind stress magnitude, $|\tau|$; eastward wind stress, τ_{east}; northward wind stress, τ^{north}; latent heat flux, Q^{lat}; sensible heat flux, Q^{sens}; net longwave radiation, Q^{lw}; net shortwave radiation, Q^{sw},; and net heat flux, Q^{net}.

0.5-1 m s^{-1} lower, 0.4 m s^{-1} lower in the mean over the IOP, and month-averaged winds were directed 13° to 22° to the left of the observed winds. The model and the observed shortwave radiation had large differences, 30 to 60 W m^{-2}. Table 4 compares the means of the WHOI IMET buoy data and the ECMWF model (at the grid point closest to the buoy, 57 km to the northeast at 1.25°S, 156.25°E) over specific, shorter intervals, during the December westerly wind burst, during a period of low winds in January, and during short-lived, squall like wind events in late January and early February. The ECMWF model overestimated the net heat loss by 17% during the westerly wind bursts, indicated a net heat gain as opposed to the observed loss during the squalls, and underestimated the net heat gain by 59% during the low wind period. During the westerly wind burst the model latent heat loss was 64 W m^{-2} greater than the observed latent heat flux, but this error was largely offset by the model net shortwave radiation being 57 W m^{-2} too large. Similar overestimation by the model of the mean shortwave radiation (89 W m^{-2} too high) was seen during the squalls, but in this case this error was not offset by error in the estimation of the latent heat flux.

We believe that many of these flux discrepancies are due to the fact that a number of subgrid scale processes affecting cloud cover and MABL properties were not parameterized in the ECMWF model used in 1992, nor in any other AGCM, then or now. Indeed, a major purpose of COARE was precisely to identify such small-scale processes, and the causes of the discrepancies just referred to are now being actively investigated. However, the impact of the resulting flux errors on SST simulation is severe. Figure 34a shows the observed SST, and the SST as simulated by the *Price et al.* [1986] model, when driven with the observed fluxes (Figure 34b; see also Figures 32a and 32c). Figure 34c shows the simulated SST when the NWP fluxes are used. The amplitude of the simulated ISO-related SST variation is in this case too small by a factor of about 3, and its phase is poorly determined. If it turns out that the observed ISO-related SST variations of order 1°C affect AGCM simulations, then such problems with AGCM fluxes will need to be identified and corrected before coupled models can be expected to generate realistic ISOs.

In October 1995 a WCRP workshop was held at ECMWF to discuss air-sea flux fields for forcing ocean models and the validation of atmospheric general circulation models. Several COARE flux investigators participated, and the issues associated with what subgrid scale variability means for the NWP models was discussed.

The large-scale models do not now have the space and time resolution required, for example, to force ocean models for the purpose of studying local response to diurnal heating or to an isolated convective system. However, mesoscale atmospheric models are able to do so, producing surface flux fields with gridding down to 1 km. Cloud-resolving models coupled to ocean mixed layer models may provide a basis for improved parameterizations of convection, cloud microphysics, radiation transfer, and the atmospheric boundary layer. Such improved mesoscale models could

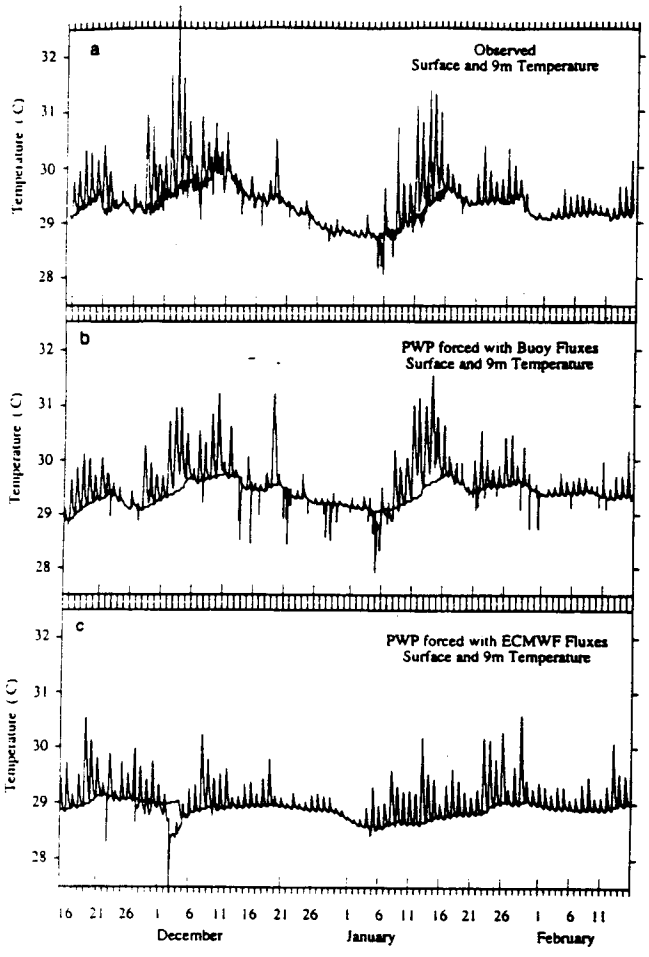

Figure 34. Comparison of (a) the observed near-surface temperature variability (0.45 and 9 m, with the shallower data showing the diurnal variability) with (b) the modeled variability using the observed fluxes and the *Price et al.* [1986] (PWP) model, and (c) using the ECMWF fluxes and the PWP model. From *Weller and Anderson* [1996].

then provide improved analyses of surface fluxes. Estimates of the low-level wind fields from the *Vickers* single-Doppler data will be valuable for checking them. Work will, in the near future, focus on simulations of case studies with cloud-resolving models and other mesoscale models and on four-dimensional data assimilation using mesoscale models. During this work, priority will be placed on the development of model parameterizations that correctly simulate physical processes. With these high-resolution models, it will be possible to study the mesoscale enhancement of monthly averaged fluxes, the effect of deep convection on fluxes, and the three-dimensionality of convection and the associated downdrafts.

The large-scale fields of fluxes will provide the context for the detailed observations made within the IFA. They will be used in atmospheric heat and moisture budget studies and in studies of large scale air-sea interaction and also for forcing three-dimensional ocean models. They will also allow validation of three-dimensional atmospheric and coupled atmosphere-ocean models. Because of the density and quality of the data within the IFA it is hoped that numerical models and satellite remote sensing techniques that have been validated by the TOGA COARE IOP data can then be used with good results in the tropics to determine the air-sea fluxes.

6. Modeling

6.1. Atmospheric Modeling

Modeling studies related to the COARE objectives can be considered as the way to synthesize all the atmospheric data collected during the field experiment. As such, numerous atmospheric modeling efforts are underway and will go on in the coming years. Use of cloud-resolving models, regional-scale models, and global circulation models have been found useful to address the multiscale and multiprocess issues of COARE. Some examples have already been mentioned in preceding sections.

Mesoscale simulations have allowed improvements in understanding the mesoscale organization of convection and its effect on the surface and troposphere. The convective organization in COARE has been found to be indeed more complex than for example in GATE (GARP Atlantic Tropical Experiment) [e.g., *Houze and Betts*, 1981]. One reason is that in the eastern Atlantic the convection is regularly forced by strong easterly waves moving westward from Africa. No such dominant and strong forcing was observed during COARE, though equatorially trapped waves were present. [*Pires et al*, 1997]. Cloud-resolving models have been able to simulate different convective organizations. *Trier et al.* [1996], *Wang et al.* [1996], and *Hong et al.* [1995] successfully simulated fast-moving squall lines organized perpendicular to the low-level shear. The simulations have shown that these systems are quite efficient in vertically redistributing heat, moisture, and momentum, as well as in enhancing the surface fluxes. Surface fluxes were found also to be important for the maintenance of such convective systems. Though still in earlier stages of development, coupled ocean-atmosphere mesoscale simulations have shown that active deep convection can regulate the sea surface temperature through ocean cooling processes [*Hong et al.*, 1995] and that the afternoon rain rate maximum in suppressed conditions seems to be a result of SST forcing [*Sui et al.*, 1998b]. Diurnally varying SST damped the amplitude of the rain rate significantly. *Redelsperger et al.* [1995a, b] looked at the initiation of a squall line observed by airborne radars [*Chong and Campos*, 1995] during the December preburst period. They were able to reproduce the formation of a convective line forming near a preexisting mesoscale convective system in a dissipating stage. A possible explanation for such initiation is the propagation of a gravity wave generated by the preexisting convective system (e.g., as derived by *Mapes* [1993]).

Radar observations indicate that shorter-lived, slower-moving convective lines were quite often organized along the low-level shear. *Guichard et al.* [1997] and *Jabouille et al.* [1996b] have successfully simulated such three-dimensional systems and have analyzed in detail the thermodynamical impact of these systems, as well as the modification of surface fluxes (see section 3.7). For such systems the convective vertical transport occurs on very fine scales (order of a kilometer), which puts into question some basic hypotheses assumed in existing convection

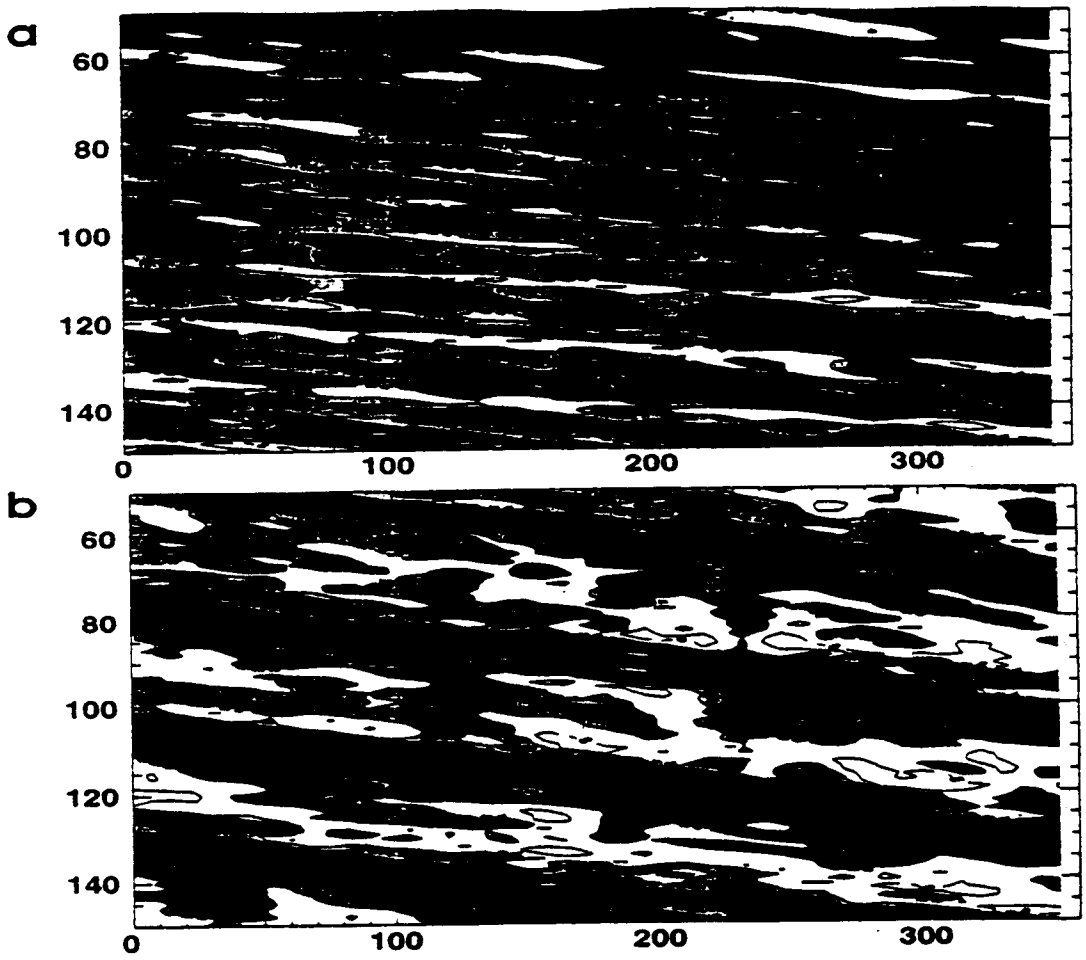

Figure 35. (a) Modeled zonal winds along the equator for an R15 AGCM running over an ocean-covered planet. SST is fixed. (b) same as for Figure 35a, but SST rises in easterly conditions and falls in westerlies, according to empirical rules derived from COARE observations. From *Flatau et al.* [1997].

parameterizations. One important result confirmed by aircraft measurements is the existence of density equilibrium (weak variations of mean buoyancy between cloud and environment) [*Lucas et al.*, 1994]. *Wu and Moncrieff* [1996] have looked at the collective effects of a two-dimensional squall line on the environment, as observed during the onset stage of the December westerly burst. They found that the shear generation of kinetic energy was comparable to the buoyancy generation and dominated the sum of buoyancy and water-loading generation. As a consequence, shear generation should also be included in convective parameterization. In some cases the large extent of some observed clusters precludes the use of cloud-resolving models. Instead, regional models are used with convective parameterization. *Holt and Raman* [1994] used a triple-nested model to look at the regional variability of surface fluxes. Over a 10-day period they found large variations of surface latent and sensible fluxes related to the convective cloud occurrence.

Precipitating convective cloud systems observed during COARE have also been studied through the framework of the GEWEX Cloud System Study (GCSS) [*Moncrieff et al.*, 1997]. This international effort is mainly based on multiday simulations performed with cloud-resolving models. The goal is to focus on the environmental effects of cloud systems as they respond to changes in atmospheric large-scale tendencies and sea surface conditions. The first workshop of model intercomparison has shown the consistency of results among models. It confirms that the bulk characteristics of convective systems are largely determined by the large-scale tendencies. This result is important since these tendencies are explicitly resolved in GCMs. Parallel to this ongoing effort, operational analysis and forecasts from ECMWF, NCEP, JMA and the Australian Bureau of Meteorology (BOM) have been extensively used by COARE researchers. *Moncrieff and Klinker* [1998] looked at the realizations of superclusters during the December westerly burst in the ECMWF T213 operational forecasting model. A supercluster-sized system having a structure analogous to a mesoscale system was well predicted but with a scale much larger than in the real atmosphere. Contrary to the assumption of scale separation used in all convective parameterizations, the transports, sources and sinks are part resolved and part parameterized. This problem leads to systematic errors in the forecasts, suggesting that physically based parameterizations of

organized convection may be required for climate models. Statistics of the differences between COARE observations and ECMWF operational analyses [*Nuret and Chong*, 1996] show a systematic underestimation of the analyzed wind speed around 1 m s^{-1}, reaching 2 m s^{-1} at the easterly jet level. Humidity was also found too dry in the midtroposphere and too moist in the low troposphere. Reanalyses are currently being performed at NCEP and ECMWF encompassing the COARE IOP, using a comprehensive observation data set and recent improvements of modeling and analysis systems. As an example, the humidity field, considered as a key feature in the tropics, is considerably better in the ECMWF reanalysis than in the operational model output, mainly because of a new cloud prognostic scheme.

One modeling result directly addresses the question of whether SST variations are an essential part of the ISO mechanism. *Flatau et al.* [1997] use data from COARE and the TAO array to obtain an empirical relation between the rate of change of SST and convection (SST warms to the east of the convection and cools to the west of it). They find that if this relation is not used in their "aquaplanet" AGCM, equatorial wind fluctuations over their (water-covered) globe have the character of Kelvin waves propagating around the globe with a phase speed of about 20 m s^{-1} (Figure 35a). With the SST relationship included, the waves slow down to about 15 m s^{-1}, and the winds strengthen, become more organized and acquire a quite well-defined 25-30-day periodicity (Figure 35b). While the model is idealistic and does not reproduce the greater slowing to about 4 m s^{-1} observed over the warm pool region, the results suggest that the observed ISO-related SST changes may feed back strongly onto the atmosphere.

6.2. Ocean Modeling

Most of the ocean modeling studies pertinent to the scientific objectives of COARE have been targeted at the response of the western Pacific warm pool to momentum and/or buoyancy forcing. A suite of one-dimensional mixed layer and three-dimensional ocean circulation models has been used to enhance understanding of the oceanic response to energetic westerly wind bursts and heavy precipitation. The heat budget of the warm pool, the downstream effects of forcing within the warm pool, and the barrier layer hypothesis of *Lukas and Lindstrom* [1991] are among the topics of many of the modeling studies to date. More recently, some ocean modeling studies to examine the effect of ISO activity on SST have been undertaken.

Prior to COARE, one-dimensional mixed layer models were used to demonstrate how a stable rain-induced mixed layer ("freshwater lens") could serve to insulate the deeper portions of the water column from changes in the surface fluxes of momentum and heat. *Miller* [1976] and *Price* [1979] illustrated how rainfall over tropical and subtropical oceans can play a key role in determining the temperature and depth of the mixed layer. *Chen and Rothstein* [1991] pursued this line of research to invoke a local forcing argument for the existence of the barrier layer. In this study the effects of idealized intermittent westerly wind bursts and episodic rainfall were analyzed within the context of a one-dimensional mixed layer model. It was demonstrated that a shallow isohaline surface layer could be formed in response to forcing by precipitation-evaporation (P-E). As a result, the deep thermocline became insulated from the surface layer by a barrier layer within which there was no active turbulent mixing.

Shinoda and Lukas [1995] utilized a Lagrangian mixed layer model in comparison studies with results from an Eulerian mixed layer model to highlight how the horizontal advection of saline waters from the central Pacific makes an important contribution to maintaining the thermohaline structure within the warm pool. *Webster* [1994] performed a series of sensitivity studies by varying the wind, precipitation, and solar radiative forcing of a mixed layer model. For realistic changes in either wind (5-10 m s^{-1}) or cloudiness effects (400-800 W m^{-2}) the overall influence on SST changes was approximately the same at 0.3°-0.4°C per 5 days. However, considerable surface cooling was noted (~1°-2°C per 5 days) when heavy precipitation was accompanied by reduced solar radiation. More recently, *Anderson et al.* [1996] used the IMET time series to demonstrate a subtle dependence of SST on rainfall, as discussed earlier. *Li et al.* [1998] analyzed the observed and simulated upper ocean response to rain, wind, and solar forcing in terms of variation of the Monin-Obukhov length scales.

These studies clearly demonstrated the potentially important role of freshwater forcing and a realistic treatment of salinity within the context of mixed layer models. The work of *Cooper* [1988] was the first to address the importance of salinity in a three-dimensional context for tropical ocean circulation. Although these experiments with and without salinity were performed with an OGCM for the Indian Ocean, there was considerable relevance to COARE. The incorporation of salinity was found to influence the thermal field, dynamic topography, and the vertical stability of the water column. The changes to SST ranged between 0.5° and 2°C, and geostrophic currents differed by 10-40 cm s^{-1} as a result of the inclusion of salinity.

Yet, during most of the TOGA decade, little progress was made at incorporating active hydrological forcing into circulation models of the tropical Pacific Ocean. Most ocean modeling studies related to surface forcing in the western Pacific have focused solely on the locally and remotely forced response to momentum and heat fluxes. For example, *Harrison and Giese* [1988] and *Giese and Harrison* [1991] showed how idealized westerly wind bursts within the western Pacific warm pool could have a significant effect on SST downstream within the equatorial waveguide. *Kindle and Phoebus* [1995] forced reduced-gravity models with analyzed fields of surface wind stress observations to simulate successfully the intense Kelvin wave activity radiating out of the western Pacific in response to a series of westerly wind bursts.

Gent [1991] used the sigma-coordinate model of *Gent and Cane* [1989] to study the annual mean heat budget for the warm pool region. It was concluded that contrary to previous climatologically based estimates, the annual mean heat flux for the warm pool was near zero. With the advent of COARE and the emphasis on the buoyancy forcing of the warm pool, explicit consideration of P-E forcing in models of the tropical Pacific Ocean became a reality. D. Chen et al. (The response of the thermocline structure in the western equatorial Pacific to combined momentum and buoyancy forcing, submitted to the *Journal of Geophysical*

Research, 1997) used a version of the *Gent and Cane* [1989] model upgraded with an embedded hybrid mixed layer model [*Chen*, 1994a] and active hydrology to examine various hypotheses for the barrier layer. In response to idealized episodic westerly wind bursts and rainfall the structure and variability of the thermohaline fields in the warm pool compared favorably with available observations. Zonal advection, meridional advection, as well as local forcing, and vertical mixing were all deemed to be important for the maintenance and variability of the unique thermohaline structure in the warm pool. It was also demonstrated that while westerly wind bursts could generate large downstream disturbances in both dynamic and thermal fields through the propagation of equatorial waves, the effect of broad-scale precipitation was confined to the forcing region. *Roemmich et al.* [1994] investigated the potential of zonal gradients in salinity to be responsible for inducing a freshwater-forced equatorial jet. Analytical results suggest that vertical shears in the zonal pressure gradients may generate a vertically sheared eastward freshwater jet that is analogous to the Yoshida jet forced by westerly wind events.

Accurate simulation of sea surface temperatures is a crucial problem for coupled modeling. *Seager and Blumenthal* [1994] and *Chen et al.* [1994b] found that provided a realistic mixed layer model was used, the amount of heat flux modification needed to eliminate the annual mean SST errors in the model was comparable to the annual mean uncertainty among the various surface heat flux products used. However, those uncertainties were substantial (>20 W m^{-2}), suggesting that the limit on obtaining accurate SSTs in ocean models is at least as much due to uncertainties in currently available flux data sets as to problems with ocean physics.

In general, most of the COARE-related ocean modeling studies to date have relied on idealized or climatological forcing functions. An important exception has been the operational OGCM run at the National Center for Environmental Prediction (NCEP). The 4-dimensional assimilated fields of ocean temperature and velocity have provided an enhanced temporal context for the four month COARE IOP and a spatial context encircling observations taken within the COARE IFA [*Lukas et al.*, 1995]. This expanded space-time scale perspective afforded by the OGCM fields has provided COARE investigators with a much better appreciation for the upstream and downstream conditions surrounding the in situ observations taken during COARE. With the generation of special flux products for the COARE domain, an entire series of model-based process oriented, simulation, and parameterization studies is anticipated for the western Pacific warm pool.

Finally, a recent study has focused on the role of the ocean in ISO episodes. *Kessler et al.* [1995] examine an idealized model of the role of intraseasonal oscillations in moving the warm pool eastward; they developed a nonlinear ordinary differential equation, which accounts fairly well for the observed eastward expansion of the warm pool in 1991-1992.

7. Discussion and Conclusions

Deep atmospheric convection over the warm pool affects the global climate in a variety of ways. (Its counterpart, deep oceanic convection in polar regions, also affects the global oceans, but the physics of oceanic and atmospheric deep convection are extremely different, e.g. contrast this article with work by *Killworth* [1983].) Deep atmospheric convection is the primary determinant of the height of the tropopause, and interannual variations of warm pool convection are reflected in interannual climate variations around the globe. Deep atmospheric convection must be thoroughly understood and parameterized if accurate modeling of climate variability and climate change is to be achieved.

7.1. Highlights of COARE

Highlights of COARE work so far, that have expanded on what was known earlier, have been as follows.

1. COARE work has provided a detailed documentation of the relationships between changes in wind, SST, lower-tropospheric moisture content and vertical distribution, and convection onset in ISO events; the depth of the MABL has been shown to be small (300-800 m); and the prominent tradewind and melting-level stable layers has been documented, along with their effects on cloud populations (sections 2.2 and 2.3).

2. There is better documentation of the relation of rain, ice, and cloud cover (sections 3.2 and 3.3), and improvements in rain rate-radar reflectivity relations (section 3.6).

3. Two distinct modes of divergence have been discovered, corresponding to convective and stratiform rain. This implies a "gregarious" nature of convection (section 3.4).

4. Detailed documentation of convective organization has been obtained in a few cases (section 3.5), and precipitating cloud population statistics have been determined from ship-based radar (section 3.2).

5. Understanding of MABL modification by convective downdrafts has been improved (section 3.7).

6. Improved time cluster tracking techniques have been used (section 3.8) to elucidate the complex diurnal cycle (and bidiurnal cycle) of convection under suppressed and active conditions (section 3.9), and several wave types have been documented (section 3.10).

7. It has been demonstrated that with an accurate flux data set, the observed COARE SST time history can be rather well simulated by a one-dimensional model (section 4.1), but that advection by Yoshida jets and perhaps by eddies; light absorption by phytoplankton; and the combined effects of freshwater input and water transparency all need attention if SSTs are to be predicted accurately (section 4.2).

8. A sobering variety of instrumental problems have been discovered and corrected, in evaluating accurate fluxes (section 5.2), and improved algorithms have been developed for turbulent fluxes at a point and on average over an AGCM grid square (section 5.3).

9. We report progress in closing ocean heat and freshwater budgets (section 5.4), and in the use of remotely sensed data to map surface fluxes; but we document severe problems with present NWP flux estimates (section 5.5).

10. Some aspects of mesoscale convection events have been realistically modeled, and it has been demonstrated in an idealized model that realistic ISO variations in SST appear to organize and strengthen the ISOs (section 6.1).

11. The effects of salinity advection on thermohaline structure and SST have been modeled, along with an

idealized model study of ocean nonlinear response to ISOs; and we report progress in developing ocean data assimilation specific to COARE needs, (section 6.2).

7.2. Future of COARE

The scope of COARE research is enormous. This report summarizes the initial stages of a long interdisciplinary effort to understand ocean-atmosphere interactions over the warm pool. In the long term we expect that analysis of COARE data will lead to (1) improved understanding of the linked processes of convection, turbulent fluxes, and radiative fluxes over the warm pool; (2) embodiment of that understanding in parameterizations, for use in numerical models; (3) improved accuracy in remotely sensed estimates of convection and fluxes; (4) improved understanding of the oceanic processes controlling SST change in the warm pool; (5) improvements in the understanding of ISOs; and (6) improvements in coupled models.

The achievement of each of these is interlinked. For example, plans for point 4 include the running of data-assimilating ocean models, with nested high-resolution regions over the COARE IFA. One product of such models should be an estimate of the net surface heat flux that the ocean model needs to generate the observed SST changes, as a function of space and time during the IOP. This will be a valuable quality control points for 2 and 3. Progress in points 1-4 will lead, naturally, to progress in the last two objectives. However, there is still a massive amount of observational analysis to be done to achieve these objectives, and, of course, the numerical modeling work is only beginning. A partial list of the tasks needed to achieve the objectives 1-6 above is given in 7.3 below.

The key to the success of the many remaining observational tasks in COARE is to be able to integrate the data from diverse platforms and sensors. Much of the multisensor fusion is sufficiently complex (either in terms of volumes of data involved, complexity of analysis techniques employed, or both) that not many examples have yet appeared in the formal literature; hence the large size of the observational component of Section 7.3.

Simultaneously with this, the essential new findings must be embodied into algorithms for use in AGCMs (mesoscale and global), OGCMs and CGCMs, and the efficacy of these algorithms must be validated. This validation will require coordinated activity by the original observational scientists; ocean modelers, and atmospheric modelers working on both the mesoscale and global scales. This effort will require ongoing planning, for it is highly likely that it will need several iterations and occupy a number of years. A COARE Modeling Workshop will be held in July 1998 to start the transition of COARE results into climate models.

One major challenge for COARE scientists will be to maintain, strengthen, and broaden the links across disciplines that have grown up over recent years. This will be difficult without the stimulus of the IOP. However, the work reported here has been characterized by painstaking and interdisciplinary attention to quality of products. In view of the complexity of the phenomena studied in COARE it is absolutely essential that this careful, interdisciplinary approach should continue through to the final stages of COARE.

7.3. Partial List of Tasks for Completion of COARE Analysis

7.3.1. Pure observational data analyses. The following list details various observational tasks that must be performed to fully analyze the remaining data.

1. There must be a combination of multichannel radiometric measurements from overflights of convective systems with volumetric flow/precipitation patterns provided by turboprop aircraft; these studies will assist the effective use of the TRMM satellite
2. The processes leading to the moistening of the lower troposphere must be analyzed and quantified, before an ISO active period; what is its relation to the "warm rain" process? can it be parameterized?
3. An understanding of how the upper ocean data in the western tropical Pacific must be analyzed to understand how the warm pool integrates in space and time the heat, freshwater, and momentum inputs from the atmosphere
4. Remote sensing data and COARE experience must be used to analyze what causes the outbreak of deep convection at the eastern end of each sequence of westward propagating disturbances in Plate 2
5. COARE aircraft data should be analyzed for spatial/temporal variability of precipitation within larger convective systems undersampled by shipborne radars, for purposes of better description of means through which the patchy surface salinity distribution is established
6. Flight level thermodynamics should be interpreted in the context of two-and three-dimensional wind fields provided by multiple-Doppler radar at lower levels. Owing to the inherent nonlinearity of air-sea transfer processes, particularly in the presence of very warm SSTs and light synoptic-scale winds that predominate in the COARE region, it is important to quantify the phasing of intermittent mesoscale perturbations of near-surface flow and modified boundary layer thermodynamics to assess their impact on the larger scale
7. The potentially significant role of organized convective systems in contributing to the overall momentum budget of the region needs to be analyzed, along the lines described by *Esbensen and McPhaden* [1996].
8. Doppler-estimated vertical motions and shearing instabilities atop MCSs need to be evaluated, as a follow-on to Stratospheric-Tropospheric Exchange Project (STEP). They may have implications for stratospheric-tropospheric exchange.
9. An investigation is needed of the degree to which boundary layer or possibly even SST modification by precipitating mesoscale systems interplay with the diurnal cycle so as to modulate convection on a 1-2 day timescales [e.g., *Chen and Houze* 1997]; advanced radiometric SST measurements obtained by the NCAR Electra aircraft in conjunction with precipitation data from scanning Doppler radar may conceivably shed additional light on this issue
10. Convective modes (namely, degree of mesoscale organization, intensity/orientation/propagation of convective precipitation features) need to be related to observed environmental conditions (e.g., ambient large-scale thermodynamics/shear, interactions with "nearby" convection comprising timeclusters), especially through exploiting long-term measurements provided by shipborne Doppler radars
11. The role played by advection in the evolution of

SST needs to be evaluated, on ISO and ENSO timescales within the warm pool, compared to the role of local fluxes

12. The analyses of a full spectrum of case studies of the coupled system needs to be completed, including quiet, clear blue sky days as well as those characterized by strong convection

13. High-resolution SST and wind maps need to be obtained for IFA and COARE domain.

7.3.2. Observations and mesoscale modeling. To facilitate the development of mesoscale modeling, in close conjunction with observational data, the folowing steps are needed.

1. A coupled boundary layer science working group should be formed.

2. A coupled boundary layer approach is needed, to further studies of air-sea interaction in the warm pool.

3. Detailed observational/numerical treatments need to be extended beyond one or two fast-moving squall lines of questionable representativeness; the role of systems embodying slow-moving or diverse combinations of convective modes needs to be evaluated.

4. The structure of convective systems in relation to the shear and stability of the atmosphere and ocean surface conditions needs to be evaluated in relation to the dominant wave modes in the tropical large-scale circulation (Kelvin waves, Rossby waves, mixed Rossby-gravity waves, inertio-gravity waves)

5. The in situ observations at the interface and in both boundary layers need to be synthesized with mesoscale observations and analyses, and with theoretical and modeling efforts

6. Mesoscale ocean and atmosphere data assimilation techniques need to be developed.

7.3.3. Atmospheric general circulation models. Two COARE-related tasks with AGCMs are as follows.

1. The TOGA COARE bulk flux algorithms need to be adapted for use in atmospheric models, both those for NWP and those with higher space/time resolution.

2. The performance of NWP models needs to be tested, with and without data assimilation, but with observed SST on short timescales, for simulating observed cloud cover, surface temperature, humidity, winds, and hence surface fluxes. Major consistent errors need to be diagnosed and (in conjunction with mesoscale modellers) corrected.

7.3.4. Ocean general circulation models. A corresponding set of tasks for OGCMs are as follows.

1. OGCMs need to be checked to see if they get the observed SST and current response, locally and remotely, when forced with observed fluxes during COARE.

2. Basin-scale assimilation analyses need to be compared with COARE observations.

3. Present estimates of ocean mixing in mixed layer models need to be compared with direct COARE observations of mixing, to test the adequacy of present parameterizations.

4. The influence of three-dimensional circulation on vertical mixing in the upper ocean needs to be characterized and quantified.

7.3.5. Coupled model experimentation. Finally, some COARE-related tasks with coupled models are as follows.

1. The sensitivity of the coupled system to initial conditions in the warm pool should be examined.

2. Observing system simulation experiments should be performed, for long-term monitoring.

3. The impact of east Asian winter monsoon on ENSO onset needs to be tested.

Acknowledgments. COARE scientists owe a massive debt to David Carlson and his team for their dedication and hard work throughout the IOP and over the preceding years and to R. Chinman and the staff of the International TOGA COARE Project Office for their efforts over several years in turning the results of the field experiment into a flexible, comprehensive, easily accessed data set. Thanks also to A. Busalacchi for providing input to Section 6.2; to B. Smull and S. Chen for many helpful comments on the manuscript; to M. J. McPhaden and W. Kessler; and to the TAO Project Office, for providing Figure 2 and detailed comments. Thanks are also due to S. Rutledge and E. Antonissen and to numerous COARE scientists for providing preprints and comments.

References

Adler, R.R., H.Y.M. Yeh, N. Prasad, W.K. Tao and J. Simpson. Microwave simulations of tropical rainfall systems with a three-dimensional cloud model, *J. Appl. Meteor ol., 30*, 924-953, 1991.

Alados-Arboledas, L., J. Vida, and J.I. Jimenez. Effects of solar radiation on the performance of pyrgeometers with silicon domes. *J. Atmos. Oceanic Technol., 5*, 666-670, 1988.

Anderson, S.P., and M.F. Baumgartner, Radiative heating errors in naturally ventilated air temperature measurements made from buoys, *J. Atmos . Oceanic Technol.*, 15, 157-173, 1998.

Anderson, S.P., R.A. Weller, and R. Lukas. Surface buoyancy forcing and the mixed layer of the western equatorial Pacific warm pool: Observations and 1-D model results. *J. Clim., 9*, 3056-3085, 1996.

Bell, G.D., and A.N. Basist, The global climate of December 1992-February 1993, Warm ENSO conditions continue in the tropical Pacific; California drought abates, *J. Clim., 7*, 1581-1605, 1994.

Bishop, J.K.B., and W.B. Rossow, Spatial and temporal variability of global surface solar irradiance, *J. Geophys. Res., 96*, 16,839-16,858, 1991.

Bradley, E.F., and R. Weller (Eds) *Third Workshop of the TOGA-COARE Air-Sea Interaction (Flux) Working Group, East-West Center, University of Hawaii, Honolulu USA, 2-4 August 1995*, TOGA-COARE International Project Office, University Corporation for Atmospheric Research 1995a.

Bradley, E.F., and R. Weller (Eds) *Joint Workshop of the TOGA COARE Flux and Atmospheric Working Groups. Boulder, Colorado, USA, 11-13 July 1995*, TOGA-COARE International Project Office, University Corporation for Atmospheric Research, 1995b.

Bradley, E.F., and R. Weller, (Eds) *Fourth Workshop of the TOGA COARE Air-Sea Interaction (Flux) Working Group. Woods Hole Oceanographic Institution, Woods Hole, MA USA, 9-11 October 1996*, TOGA-COARE International Project Office, University Corporation for Atmospheric Research, 1996.

Bradley, E.F., P.A. Coppin, and J.S. Godfrey, Measurements of sensible and latent heat flux in the western equatorial Pacific Ocean, *J. Geophys. Res., 96*, suppl., 3375-3389, 1991.

Bradley, E. F., J. S. Godfrey, P. A. Coppin, and J. A. Butt. Observations of net heat flux into the surface mixed layer of the western equatorial Pacific Ocean. *J. Geophys. Res., 98*, 22,521-22,532, 1993.

Cane, M.A., and S.E. Zebiak, A theory for El Nino and the Southern Oscillation, *Science, 228*, 1084-1087, 1985.

Chang, C.P., and K.G. Lim Tropical-midlatitude interactions over Asia and the western Pacific Ocean during the 1983/84 northern winter, *Mon. Weather. Rev., 113*, 1345-1358, 1985.

Charnock, H., Wind stress on a water surface, *Q. J. R. Meterol. Soc., 81*, 639-640, 1955.

Chen, D., and L.M. Rothstein, Modeling the mixed layer structures of the western equatorial Pacific. *TOGA Notes 2*, pp.13-16, Oceanogr. Cent., Nova Southeastern Unit. Dania, Fla., 1991.

Chen, D., L. Rothstein, and A. Busalacchi, A hybrid vertical mixing scheme and its application to tropical ocean models, *J. Phys. Oceanogr., 24*, 2156-2179, 1994a.

Chen, D., A.J. Busalacchi, and L.M. Rothstein, The roles of vertical mixing, solar radiation, and wind stress in a model simulation of the sea surface temperature in the tropical Pacific Ocean, *J. Geophys. Res., 99*, 20,345-20,359, 1994b.

Chen, S.S., and Robert A. Houze Jr., Diurnal variation of deep convective systems over the tropical Pacific warm pool. *Q. J. R. Meteorol. Soc.* , 123, 357-388, 1997.

Chen, S.S., R.A. Houze, B.E. Mapes, S.R. Brodzik, and S.E. Yuter. TOGA COARE satellite data summaries available on the World Wide Web., *Bull. Am. Meteorol. Soc., 76*, 329-333, 1995.

Chen, S.S., R.A. Houze Jr., and B.E. Mapes, Multiscale variability of deep convection in relation to large-scale circulation in TOGA COARE, *J. Atmos. Sci., 53*, 1380-1409, 1996.

Chong, M., and C. Campos, Characteristics of the tropical convective cloud system observed on the 12 December 1992 during TOGA-COARE. Paper presented at the 21st Conference on Hurricanes and Tropical Meteorology, Am. Meteorol. Soc., Miami, Fla., April 24-28, 1995.

Chou, M.D., and W. Zhao, Estimation and model validation of surface solar radiation and cloud radiative forcing using TOGA COARE measurements, *J. Clim., 10*, 610-620, 1997.

Clayson, C.A., and J.A. Curry, Determination of surface turbulent fluxes for TOGA COARE: Comparison of satellite retrievals and in situ measurements, *J. Geophys. Res., 101*, 28,515-28,528, 1996.

Cooper, N.S., The effect of salinity on tropical ocean models, *J. Phys. Oceanogr., 18*, 697-707. 1988.

Cronin, M.F., and M.J. McPhaden, The upper ocean heat balance in the western equatorial Pacific during September-December 1992, *J. Geophys. Res.,102*, 8533-8554, 1997.

Ding, Y.H., and A. Sumi, Large-scale atmospheric circulation features during TOGA-COARE IOP, *J. Meteorol. Soc. Jpn., 73*, 339-351, 1995.

Eldin, G., T. Delcroix, C. Henin, K. Richards, Y. du Penhoat, J. Picaut and P. Rual, The large-scale structure of currents and hydrology along 156°E during the COARE Intensive Observation Period. *Geophys. Res. Lett., 21*, 2681-2684, 1994.

Emanuel, K.A., An air-sea interaction model of intraseasonal oscillations in the tropics. *J. Atmos. Sci., 44*, 2324-2340, 1987.

Esbensen, S.K. and M.J. McPhaden, Enhancement of tropical ocean evaporation and sensible heat flux by atmospheric mesoscale systems, *J. Clim., 9*, 2307-2325, 1996.

Fairall, C.W., E.F. Bradley, D.P. Rogers, J.B. Edson, and G.S. Young, Bulk parameterization of air-sea fluxes for Tropical Ocean-Global Atmosphere Coupled Ocean-Atmosphere Response Experiment, *J. Geophys. Res., 101*, 3747-3764, 1996a.

Fairall, C.W., E.F. Bradley, J.S. Godfrey, G.A. Wick, J.B. Edson, and G.S. Young, Cool- skin and warm layer effects on sea surface temperature, *J. Geophys. Res., 101*, 1295-1308, 1996b.

Feng, M., P. Hacker, and R. Lukas. Upper ocean heat and salt balances in response to a westerly wind burst in the western equatorial Pacific during TOGA COARE, *J. Geophys. Res.*, in press, 1998.

Flatau, M., P.J. Flatau, P. Phoebus, and P.P. Niiler, The feedback between equatorial convection and local radiative and evaporative processes: the implications for intraseasonal oscillations, *J. Atmos. Sci., 54*, 2373-2386, 1997.

Gadgil, S., P.V. Joseph, and N.V. Joshi, Ocean-atmosphere coupling over monsoon regions, *Nature, 312*, 141-153, 1984.

Gent, P.R., The heat budget of the TOGA-COARE domain in an ocean model, *J. Geophys. Res. ,96*, suppl, 3323-3330, 1991.

Gent, P.R., and M.A. Cane, A reduced gravity, primitive equation model of the upper equatorial ocean, *J. Comput. Phys., 81*, 444-480, 1989.

Giese, B.S., and D.E. Harrison, Eastern equatorial Pacific response to three composite westerly wind types, *J. Geophys. Res., 96*, Suppl., 3239-3248, 1991.

Gill, A.E., and E. Rasmusson, The 1982-83 climate anomaly in the equatorial Pacific, *Nature, 306*, 229-234, 1983.

Gill, G.C., Comparison testing of selected naturally ventilated solar radiation shields, report, contract NA-82-0A-A-266, Nat., Data Buoy Cent., Stennis Space Center, Miss., 1983.

Godfrey, J.S., and E.J. Lindstrom, The heat budget of the equatorial western Pacific Ocean, *J. Geophys. Res., 94*, 8007-8017, 1989.

Godfrey, J.S., M. Nunez, E.F. Bradley, P.A. Coppin, and E.J. Lindstrom, On the net surface heat flux into the western equatorial Pacific. *J. Geophys. Res., 96* suppl, 3391-3400, 1991.

Godfrey, J.S., E.F. Bradley, J.A. Butt, P.A. Coppin, I. Helmond, T.J. McDougall, and L. Pender, Measurements of upper ocean heat budget near a drifting buoy during the TOGA-COARE experiment, paper presented at the International Scientific Conference on Tropical Oceans - Global Atmosphere, World Meteorol. Organ., Melbourne, Australia, April 2-7, 1995.

Graham, N.E., and T.P. Barnett, Sea surface temperature, surface wind divergence and convection over tropical oceans, *Science, 238*, 657-659, 1987.

Guichard, F., J.P. Lafore, and J.L. Redelsperger. Thermodynamical impact and internal structure of a tropical convective cloud system, *Q. J. R. Meteorol. Soc.*, 123, 2297-2324, 1997.

Gutzler, D.S., G.N. Kiladis, G.A. Meehl, K.M. Weickmann, and M. Wheeler, The global climate of December 1992-February 1993, Large-scale variability across the tropical western Pacific during TOGA COARE, *J. Clim.*, *7*, 1606-1622, 1994.

Hacker, P.W., and R. Lukas, Spinup of a submesoscale eddy in the TOGA COARE intensive flux array during the spindown of an intense eastward jet, paper presented at the IAPSO XXI General Assembly, Int. Assoc. for the Phys. Sci. of the Oceans, Honolulu, Hawaii, August 5-12, 1995.

Haertel, P.T., The structure of the western Pacific westward-propagating equatorial disturbance, paper presented at the 21st Conference on Hurricanes and Tropical Meteorology, Am. Meteorol. Soc., Miami, Fla., April 24-28, 1995.

Harrison, D.E., and B.S. Giese, Remote westerly forcing of the eastern equatorial Pacific: Some model results, *Geophys. Res. Lett., 15*, 804-807, 1988.

Hartten, L.M., Synoptic settings of westerly wind bursts, *J. Geophys. Res., 101*, 16,997-17,019, 1996.

Hayes, S.P., L.J. Mangum, J. Picaut, A. Sumi, and K. Takeuchi.

TOGA-TAO: A moored array for real-time measurements in the tropical Pacific Ocean. *Bull. Am. Meteorol. Soc., 72*, 339-347, 1991.

Hendon, H., and B. Liebmann, A composite study of the onset of the Australian summer monsoon, *J. Atmos. Sci. 47*, 2227-2240, 1990.

Heymsfield, G.M., and R. Fulton, Comparison of high-altitude remote aircraft measurements with radar structure of an Oklahoma thunderstorm: Implications for precipitation estimation from space. *Mon. Weather Rev., 116*, 1157-1174, 1988.

Hildebrand, P.H., and W.C. Lee, Structure and evolution of a tropical squall line in TOGA COARE using the NCAR ELDORA airborne Doppler weather radar, paper presented at the 6th Conference on Mesoscale Processes, Am. Meteorol. Soc., Portland, Oreg., July 18-22, 1994.

Hildebrand, P.H., et al., The ELDORA/ASTRAIA airborne Doppler weather radar: High resolution observations from TOGA COARE, *Bull. Am. Meteorol. Soc., 77*, 213-232, 1996.

Holt, T.R., and S. Raman, Synergistic interaction of air-sea fluxes and clouds in the TOGA-COARE warm pool system, paper presented at the 6th Conference on Mesoscale Processes, Am. Meteorol. Soc., Portland, Oreg., July 18-22, 1996.

Hong X., S. Raman, and R.V. Madala, Effect of air-sea coupling on the development and the maintenance of deep tropical convection, in *Proceedings of the International Scientific Conference on TOGA*, vol. I, *Rep. WMO/TD 177*, pp. 398-402, World Meteorol. Organ., Geneva, 1995.

Houze, R.A., Jr., Structure and dynamics of a tropical squall-line system, *Mon. Weather Rev., 105*, 1540-1567, 1977.

Houze, R.A., Jr., and A.K. Betts, Convection in GATE, *Rev. Geophys., 19*, 541-576, 1981.

Houze, R.A., Jr., and C.P. Cheng, Radar characteristics of tropical convection observed during GATE: Mean properties and trends over the summer season, *Mon. Weather Rev., 105*, 964-980, 1977.

Houze, R.A., Jr., and D.D. Churchill, Mesoscale organization and cloud microphysics in a Bay of Bengal depression, *J. Atmos. Sci., 44*, 1845-1867, 1987.

Hu, J., and G. Barnes, A fast-moving MCS parallel to the environmental shear over the oceanic warm pool, paper presented at the 6th Conference on Mesoscale Processes, Am. Meteorol. Soc., Portland, Oreg., July 18-22, 1994.

Huyer, A., P.M. Kosro, R. Lukas, and P. Hacker, Upper ocean thermohaline fields near 2° S, 156° E, during the Tropical Ocean-Global Atmosphere Coupled Ocean-Atmosphere Response Experiment, November 1992 to February 1993, *J. Geophys. Res., 102*, 12,749-12,784, 1997.

Jabouille, P., J.L. Redelsperger, and J.P. Lafore, Mesoscale variability of surface fluxes due to atmospheric convection as simulated and observed during TOGA-COARE, paper presented at the 8th Conference on Air-Sea Interaction, Am. Meteorol. Soc., Atlanta, Ga., Jan. 28 to Feb. 2, 1996a.

Jabouille, P., J.L. Redelsperger, and J.P. Lafore, Modification of surface fluxes by atmospheric convection in the TOGA-COARE region, *Mon. Weather Rev., 124*, 816-837, 1996b.

Johnson, R.H., and J.A. Dickey, Effects of convection on the atmospheric boundary layer as revealed by TOGA-COARE sounding data, paper presented at the 8th Conference on Air-Sea Interaction, Am. Meteorol. Soc., Atlanta, Ga., Jan. 28 to February 2, 1996.

Johnson, R.H., P.E. Cieselski, and K.E. Hart, Tropical inversions near the 0°C level, *J. Atmos. Sci., 53*, 1838-1855, 1996.

Jorgensen, D. P., and and T. Matejka, Over determined quadruple Doppler synthesis from airborne Doppler radars. Paper presented at the 26th Conference on Radar Meteorology, Am. Meteorol. Soc., Norman, OK, 1993.

Jorgensen, D.P., T.J. Matejka, and M.A. LeMone, Structure and momentum fluxes within a TOGA COARE squall line system observed by airborne Doppler radar, paper presented at the 21st Conference on Hurricanes and Tropical Meteorology, Am. Meteorol. Soc., Miami, Fla., April 24-28, 1995.

Kaneko, A., X.H. Zhu, and M.H. Radenac, Diurnal variability and quantification of subsurface sound scatterers in the western equatorial Pacific, *J. Oceanogr., 52*, 655-674, 1996.

Keen, R., The role of cross-equatorial tropical cyclone pairs in the Southern Oscillation, *Mon. Weather Rev., 110*, 1405-1416, 1982.

Kessler, W.S., and M.J. McPhaden, Oceanic equatorial waves and the 1991-93 El Nino., *J. Clim., 8*, 1757-1774, 1995.

Kessler, W.S., M.J. McPhaden, and K.M. Weickmann, Forcing of intraseasonal Kelvin waves in the equatorial Pacific, *J. Geophys. Res., 100*, 10,613-10,631, 1995.

Kiladis, G.N., G.A. Meehl, and K.M. Weickmann, Large-scale circulation associated with westerly wind bursts and deep convection over the western equatorial Pacific, *J. Geophys. Res., 99*, 18,527-18,544, 1994.

Killworth, P.D., Deep convection in the world ocean, *Rev. Geophys., 21*, 1-26, 1983.

Kindle, J.C., and P.A. Phoebus, The ocean response to operational westerly wind bursts during the 1991-1992 El Nino, *J. Geophys. Res., 100*, 4893-4920, 1995.

Kingsmill, D.E., and R.A. Houze Jr., Airborne Doppler-radar observations of gust fronts and midlevel inflow in COARE mesoscale convective systems, paper presented at the 27th Conference on Radar Meteorology, Am. Meteorol. Soc., Vail, Colo., Oct. 9-13, 1995.

Knutson, T.R., and K.M. Weickmann, 30-60 day atmospheric oscillations: Composite life cycles of convection and circulation anomalies, *Mon. Weather Rev., 115*, 1407-1436, 1987.

Koschmeider, H., Methods and results of definite rain measurements, *Mon. Weather Rev., 62*, 5-7, 1934.

Krishnamurti, T.N., D.K. Oosterhof, and A.V. Mehta, Air-sea interaction on the time-scale of 30 to 50 days. *J. Atmos. Sci., 45*, 1304-1322, 1988.

Kristensen, L., J. Mann, S.P. Oncley, and J.C. Wyngaard, How close is close enough when measuring scalar fluxes with displaced sensors?, *J. Atmos. Oceanic Technol.*, 14, 814-821, 1997.

Lau, K.M., Equatorial response to northeasterly cold surges as inferred from satellite cloud imagery, *Mon. Weather Rev., 110*, 1306-1313, 1982.

Lau, K.M., and P.H. Chan, Intraseasonal and interannual variations of tropical convection: A possible link between the 40-day mode and ENSO, *J. Atmos. Sci., 45*, 950-972, 1988.

Lau, K.M., and C.-H. Sui, Mechanisms of short-term sea surface temperature regulation: observations during TOGA COARE, *J. Clim., 10*, 465-472, 1997.

Lau, K.M., T. Nakazawa, and C.H. Sui, Observations of cloud cluster hierarchies over the tropical western Pacific, *J. Geophys. Res., 96*, 3197-3208, 1991.

Lau, K.M., P.J. Sheu, S. Schuber, D. Ledvina, and H. Weng, Evolution of large scale cirucaltion during TOGA-COARE: Model intercomparison and basic features. *J. Clim., 5*, 986-1003, 1996.

LeMone, M.A., and M.W. Moncrieff, Momentum and mass transport by convective bands: Comparison of highly idealized dynamical models to observations, *J. Atmos. Sci., 51*, 281-305, 1994.

LeMone, M.A., D.P. Jorgensen, and B.F. Smull, The impact of two convective systems on sea surface stresses in COARE, paper presented at the 6th Conference on Mesoscale Processes, Am. Meteorol. Soc., Portland, Oreg., July 18-22, 1994.

LeMone, M.A., D.P. Jorgensen, S. Lewis, B. Smull, and T.

Matejka, Boundary-layer recovery in the stratiform region of mesoscale convective systems in TOGA COARE, paper presented at the 21st Conference on Hurricanes and Tropical Meteorology, Am. Meteorol. Soc., Miami, Fla., April 24-28, 1995.

Lewis, M.R., M.E. Carr, G.C. Feldman, W. Esaias, and C. McLain, Satellite estimates of the influence of penetrating solar radiation on the heat budget of the equatorial Pacific Ocean, *Nature*, *347*, 543-545, 1990.

Lewis, S.A., M.A. LeMone, and D.P. Jorgensen, The precipitation and circulation of a slow-moving convective band observed in TOGA COARE, paper presented at the 21st Conference on Hurricanes and Tropical Meteorology, Am. Meteorol. Soc., Miami, Fla., April 24-28, 1995.

Li, X., C. H. Sui, D. Adamec, and K. M. Lau, Impacts of precipitation in the upper ocean in the western Pacific warm pool during TOGA COARE, *J. Geophys. Res.*, *103*, 5347-5360, 1998.

Lilly, D.K., Cirrus outflow dynamics, *J. Atmos. Sci.*, *45*, 1594-1605, 1988.

Lin, X., and R.H. Johnson, Kinematic and thermodynamic characteristics of the flow over the western Pacific warm pool during TOGA COARE, *J. Atmos. Sci.*, *53*, 695-715, 1996a.

Lin, X., and R.H. Johnson, Heating, moistening and rainfall over the western Pacific warm pool during TOGA COARE, *J. Atmos. Sci.*, *53*, 3367-3383, 1996b.

Liu, W.K., K.B. Katsaros, and J.A. Businger, Bulk parameterization of air-sea exchanges of heat and water vapor including the molecular constraints at the interface, *J. Atmos. Sci.*, *36*, 1722-1735, 1979.

López, R.E., Radar characteristics of the cloud populations of tropical disturbances in the northwest Atlantic, *Mon. Weather Rev.*, *104*, 268-283, 1976.

López, R.E., The lognormal distribution and cumulus cloud populations, *Mon. Weather Rev.*, *105*, 865-872, 1977.

López, R.E., Internal structure and development processes of C-scale aggregates of cumulus clouds, *Mon. Weather Rev.*, *106*, 1488-1494, 1978.

Lucas, C., and R.E. Orville, TOGA-COARE: Oceanic Lightning, paper presented at the 5th Symposium on Global Change Studies,. Am. Meteorol. Soc., Nashville, Tenn., Jan. 23-28, 1994.

Lucas, C., and E. Zipser, The variability of vertical profiles of wind, temperature and moisture during TOGA COARE, paper presented at the 7th Conference on Mesoscale Processes, Am. Meteorol. Soc., Reading, England, Sept. 9-13, 1996.

Lucas, C., E.J. Zipser, and M.A. LeMone, Vertical velocity in oceanic convection off tropical Australia, *J. Atmos. Sci.*, *51*, 3183-3193, 1994.

Lucas, C., E.J. Zipser, and B.S. Ferrier, The impact of dry air intrusions on mesoscale convective systems, paper presented at the 8th Conference on Air-Sea Interaction, Am. Meteorol. Soc., Atlanta, G.,Jan. 28 to Feb. 2, 1996.

Lukas, R., and E. Firing, The geostrophic balance of the Pacific Equatorial Undercurrent, *Deep Sea Res., Part A*, *31*, 61-66, 1984.

Lukas, R., and E.J. Lindstrom, The mixed layer of the western equatorial Pacific Ocean, *J. Geophys. Res.*, *96*, suppl., 3343-3357, 1991.

Lukas, R., P.J. Webster, M. Ji, and A. Leetmaa, The large-scale context for the TOGA Coupled Ocean-Atmosphere Response Experiment, *Meteorol. Atmos. Phys.*, *56*, 3-16, 1995.

Madden, R.A., and P.R. Julian, Detection of a 40-50 day oscillation in the zonal wind in the tropical Pacific, *J. Atmos. Sci.*, *28*, 702-708, 1971.

Madden, R.A., and P.R. Julian, Observations of the 40-50 day tropical oscillation — A Review, *Mon. Weather Rev.*, *122*, 814-837, 1994.

Maddox, R.A., K.W. Howard, D.L. Bartels, and D.M. Rodgers, Mesoscale convective complexes in middle latitudes, in *Mesoscale Meteorology and Forecasting*, edited by P.S. Ray, pp. 390-413, Am. Meteorol. Soc., Boston, Mass., 1986.

Mapes, B.E., Gregarious tropical convection, *J. Atmos. Sci.*, *50*, 2026-2037, 1993.

Mapes, B.E., The large-scale part of tropical mesoscale convective system circulations: A linear vertical spectral band model, *J. Meteorol. Soc. Jpn.*, in press, 1998.

Mapes, B.E., and R.A. Houze Jr., Cloud clusters and superclusters over the oceanic warm pool, *Mon. Weather Rev.*, *121*, 1398-1415, 1993.

Mapes, B.E., and R.A. Houze Jr., Diabatic divergence profiles in western Pacific mesoscale cloud systems, *J. Atmos. Sci.*, *52*, 1807-1828, 1995.

Mapes, B.E., and P. Zuidema, Radiative-dynamical consequences of dry tongues in the tropical atmosphere, *J. Atmos. Sci.*, *53*, 620-638, 1995.

McBride, J., and G. Holland, The Australian Monsoon Experiment (AMEX): Early results, *Aust. Meteorol. Mag.*, *37*, 23-35, 1989.

McBride, J.L., N.E. Davidson, K. Puri, and G.C. Tyrell, The flow during TOGA COARE as diagnosed by the BMRC Tropical Analysis and Prediction System, *Mon. Weather Rev.*, *123*, 717-736, 1995.

McGaughey, G., and E.J. Zipser, Passive microwave observations of the stratiform regions of two tropical oceanic mesoscale convective systems, *J. Appl. Meteorol.*, *35*, 1949-1962, 1996.

McGaughey, G., E.J. Zipser, R.W. Spencer, and R.E. Hood, High-resolution passive microwave observations of convective systems over the tropical Pacific Ocean, *J. Appl. Meteorol.*, *35*, 1921-1947, 1996.

McPhaden, M.J., and S.P. Hayes, On the variability of winds, sea surface temperature, and surface layer heat content in the western equatorial Pacific, *J. Geophys. Res.*, *96*, suppl., 3331-3342, 1991.

McPhaden, M.J., H.P. Freitag, S.P. Hayes, and B.A. Taft, The response of the equatorial Pacific Ocean to a westerly wind burst in May 1986, *J. Geophys. Res.*, *93*, 10,589-10,603, 1988.

McPhaden, M.J., F. Bahr, Y. du Penhoat, E. Firing, S.P. Hayes, P.P. Niiler, P.L. Richardson, and J.M. Toole, The response of the western equatorial Pacific to westerly wind bursts during November 1989 to January 1990, *J. Geophys. Res.*, *97*, 14,289-14,303, 1992.

McPhaden, M.J., et al., Tropical Ocean-Global Atmosphere (TOGA) observing system: A decade of progress, *J. Geophys. Res.*, this issue.

Meehl, G.A., G.N. Kiladis, K.M. Weickmann, M. Wheeler, D.S. Gutzler, and G.P. Compo, Modulation of equatorial subseasonal convective episodes by tropical-extratropical interaction in the Indian and Pacific Ocean regions, *J. Geophys. Res*, *101*, 15,033-15,049, 1996.

Meyers G., J.R. Donguy, and R.K. Reed, Evaporative cooling of the western equatorial Pacific Ocean by anomalous winds, *Nature*, *323*, 523-526, 1986.

Miller, J.R., The salinity effect in a mixed layer ocean model, *J. Phys. Oceanogr.*, 6, 29-35, 1976.

Miller, M.J., A.C.M. Beljaars, and T.N. Palmer, The sensitivity of the ECMWF model to the parameterisation of evaporation from the tropical oceans, *J. Clim.*, *5*, 418-434, 1992.

Milliff, R.F., and R.A. Madden, The existence and vertical structure of fast, eastward-moving disturbances in the equatorial troposphere, *J. Atmos. Sci.*, *53*, 586-597, 1996.

Moncreiff, M.W. and J.S.A. Green, The propagation and

transfer properties of steady convective overturning in shear, *Q. J. R. Meteorol. Soc., 98*, 336-352, 1972.

Moncrieff, M.W., and E. Klinker, Organised convective systems in the tropical western Pacific as a process in general circulation models: A TOGA COARE case study *Q. J. R. Meteorol. Soc.*, in press, 1998.

Moncrieff M.W., D. Gregory, S.K. Krueger, J.L. Redelsperger, and W.K. Tao, GEWEX Cloud System Study (GCSS) Working Group 4: Precipitating convective cloud system, *Bull. Am. Meteorol. Soc., 78*, 831-852, 1997.

Nakazawa, T., Tropical cloud clusters within intraseasonal variations over the western Pacific. *J. Meteorol. Soc. Jpn., 66*, 823-839, 1988.

Nakazawa, T., Intraseasonal oscillations during the TOGA-COARE IOP. *J. Meteorol. Soc. Jpn., 73*, 305-319, 1995.

Neelin, J.D., I.M. Held, and K.H. Cook, Evaporation-wind feedback and low-frequency variability in the tropical atmosphere, *J. Atmos. Sci., 44*, 2341-2348, 1987.

Nitta, T., Energy budget of wave disturbances over the Marshall Islands during the years of 1956 and 1958, *J. Meteorol. Soc. Jpn., 50*, 71-84, 1972.

Numaguti, A., Characteristics of 4-to-20-day-period disturbances observed in the equatorial Pacific during the TOGA COARE IOP, *J. Meteorol. Soc. Jpn., 73*, 353-377, 1995.

Numaguti, A., R. Oki, K. Nakamura, K. Tsuboki, N. Misawa, T. Asai, and Y. Kodama, 4-5 day-period variation and low-level dry air observed in the equatorial western Pacific during the TOGA-COARE IOP, *J. Meteorol. Soc. Jpn., 73*, 267-290, 1995.

Nuret, M., and M. Chong, Monitoring the performance of the ECMWF operational analysis using the enhanced TOGA-COARE observational network, *Weather Forecasting, 11*, 53-65, 1996.

Palmer, T.N., and D.A. Mansfield, Response of two atmospheric general circulation models to sea-surface temperature anomalies in the tropical east and west Pacific, *Nature, 310*, 483-485, 1984.

Panofsky, H.A., and J.A. Dutton, *Atmospheric Turbulence*. 397 pp., Wiley-Interscience, New York, 1984.

Parsons, D., et al., The Integrated Sounding System: Description and preliminary observations from TOGA-COARE, *Bull. Am. Meteorol. Soc., 75*, 553-567, 1994.

Petersen, W.A., S.A. Rutledge, and R.E. Orville, Cloud-to-ground lightning observations from TOGA COARE: Selected results and lightning location algorithms, *Mon. Weather Rev., 124*, 602-620, 1996.

Picaut, J., and T. Delcroix, Equatorial wave sequence associated with warm pool displacements during the 1986-1989 El Nino-La Nina, *J. Geophys. Res., 100*, 18,393-18,408, 1995.

Pires, P., J.P. Lafore, and J.L. Redelsperger, Analysis of atmospheric wave modes during the TOGA–COARE intensive observation period, paper presented at the 6th Conference on Mesoscale Processes, Am. Meteorol. Soc., Portland, Oreg., July 18-22, 1994.

Pires P., J.L. Redelsperger, and J.P. Lafore, Equatorial atmospheric waves and their association to convection, *Mon. Weather Rev., 125,1167-1184*, 1997.

Price, J.F., Observations of a rain-formed mixed layer, *J. Phys. Oceanogr., 9*, 643-649, 1979.

Price, J.F., R.A. Weller, and R. Pinkel, Diurnal cycling: Observations and models of the upper ocean response to diurnal heating, cooling, and wind mixing, *J. Geophys. Res., 91*, 8411-8427, 1986.

Protat, A., Y. Lemaitre, and G. Scialom, Scale interactions involved in the initiation and evolution of mesoscale convective systems observed during TOGA COARE, paper presented at the 27th Conference on Radar Meteorology, Am. Meteorol. Soc., Vail, Colo., Oct. 9-13, 1995.

Pueschel, R.F., D.A. Allen, C. Black, S. Faisant, G.V. Ferry, S.D. Howard, J.M. Livingston, J. Redemann, C.E. Sorenson, and S. Verma, Condensed water in tropical cyclone "Oliver," 8 February 1993.*Atmos. Res., 38*, 297-313, 1995.

Ralph, E.A., K. Bi, P.P. Niiler, and Y. du Penhoat, A Lagrangian description of the western equatorial Pacific response to the wind burst of December 1992, *J. Clim., 10*, 1706-1721, 1997.

Randall, D.A., Harshvardan, and D.A. Dazlich, Diurnal variability of the hydrological cycle of a GCM, *J. Atmos. Sci., 48*, 40-62, 1991.

Rasmusson, E.M., and T.H. Carpenter, Variations in tropical sea surface temperature and surface wind fields associated with the Southern Oscillation/El Nino, *Mon. Weather Rev., 110*, 354-384, 1982.

Raymond, D.J., Regulation of moist convection over the western Pacific warm pool, *J. Atmos. Sci., 52*, 3945-3959, 1995.

Redelsperger, J.L., F. Guichard, P. Jabouille, and J.P. Lafore, Numerical studies of precipitating systems observed during COARE: organization, surface flux and troposphere modifications, in *Proceedings of the International Scientific Conference on TOGA*, Vol. I, Rep. *WMO/TD 177*, pp. 449-453, World Meteorol. Organ., Geneva, 1995a.

Redelsperger, J.L., P. Jabouille, and J.P. Lafore, Numerical studies of convective organization observed during COARE, paper presented at the 21st Conference on Hurricanes and Tropical Meteorology, Am. Meteorol. Soc., Miami, Fla., April 24-28, 1995b.

Reed, R.J., and E.E. Recker, Structure and properties of synoptic-scale wave disturbances in the equatorial western Pacific, *J. Atmos. Sci., 28*, 1117-1133, 1971.

Rickenbach, T.M., Rainfall production from the spectrum of convection observed by shipboard radar during TOGA COARE, paper presented at the 21st Conference on Hurricanes and Tropical Meteorology, Am. Meteorol. Soc., Miami, Fla., April 24-28, 1995.

Rickenbach, T.M., and S.A. Rutledge, Convection in TOGA COARE: Horizontal scale, morphology, and rainfall production, *J. Atmos. Sci.*, (in press), 1998.

Riehl, H., *Tropical Meteorology*, McGraw-Hill, New York, 392 pp., 1954.

Roemmich, D., M. Morris, W.R. Young, and J.R. Donguy, Fresh equatorial jets, *J. Phys. Oceanogr., 24*, 540-558, 1994.

Rossow, W.B., and R.A. Schiffer, ISCCP cloud data products, *Bull. Am. Meteorol. Soc., 72*, 2-20, 1991.

Roux, F., and O. Bousquet, Heat and momentum budgets and mesoscale convective systems observed during TOGA COARE, paper presented at the 27th Conference on Radar Meteorology, Am. Meteorol. Soc., Vail, Colo., Oct. 9-13, 1995.

Schubert, W.H., P.E. Ciesielski, C. Lu, and R.H. Johnson, Dynamical adjustment of the trade wind inversion layer, *J. Atmos. Sci., 52*, 2941-2952, 1995.

Seager, R. and B. Blumenthal, Modeling tropical Pacific sea surface temperature with satellite-derived solar radiative forcing, *J. Clim., 7*, 1943-1957, 1994.

Shinoda, T., and R. Lukas, Lagrangian mixed layer modeling of the western equatorial Pacific, *J. Geophys. Res., 100*, 2523-2541, 1995.

Short, D.A., P.A. Kucera, B.S. Ferrier and O.W. Thiele, COARE IOP rainfall from shipborne radars, 1, Rainmapping algorithms, paper presented at the 27th Conference on Radar Meteorology, Am. Meteorol. Soc., Vail, Colo., Oct. 9-13, 1995.

Siegel, D.A., J.C. Ohlmann, L. Washburn, R.R. Bidigare, C.T. Nosse, E. Fields, and Y. Zhou, Solar radiation, phytoplankton pigments and the radiant heating of the

equatorial Pacific warm pool, *J. Geophys. Res., 100*, 4885-4891, 1995.

Smith, E.A., X. Xiang, A. Mugnai, R.E. Hood, and R.W. Spencer, Behavior of an inversion-based precipitation retrieval algorithm with high-resolution AMPR measurements including a low-frequency 10.7 GHz channel, *J. Atmos. Oceanic Technol., 11*, 858-873, 1994.

Smith, S.D., Coefficients for sea surface wind stress, heat flux, and wind profiles as a function of wind speed and temperature, *J. Geophys. Res, 93*, 15,467-15,472, 1988.

Smull, B.F., and R.A. Houze Jr., Rear inflow in squall lines with trailing stratiform precipitation, *Mon. Weather Rev., 115*, 2869-2889, 1987.

Smull, B.F., D.P. Jorgensen, T.J. Matejka, and M.A. LeMone, Airborne Doppler radar and in situ measurements of a slow-moving convective band observed during TOGA COARE, paper presented at the 21st Conference on Hurricanes and Tropical Meteorology, Am. Meteorol. Soc., Miami, Fla., April 24-28, 1995.

Smyth, W.D., D. Hebert, and J.N. Moum, Local ocean response to a multiphase westerly wind burst, Thermal and freshwater responses, *J. Geophys. Res., 101*, 22,513-22,533, 1995.

Soloviev, A., and R. Lukas, Observation of spatial variability of diurnal thermocline and rain-formed halocline in the western equatorial Pacific warm pool, *J. Phys. Oceanogr., 26*, 2529-2538, 1996.

Soloviev, A., and R. Lukas, Observation of large diurnal warming events in the near-surface layer of the western equatorial Pacific warm pool. *Deep Sea Res., I, 44*, 1055-1076, 1997a.

Soloviev, A., and R. Lukas, Sharp frontal interfaces in the near-surface layer of the ocean in the western equatorial Pacific warm pool, *J. Phys. Oceanogr. 27*, 999-1017, 1997b.

Sui, C.H., K.M. Lau, Y. Takayabu, and D. Short, Diurnal variations in tropical oceanic cumulus ensemble during TOGA-COARE, *J. Atmos. Sci., 54* , 637-655, 1997.

Sui, C.-H., X. Li, and K.-M. Lau, Selective absorption of solar radiation and upper ocean temperature in the equatorial western Pacific,*J. Geophys. Res.*, (in press), 1998a.

Sui, C.H., X. Li, and K.M. Lau, Radiative-convective processes in simulated diurnal variations of tropical oceanic convection, *J. Atmos. Sci.*, (in press), 1998b.

Sun, J., J.F. Howell, S.K. Esbenson, L. Mahrt, C.M. Greb, R. Grossman, and M.A. Le Mone, Scale dependence of air-sea fluxes over the western equatorial Pacific, *J. Atmos. Sci., 53, 2997-3012*, 1996.

Takahashi, N., and H. Uyeda, Doppler radar observation of the structure and characteristics of tropical clouds during the TOGA-COARE IOP in Manus, Papua New Guinea: Three case studies on November 23 and December 16, 1992, *J. Meteorol. Soc. Jpn., 73*, 427-442, 1995.

Takahashi, T., K. Suzuki, M. Orita, M. Tokuno, and R. de la Mar, Videosonde observations of precipitation processes in equatorial cloud clusters, *J. Meteorol. Soc. Jpn., 73*, 509-534, 1995.

Takayabu, Y.N., Large-scale cloud disturbances associated with equatorial waves, II. Westward-propagating inertio-gravity waves, *J. Meteorol. Soc. Jpn., 72*, 451-465, 1994.

Takayabu, Y.N., K.M. Lau, and C.H. Sui, Observation of quasi two-day wave during TOGA COARE, *Mon. Weather Rev., 124*, 1892-1913, 1996.

TOGA COARE International Project Office (TCIPO), TOGA COARE experiment design, report Univ. Corp. for Atmos. Res., Boulder, Colo., 1991.

TOGA COARE International Project Office (TCIPO), TOGA COARE operations plan, report, 95 pp., Univ. Corp. for Atmos. Res., Boulder, Colo., 1992.

TOGA COARE International Project Office (TCIPO), TOGA COARE intensive observing period operations summary, report, Univ. Corp. for Atmos. Res., Boulder, Colo., 1993.

TOGA COARE International Project Office (TCIPO), Summary report of the TOGA COARE International Data Workshop, report Univ. Corp. for Atmos. Res., Boulder, Colo., 1995.

Tokay, A., and D.A. Short, Evidence from tropical raindrop spectra of the origin of rain from stratiform vs. convective clouds, *J. Appl. Meteorol., 35*, 355-371, 1996.

Tomczak, M., Salinity variability in the surface layer of the tropical western Pacific Ocean, *J. Geophys. Res., 100*, 20,499-20,515, 1995.

Trier, S.B., D.B. Parsons, and M.A. LeMone, A three-dimensional numerical simulation of a tropical squall line observed during TOGA COARE, paper presented at the 6th Conference on Mesoscale Processes, Am. Meteorol. Soc., Portland, Oreg., July 18-22, 1994.

Trier, S.B., W.C. Skamarock, and M.A. LeMone, Structure and evolution of the 22 February 1993 TOGA-COARE squall line: Numerical simulations. *J. Atmos. Sci., 54*, 386-407, 1996.

Tsukamoto, O. and H. Ishida, Turbulent flux measurements and energy budget analysis over the equatorial Pacific during TOGA-COARE IOP, *J. Meteorol. Soc. Jpn., 73*, 291-302, 1995.

Ushiyama, T., S. Satoh and K. Takeuchi, Time and spatial variations of mesoscale rainfalls and their relation to the large-scale field in the western tropical Pacific, *J. Meteorol. Soc. Jpn., 73*, 379-392, 1995.

Uyeda, H., et. al., Doppler radar observations on the structure and characteristics of tropical clouds during the TOGA-COARE IOP in Manus, Papua New Guinea — Outline of the observations. *J. Meteorol. Soc. Jpn., 73*, 415-426, 1995.

Velden, C.S., and J.A. Young, Satellite observations during TOGA-COARE:Large-scale descriptive overview, *Mon. Weather Rev., 122*, 2426-2441, 1994.

Waliser, D.E., W.D. Collins, and S.P. Anderson, An estimate of the surface shortwave cloud forcing over the western Pacific during TOGA-COARE, *Geophys. Res. Lett., 23*, 519-522, 1996.

Walsh, E.J., D.E. Hagan, D.P. Rogers, R. Pinkel, R.A. Weller, C.W. Fairall, D.C. Vandemark, R.N. Swift, and J.F. Scott, Correlations between sea surface mean square slope, SST and wind speed under light wind conditions during TOGA COARE, paper presented at the 8th Conference on Air-Sea Interactions, Am. Meteorol. Soc., Atlanta, Ga., Jan. 28-Feb. 2, 1996.

Wang, Y., W.K. Tao, and J. Simpson, The impact of ocean surface fluxes on a TOGA-COARE convective system, *Mon. Weather Rev., 124*, 2753-2763, 1996.

Webb, E. K, On the correction of flux measurements for effects of heat and water vapor transfer, *Boundary Layer Meteorol., 23*, 251-254, 1982.

Webster, P.J., The large-scale structure of the tropical atmosphere, *in General Circulation of the Atmosphere*, edited by B. Hoskins and R. Pearce, pp. 235-275, Academic, San Diego, Calif., 1983.

Webster, P.J., The role of hydrological processes in ocean-atmosphere interactions, *Rev. Geophys., 32*, 427-476, 1994.

Webster, P.J., and R.A. Houze Jr., The Equatorial Mesoscale Experiment (EMEX): An overview, *Bull. Am. Meteorol. Soc., 72*, 1481-1505, 1991.

Webster, P.J., and R. Lukas, TOGA COARE: The Coupled Ocean-Atmosphere Response Experiment, *Bull. Am. Met.eorol Soc., 73*, 1377-1416, 1992.

Weisman, M.L., J.B. Klemp, and R. Rotunno, Structure and evolution of numerically simulated squall lines, *J. Atmos. Sci., 45*, 1990-2013, 1988.

Weller, R.A., and S.P. Anderson, Surface meteorology and air-sea fluxes in the western equatorial Pacific warm pool during the TOGA Coupled Ocean-Atmosphere Response Experiment, *J. Clim., 9*, 1959-1990, 1996.

Wick, G. A., Evaluation of the variability and predictability of the bulk-skin sea surface temperature difference with application to satellite-measured sea surface temperature, Ph.D. thesis, 146 pp., Univ. of Colo., Boulder, 1995.

Williams, A.G., H. Kraus, and J.M. Hacker, Transport processes in the tropical warm pool boundary layer, I, Spectral composition of fluxes, *J. Atmos. Sci.*, 53, 1187-1202, 1996.

Williams, M., and R.A. Houze Jr., Satellite-observed characteristics of winter monsoon cloud clusters, *Mon. Weather Rev.*, *115*, 505-519, 1987.

Willis, P.T., R.A. Black, and F.D. Marks Jr., Airborne rain drop size distributions in TOGA COARE, paper presented at the 21st Conference on Hurricanes and Tropical Meteorology, Am. Meteorol. Soc., Miami, Fla., April 24-28, 1995.

Wu, X., and M. W. Moncrieff, Collective effects of mesoscale convection and its approximation in general circulation models, *J. Atmos. Sci.*, *53*, 1477-1495, 1996.

Wyrtki, K., and G. Meyers, The trade wind field over the Pacific Ocean, The mean field and the mean annual variations, *Rep. HIG-75-1*, Hawaii Inst. of Geophys., Univ. of Hawaii, 1975.

Yanai, M., S. Esbensen, and J.H. Chu, Determination of bulk properties of tropical cloud clusters from large-scale heat and moisture budgets, *J. Atmos. Sci.*, *30*, 611-627, 1973.

Yoneyama, K., and T. Fujitani, The behavior of dry westerly air associated with convection observed during the TOGA-COARE Natsushima cruise, *J. Meteorol. Soc. Jpn.*, *73*, 25-38, 1995.

Yoshizaki, M., On the selection of eastward-propagating modes appearing in the wave-CISK model as tropical intraseasonal (30-60 day) oscillations. Linear response to localized heating moving in an east-west direction on the equatorial beta plane, *J. Meteorol. Soc. Jpn.*, *69*, 595-608, 1991.

Young, G.S., S.M. Perugini, and C.W. Fairall, Convective wakes in the equatorial western Pacific during TOGA, *Mon. Weather Rev.*, *123*, 110-123, 1995.

Yuter, S.E., and R.A. Houze, The natural variability of precipitating clouds over the western Pacific warm pool, *Q. J. R. Meteorol. Soc.*, in press, 1998.

Yuter, S.E., and R.A. Houze Jr., Measurements of raindrop size distributions over the Pacific warm pool and implications for Z-R relations, *J. Appl. Meteorol.*, *36*, 847-867, 1997.

Yuter, S.E., R.A. Houze Jr., B.F. Smull, F.D. Marks Jr., J.R. Daugherty, and S.R. Brodzik, TOGA COARE aircraft mission summary images: An electronic atlas. *Bull. Am. Meteorol. Soc.*, *76*, 319-328, 1995.

Zhang, C., Atmospheric intraseasonal variability at the surface in the tropical western Pacific Ocean, *J. Atmos. Sci.*, *53*, 739-758, 1996.

Zipser, E.J., The role of organized unsaturated convective downdrafts in the structure and rapid decay of an equatorial disturbance, *J. Appl. Meteorol.*, *8*, 799-814, 1969.

Zipser, E.J., Mesoscale and convective scale downdrafts as distinct components of squall line circulation, *Mon. Weather Rev.*, *105*, 1568-1589, 1977.

Zipser, E.J., The evolution of mesoscale convective systems: Evidence from radar and satellite observations in *Tropical Rainfall Measurements*, edited by J. S. Theon and N. Fugono, pp. 159-166, Deepak Pub., Hampton, Va., 1988.

Zipser, E.J., and K.A.L. Caesar, The structure of cold pools produced by mesoscale convective systems during TOGA COARE, paper presented at the 6th Conference on Mesoscale Processes, Am. Meteorol. Soc., Portland, Oreg., July 18-22, 1994.

J. S. Godfrey, CSIRO Marine Research, GPO Box 1538, Hobart, Tasmania 7001, Australia. (e-mail: godfrey@marine.csiro.au)

R. A. Houze Jr., Department of Atmospheric Sciences, Box 351640, University of Washington, Seattle, WA 98195. (e-mail: houze@atmos.washington.edu)

R. H. Johnson, Department of Atmospheric Science, Colorado State University, Fort Collins, CO 80523. (e-mail: dick@vortex.atmos.colostate.edu)

R. Lukas, Department of Oceanography, MSB 312, University of Hawaii at Manoa/JIMAR, 1000 Pope Road, Honolulu, HI 96822. (e-mail: rlukas@iniki.soest.hawaii.edu)

J.-L. Redelsperger, Meteo-France CNRM, 42, ave Gustave Coriolis, 31057 Toulouse Cedex, France. (e-mail: redels@meteo.fr)

A. Sumi, Center for Climate System Research, University of Tokyo, 4-6-1, Komaba, Meguro-ku, Tokyo 113, Japan. (e-mail: sumi@ccsr.u-tokyo.ac.jp)

R. Weller, Woods Hole Oceanographic Institute, Woods Hole, MA 02543. (e-mail: bob@altair.whoi.edu)

(Received May 23, 1996; revised April 22, 1997; accepted November 3, 1997.)